

OPTOGENETIC, VOLTAMMETRIC, AND HISTOCHEMICAL
CHARACTERIZATION OF STRIATAL TYROSINE HYDROXYLASE
INTERNEURONS

By

HARRY S. XENIAS

A dissertation submitted to the Faculty of the Graduate School-Newark of
Rutgers, The State School of New Jersey in the partial fulfillment of the

requirement for the degree of Doctorate of Philosophy

Graduate Program in Behavioral and Neural Science

Written under the direction of Professor James M. Tepper

And approved by

Elizabeth D. Abercrombie

Ian Creese

Tibor Koós

Denis Paré

Margaret E. Rice

James M. Tepper

Mark R. Wightman

Newark, New Jersey

October, 2014

© 2014

by

HARRY S. XENIAS

ALL RIGHTS RESERVED

ABSTRACT OF THE DISSERTATION

Optogenetic, Voltammetric, and Histochemical Characterization of Striatal
Tyrosine Hydroxylase Interneurons

By Harry S. Xenias

Thesis Director: Professor James M. Tepper

The traditional view of striatal dopamine originating from the midbrain remained unchallenged until a publication by Dubach et al. (1987) showed that in primates there are striatal interneurons immunoreactive for tyrosine hydroxylase (TH), the rate-limiting enzyme for catecholamine synthesis. It has generally been assumed in subsequent publications that striatal TH interneurons (THINs) are an intrinsic striatal source of dopamine (DA). The possibility that THINs could be DAergic has deep implications for both normal and pathological states, such as Parkinson's disease. However, despite nearly three decades since the first report of striatal TH⁺ neurons, no direct evidence that THINs are DAergic or can compensate for the loss of nigrostriatal DA has been reported.

To examine if THINs contain and release DA, two bacterial artificial chromosome (BAC) transgenic mouse lines were used that express either the Cre recombinase enzyme or the enhanced green fluorescent protein (EGFP) reporter. Both transgenes are under the control of the regulatory elements of TH and each respective mouse line is referred to as TH-Cre or EGFP-TH. Immunofluorescent cytochemistry revealed no colocalization of EGFP⁺ striatal cells with DA in TH-EGFP mice. Neither was there any colocalization of

EGFP⁺ striatal cells with aromatic L-amino acid decarboxylase (AADC), the vesicular monoamine transporter-2 (VMAT2), or the dopamine transporter (DAT). Additionally, TH-Cre mice that were unilaterally lesioned by 6-OHDA in the midbrain were also bilaterally injected into the striatum with Cre-dependent recombinant adeno-associated virus (AAV), encoding the opsin protein channelrhodopsin-2 (ChR2) fused to the enhanced yellow fluorescent protein (EYFP) to transduce THINs to express ChR2.

THINs were then light-activated by 2-5 ms blue light pulses during simultaneous fast-scan cyclic voltammetry (FSCV) and found to not release any detectable amounts of DA, even in the presence of nomifensine, a potent DA reuptake inhibitor. Lastly, it was found that THINs are powerfully modulated by DA and provide a widespread and powerful inhibition on SPNs. THINs then, despite containing TH, are not DAergic but a novel class of GABAergic interneuron that regulates the timing of the output responses of SPNs and add to the complexity of the striatal microcircuitry.

PREFACE

A Biased Perspective

My undergraduate background is in physics and mathematics, studies that I have never regretted undertaking, as they offer, with an elegant economy of principles, an at once rich and precise understanding of the world at large. In sharp contrast, the biological world is far less exact; it is messy, both literally and figuratively. It lacks the comforting regularity and controlled repeatability that the physical sciences enjoy. Still, for anyone who has contemplated the inner workings of the machinery of a single cell let alone ensembles of them working in unison, there is an underlying beauty to be found. We have evolved toward a more detailed quantitative, biophysical understanding of this inner realm but still have far to go in terms of our understanding of network level phenomena and how it is that the brain as a whole performs the incredible computational feats of adaptive learning, memory, and behavior.

In 1982, a visionary outline of how to proceed towards a deeper computational understanding was posthumously published in a book written by David Marr, *Vision: A Computational Investigation Into the Human Representation and Processing of Visual Information*. Marr describes his view of how to understand brain function in terms of three levels of organization. The first level relates to the computation goal, or logic of a functional execution. The second is the algorithmic level, or how the computational goal is represented in input-output terms along with their associated transformations. The last is the so-called “hardware” implementation level, which specifies how the computational algorithm is physically realized. Recently, I had the

pleasure of speaking with Dr. Peter Redgrave at the first Gordon Conference for the basal ganglia (2014). We spoke about the potential impact of adopting Marr's ideas on basal ganglia research. While it seemed clear to both of us that Marr's philosophical view is largely ignored by those outside of the vision community, it was gratifying to have an agreement that Marr's philosophy of approach could be applied to any brain region. Given the plethora of behavioral and cellular-level data about the basal ganglia, which will only grow as a result of the new molecular and transgenic tools already have and are rapidly emerging, now more than any other time, the basal ganglia community needs to embrace this multi-tiered Marrian viewpoint. Moreover, it should also do so while not mistaking understanding of top-level organizations for understanding underlying bottom-up mechanisms.

Arguably, Marr's ideas have not been readily incorporated into research because of their lack of immediate utility stemming from our still largely ignorant understanding of the neuronal basis for behavior. Often we know little if anything of the computational goals of a microcircuit, which in turn makes elucidating a neural algorithm difficult. Complicating matters even further, as we have now found ourselves in recent years, there is an emerging embarrassment of riches in newly discovered striatal interneurons and subtypes, which heretofore were neither recognized nor fully appreciated. Their existence and associated microcircuitry undoubtedly adds to a greater complex, computational architecture responsible for the algorithmic realization of behavioral output. The discovery of striatal tyrosine hydroxylase interneurons, the subject of this thesis, adds to this complexity.

Although small in terms of the percentage of the total striatal neuronal population, interneurons comprise an important portion of the “hardware” of the basal ganglia and help determine the output of projection neurons. How they interact with one another and affect output therefore informs us of the next Marrian hierarchical level of an algorithmic realization. This bottom-up view is no less important and complementary to the top-down view of basal ganglia function and cannot be ignored. It remains to be determined how striatal interneurons are selected in implementing an algorithmic realization of a computational goal, which would then elucidate the functional contributions of the diverse heterogeneity of interneuron subtypes.

While this is a biased, reductionist view, the alternative view is that there is no underlying principle of neural dynamics. Each computational goal must have either a dedicated and unique set of interneurons for its realization or be comprised of intersecting sets of interneurons that are involved in different computational goals but which somehow do not interfere with the other goals. If the former case, then our task is to unravel the one-to-one mappings of specific microcircuits to behavioral outputs. If the latter case, then some deeper, meta-level principle of interneuron microcircuit mapping to behavior must exist. If nature is any teacher, however, the workings of the physical world, which biology is subject, often reveal an underlying principle of operation that can give rise to diverse and disparate outcomes.

Although we are still in a nascent stage of our understanding, there is reason for being excited: we are now armed with research tools, which only a few years ago were the stuff of science fiction, and which will permit us to understand and bridge these multiple tiers of behavioral organization and

hopefully reconcile an otherwise disparate and daunting wealth of neuroscientific data.

ACKNOWLEDGEMENTS

As is always the case upon the completion of a doctorate, a good deal of gratitude is owed to the many people who enabled and facilitated the endeavor to be successful. To our center's animal care staff, I am grateful for their professionalism of maintaining our animal colonies, especially during the bitter cold Mid-Atlantic winters, when often our university was shut down and staff members still managed to tirelessly come in for their proverbial appointed rounds. To our center's administrative staff, Wayne Brown, Ann Kutyla, Shivangiben "Shiva" Patel, and Celina Nieves-Caban, I am indebted for their help over these past years with the red-tape formalities and ensuring a smooth transition from semester to semester. I wish to also thank Sandy Reyes of the Office of the Dean, Graduate School for her help with the final process of submitting this doctoral thesis.

As also is often the case, the mastery of scientific techniques has its roots in first being mentored and then mimicking the success of others, hopefully finding your own unique style along the way. For something like patch clamping, there is as much an art as there is a science to the practice of effectively softly kissing a cell with a thin tube of glass and gently coaxing it to let you in to spy on its inner functions. It was Dr. Fatuel Tecuapetla, a post-doctoral researcher in our lab, who first taught me how to patch. His Zen-like patience and ability to suppress the urge to utter colorful language during frustrating sessions of patching axon blebs always impressed me. I was also very fortunate to have known Dr. Osvaldo Ibáñez-Sandoval, another patient, hard-working post-doctoral researcher, from whom I learned a good deal and

whom I came to call a friend. I was privileged to have known and worked with both of them.

In addition, I am grateful in general to Fulva Shah, our lab's senior technician, and to our former research technicians Ibrahim Tadros, Janish Kothari, and Parth Gandhi. I am especially indebted to our most recent technician, Arpan Garg, for his very helpful assistance during the final end of my stay in the Tepper lab and his friendship. In addition, I thank my fellow lab research members, past and present, and departmental colleagues for their support and friendship.

I also wish to especially thank my committee members, whose larger than typical size is reflective of the multidisciplinary approaches used for my doctoral research. I am indebted to Dr. Margaret E. Rice, who I first met in 2010 at the International Basal Ganglia Society (iBAGs) meeting and who graciously invited me to her lab at NYU. It was there that I learned the art of carbon fiber electrode making and imported the skill back to our lab. I am also indebted to Dr. R. Mark Wightman of UNC. He and his lab personnel were instrumental in helping me with the finer points of the Ensman EI-400 biopotentiostat, which their laboratory designed and from which I have gotten lots of mileage over the years. To Dr. Ian Creese and Dr. Denis Paré, I owe thanks for them being not only the former (Ian) and current (Denis) director of our program, advising me during my stay at Rutgers, but also for their good recommendations as committee members, especially during my thesis proposal. With Dr. Tibor Koós, one of the most intellectually driven minds I have known, along the way with the endless discussions on everything from the frustrated musings over the reasons for serotype-specific cytotoxicity of

given cell types to the science of politics and the politics of science, I was first exposed to the magic of optogenetics. To Dr. Elizabeth D. Abercrombie, my committee chair member, I am grateful for her gentle guidance and open-door policy—and the occasional coffee.

Last but not least, to Dr. James M. Tepper, my mentor: I am truly grateful for his trust and high expectations of me. Dr. Tepper did not simply accept me into his lab but entrusted me early on with the task of setting up a complete electrophysiology rig and giving me a wonderfully intellectually enriching project. On both a technical and scientific level, I could not have asked for either a more challenging or rewarding experience, which evolved into a multidisciplinary thesis. Thank you Jim.

DEDICATION

I lovingly dedicate this dissertation to my mother and father, Constance and Stylianos Xenias, whose love and support I can never possibly repay except with the love they showed me.

Τα φαινόμενα συχνά απατούν.
“Appearances often are deceiving,”
Aesop, The Wolf in Sheep’s Clothing.

TABLE OF CONTENTS

CHAPTER I: INTRODUCTION	1
The basal ganglia: an overview	2
The striatum and its functional significance	3
The rodent as an ideal model	4
Striatal interneurons	6
Striatal interneuron processing of output neurons	9
Diversity of striatal interneurons	11
Striatal tyrosine hydroxylase interneurons (THINS)	12
Immunocytochemical evidence for striatal TH+ neurons	12
Evidence that striatal TH+ neurons are “dopaminergic”	13
Striatal TH+ neurons increase in number following nigrostriatal deletion	15
Striatal TH+ neurons detected after nigrostriatal DA loss are from pre-existing neurons	17
Striatal TH+ neurons are GABAergic interneurons with four distinct subtypes	20
Subtype specific electrophysiology of THINs	22
Striatal THIN distribution obeys a striosome-matrix-based cytoarchitecture	24
Neuromodulation of Striatal THINs	26
Striatal THINs: Are they DAergic?	26
CHAPTER II: METHODS	30
Subjects	31
Optogenetics	31
Viral mediated gene transfer	32
Stereotaxic intracerebral viral and 6-hydroxydopamine injections	33
Preparation of brain slices	34
Imaging of slices	35
In vitro electrophysiology	35
Whole-cell patch recording	35

Subthreshold membrane oscillation induction	36
In vitro voltammetry	37
Stimulation protocols	39
Electrical stimulation	39
Optical stimulation.....	40
Biocytin histochemistry	40
Fluorescent immunocytochemistry	41
Immunocytochemistry for TH and DA.....	41
Immunocytochemistry for AADC	43
Immunocytochemistry for VMAT2	44
Immunocytochemistry for DAT.....	45
Statistical analysis and graphical representations	46
 CHAPTER III: RESULTS	 48
Immunofluorescent characterization of striatal THINs.....	49
DA immunofluorescence.....	50
Characterization of DA in the midbrains of unilaterally lesioned EGFP-TH mice	50
Characterization of DA in the striatum of unilaterally lesioned EGFP-TH mice	52
AADC immunofluorescence.....	56
Control characterization of AADC in the midbrains of EGFP-TH mice.....	56
Characterization of AADC in the striatum of EGFP-TH mice	57
VMAT2 immunofluorescence.....	60
Control characterization of VMAT2 in the midbrains of EGFP TH mice	60
Characterization of VMAT2 in the striatum of EGFP-TH mice	60
DAT immunofluorescence	62
Control characterization of DAT in the midbrains of EGFP TH mice.....	62
Characterization of DAT in the striatum of EGFP-TH mice	63
Voltammetry	65
Characterization of in vitro fast-scan cyclic voltammetric detection of DA.....	65

Optogenetics with simultaneous voltammetry	70
Selective targeting and optogenetic activation of striatal THINs.....	70
Electrophysiology with simultaneous FSCV	72
Optogenetic evoked release of nigrostriatal DA during FSCV in the striatum	75
Optogenetic activation of striatal THINs during FSCV in the striatum.....	77
Electrophysiology and modulation of striatal THINs.....	82
Inhibitory Effects of Striatal THINs on SPNs.....	82
THINs alter the spike timing of SPNs.....	82
THINs elicit robust GABA _A -mediated IPSCs into SPNs	83
Neuromodulation of striatal THINs	85
SMOs and their modulation by DA.....	87
 CHAPTER IV: DISCUSSION	 94
Dopaminergic neurons are a very small minority of striatal TH neurons.....	95
Immunocytochemical evidence that THINs are non-dopaminergic	98
Absence of colocalization of EGFP-TH with Dopamine in THINs.....	100
Absence of colocalization of EGFP-TH with AADC in THINs	105
Absence of colocalization of EGFP-TH with VMAT2 in THINs	108
Absence of colocalization of EGFP-TH with DAT in THINs.....	108
Voltammetric evidence that striatal THINs are non-dopaminergic	111
Electrophysiological properties of THINs	117
THINs control spike-timing and inhibit SPNs.....	118
Neuromodulation of THINs	120
DA modulation of plateau potentials.....	121
DA modulation of subthreshold membrane oscillations	125
ACh modulation of THINs	128
But why TH? : The monoenzymatic cooperativity hypothesis.....	130
Functional significance and concluding remarks	135

REFERENCES	144
-------------------------	-----

Vita	164
-------------------	-----

LIST OF FIGURES

Chapter I:

Figure 1:	Simplified schematic of the basal ganglia	3
-----------	---	---

Chapter II:

Figure 2:	Fast-scan cyclic voltammetry and detection of DA	37
-----------	--	----

Chapter III:

Figure 3:	Immunofluorescent detection of DA in the midbrain.....	50
Figure 4:	High-magnification of DA immunofluorescent midbrain neurons	51
Figure 5:	DA fluorescent immunocytochemistry in dorsal striatum	54
Figure 6:	DA fluorescent immunocytochemistry in ventral striatum	55
Figure 7:	AADC fluorescent immunocytochemistry in midbrain	56
Figure 8:	Negative detection of AADC immunofluorescence in THINs	58
Figure 9:	Example of a non-THIN AADC+ only cell in the striatum	59
Figure 10:	VMAT2 fluorescent immunocytochemistry in midbrain	60
Figure 11:	Negative detection of VMAT2 immunofluorescence in THINs	61
Figure 12:	DAT fluorescent immunocytochemistry in midbrain	63
Figure 13:	Negative detection of DAT immunofluorescence in THINs	64
Figure 14:	Calibration of carbon fiber electrode for FSCV	66
Figure 15:	FSCV detection of DA	67
Figure 16:	Neuropharmacology to maximize FSCV DA detection	68
Figure 17:	Carbon fiber electrode sensitivity of DA detection	69
Figure 18:	Fluorescent photomicrograph of transduced THINs in TH-cre mouse	70
Figure 19:	Optogenetic activation of THINs	72
Figure 20:	Simultaneous FSCV with electrophysiology	73
Figure 21:	Optogenetic activation of THINs during simultaneous FSCV	74
Figure 22:	FSCV during optogenetically activated TH+ midbrain neurons.....	76

Figure 23:	FSCV and optogenetic activation of THINs in the striatum.....	79
Figure 24:	Pharmacology with FSCV in striatum during activation of THINs.....	80
Figure 25:	Statistical summary of FSCV results	81
Figure 26:	THINs generate IPSPs onto SPNs	83
Figure 27:	GABA _A -mediate inhibition of THINs	84
Figure 28:	Population vs. unitary responses of THINs onto SPNs	85
Figure 29:	Plateau potentials and subthreshold membrane oscillations.....	86
Figure 30:	Lomb-Scargle analysis plot of subthreshold membrane oscillations	87
Figure 31:	Dopamine modulation of subthreshold membrane oscillations	90
Figure 32:	SMOs are dependent on Ca and TTX-sensitive Na channels.....	91
Figure 33:	Heat map and statistics of averaged SMOs	93
Figure 34:	Monoenzymatic cooperativity	134
Figure 35:	Proposed coordinated neuromodulation of THINs	142

LIST OF ABBREVIATIONS

6-OHDA : six hydroxydopamine

AADC: Aromatic L-amino acid decarboxylase

AAV: Adeno-associated virus

ACh: Acetylcholine

ADP: Afterdepolarization potential

AMP: Cyclic adenosine monophosphate

AN: Arcuate nucleus of the hypothalamus

AP: Action potential

BG: Basal ganglia

BrdU: Bromodeoxyuridine

CIN: Cholinergic interneuron

ChR2: Channelrhodopsin-2

CFE: Carbon fiber electrode

Cre: Cre recombinase

DA: Dopamine

DAB: 3,3'-diaminobenzidine

DNQX: 6,7-dinitroquinoxaline-2,3-dione

DREADD: Designer receptors exclusively activated by designer drugs

ERK: Extracellular signal-regulated kinases

EGFP: Enhance green fluorescent protein

EYFP: Enhanced yellow fluorescent protein

EPSP: Excitatory postsynaptic potential

FFA: Flufenamic acid

FLU: Flufenamic acid

FSCV: Fast-scan cyclic voltammetry

FS: Fast-spiking

GABA: Gamma-aminobutyric acid

cAMP: cyclic AMP

cAMP-PKA: cyclic AMP-dependent protein kinase A

GP: Globus pallidus

GPCR: G-protein coupled receptors

HCN: Hyperpolarization-activated cyclic nucleotide-gated

HPLC: High performance liquid chromatography

ICAN: Ca²⁺-activated non-specific cation conductance

I_h: Hyperpolarization-activated current

IPSC: Inhibitory postsynaptic current

IPSP: Inhibitory postsynaptic potential

Kir: Potassium inward rectifier

L-DOPA: L-Dihydroxyphenylalanine

LoxP: Locus of X-over P1

LTD: Long-term depression

LTP: Long-term potentiation

MEC: Mecamylamine

MOR: μ -opioid receptor

MPTP: 1-methyl-4-phenyl-1,2,3, 6-tetrahydropyridine

MPP⁺ : 1-methyl-4-phenylpyridinium

nAChR: nicotinic acetylcholine receptor

NADPH: Nicotinamide adenine dinucleotide phosphate

NIM: Nimodipine
Nom: Nomifensine
NOS: Nitric oxide synthase
NPY: Neuropeptide Y
NPY-NGF: NPY neurogliaform
PKA: Protein kinase A
PLTS: Persistent and low-threshold spike cell
PP: Plateau potential
PV: Parvalbumin
RAC: Raclopride
RMP: Resting membrane potential
SMB: Sodium metabisulfite
SMO: Subthreshold membrane oscillation
SNc: Substantia nigra, pars compacta
SNr: Substantia nigra, pars reticulata
SOM: Somatostatin
SPN: Spiny projection neuron
STDP: Spike-timing-dependent plasticity
STN: Subthalamic nucleus
TAN: Tonically active neurons
TEA: Tetraethylammonium chloride
TH: Tyrosine hydroxylase
THIN: Tyrosine hydroxylase interneuron
TRPM: Transient receptor potential melastatin
TTX: Tetrodotoxin

CHAPTER I

INTRODUCTION

The basal ganglia: an overview

The evolutionary success of a complex organism such as a vertebrate depends in large part on its ability to negotiate between competing behavioral actions to maximize its survival (Cerri and F., 1983; Lima et al., 1985; Aslan and Bauml, 2012; Dezfouli and Balleine, 2012). In ever changing, unpredictable environments, a flexible ability to switch between and select among different actions in a goal-directed manner is crucial to the long-term survival and normal functioning (Dezfouli and Balleine, 2012, 2013). This ability must be adaptive over the organism's lifetime because learning from experience increases survival (Nairne et al., 2008; Nairne and Pandeirada, 2008; Aslan and Bauml, 2012). Moreover, while changing environmental conditions have evolutionarily and markedly shaped the external morphologies of animals (Darwin, 1859), the requirement for an information integrative system that incorporates an memory with the ability to appropriately select actions among many alternatives is an evolutionary necessity. The biological solution to this problem was the emergence of a highly conserved set of interconnected brain nuclei collectively termed the basal ganglia (Medina and Reiner, 1995; Reiner et al., 1998; Redgrave et al., 1999; Smeets et al., 2000; Stephenson-Jones et al., 2012; Ericsson et al., 2013a; Grillner et al., 2013). These structures have remained conserved for over 560 million years of vertebrate evolution and can be traced back to the earliest vertebrates, the cyclostomes, which include the jawless fishes, the hagfish and the lamprey (Grillner et al., 2013) and found in many other vertebrates (Medina and Reiner, 1995; Reiner et al., 1998), including birds (Veenman, 1997; Reiner, 2002) and mammals (Gerfen, 1992; Graybiel et al.,

1994; Smeets et al., 2000; Hikosaka et al., 2006; Pennartz et al., 2009; Jin et al., 2014).

In rodents, these interconnected nuclei of the basal ganglia (BG), include the corpus striatum (Str), the globus pallidus, external segment (GPe), the substantia nigra, pars reticulata (SNr),

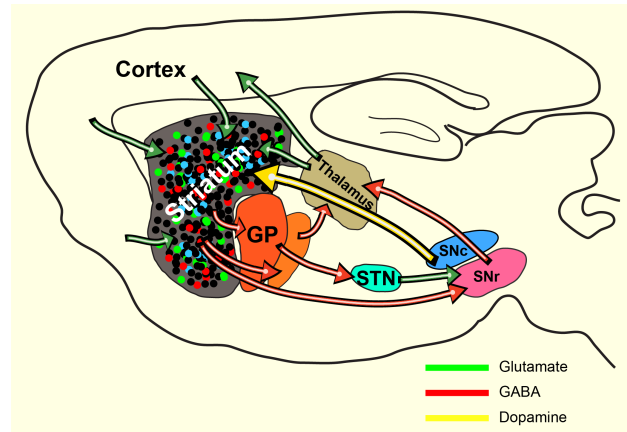


Figure 1. Simplified schematic representation of the basal ganglia, highlighting the major intrabasical ganglia subcortical nuclei, their gross pathways, and neurotransmitters. GP = globus pallidus; STN = subthalamic nucleus; SNc = substantia nigra, pars compacta; and SNr = substantia nigra, pars reticulata.

the substantia nigra, pars compacta (SNc), and the subthalamic nucleus (STN) (Gerfen C. R., 1996; Groenewegen, 2003; Lanciego et al., 2012). A simplified representation of these nuclei, their corresponding gross intrabasical ganglia connections, and major neurotransmitters are shown in Figure 1.

The Striatum and its functional significance

Much attention has been given to the striatum, not simply because it is the largest subcortical nucleus of the basal ganglia but also the main input nucleus. The striatum receives excitatory innervation from the cortex and thalamus, and forms closed loops with the cortex via the thalamus (Gerfen, 1992; Graybiel et al., 1994; Gerfen C. R., 1996; Holt et al., 1997; Bolam et al., 2000; Groenewegen, 2003; Tepper, 2006; Gerfen and Surmeier, 2011; Kress et al.,

2013). Another distinguishing property of the striatum is that it contains the most numerous and heterogeneous population of neurons of any nucleus of the basal ganglia. The striatum has two major outputs, referred to as the direct and indirect pathway, often referred to as the “go” or “no-go” pathways, respectively (Gerfen C. R., 1996; Bolam et al., 2000; Bateup et al., 2010; Jin and Costa, 2010; Chuhma et al., 2011; Gerfen and Surmeier, 2011; Cui et al., 2013).

More importantly, the striatum plays a pivotal role in shaping cortical dynamics through this parallel closed loop architecture by processing the cortical input it receives and ultimately modifying BG output via the thalamus back to the cortex (Alexander et al., 1990; Graybiel et al., 1994; Joel and Weiner, 1994; McHaffie et al., 2005; Tepper, 2006). Lastly, the striatum is involved in goal-directed behavior (Hollerman et al., 2000; Johnson et al., 2007; Grillner et al., 2008; Redgrave et al., 2010; Pennartz et al., 2011; Dezfouli and Balleine, 2013), in which dopamine (DA) from the mesencephalon serves to both modulate and direct behaviors by predicting reward outcome and effecting long-term plasticity (Schultz, 2002, 2006; Lovinger, 2010; Schultz, 2010b; Parush et al., 2011).

The rodent as an ideal model

For this thesis, the mouse was chosen for two main reasons. First, the BG of the mouse is identical to that of other vertebrates with only few differences (Smeets et al., 2000; Zeiss, 2005). One notable difference between the BG of rodent and higher mammals is that rodents lack a clear division

between the caudate and putamen of the corpus striatum (Bolam et al., 1988; Aoki and Pickel, 1989; Aosaki et al., 1994a; Hikosaka et al., 2006). In rodents, the striatum is simply referred to as the neostriatum (Bolam et al., 1983; Kawaguchi, 1992; Kubota and Kawaguchi, 1993; Tepper and Bolam, 2004; Tepper et al., 2004). Second, there are now many readily commercially available transgenic mice lines, which greatly aid basic research in the basal ganglia. These include mice lines of conditional models (Bockamp et al., 2008) used for Parkinson's disease models (Martin, 2007; Skaper and Giusti, 2010) and Huntington's research (Li et al., 2005; Ehrnhoefer et al., 2009; Skaper and Giusti, 2010). There are also a variety of bacterial artificial chromosome (BAC) transgenic lines that express the cre recombinase enzyme for use with optogenetics (Deister et al., 2009; Gradinaru et al., 2009; Gradinaru et al., 2010; Tecuapetla et al., 2010; Zhang et al., 2010; Deisseroth, 2011; English et al., 2012; Williams and Deisseroth, 2013) and used in conjunction with other genetically engineered tools for the light and drug-activated control of G-protein coupled receptors (GPCRs) to recruit and initiate selective intracellular pathways, such as with light-activated so-called "optoXRs" (Airan et al., 2009) or designer receptors exclusively activated by designer drugs (DREADDs) (Pei et al., 2008).

The majority of the neostriatum is comprised of the spiny projection neurons (SPNs) (Parent, 1986; Gerfen C. R., 1996; Bolam et al., 2000; Tepper et al., 2004; Kress et al., 2013). These are medium sized, densely spiny GABAergic output neurons (Gerfen et al., 1990; Kita, 1993; Gerfen C. R., 1996; Gittis and Kreitzer, 2012), their somata typically ranging between 12-20 μm in diameter, and emitting 5-10 smooth primary dendrites, which quickly become densely studded with spines beginning 20 μm away from the soma (Gerfen C. R., 1996).

They have a modest dendritic branching, usually of 30-35 dendritic tips, which spherically arborize to a diameter of about 200-300 μm (Tepper et al., 1998).

In addition, the SPNs have two functionally and neurochemically distinct populations: a D1 dopamine receptor expressing subtype that projects to the substantia, par reticulata (SNr) and comprise the so-called “direct pathway” and a D2 dopamine receptor expressing subtype that innervates the globus pallidus (GP) and known as the “indirect pathway” (Gerfen et al., 1990; Surmeier and Kitai, 1993; Gerfen C. R., 1996; Surmeier et al., 2007; Shen et al., 2008).

Another difference between the neostriatum of rodents and the striatum of higher vertebrates such as primates is the significantly higher percentage of SPNs in the neostriatum that comprise approximately 95% of the neostriatum (Graveland and DiFiglia, 1985; Tepper, 2006; Tepper et al., 2010). This lower percentage of SPNs in the primate suggests that the correspondingly higher percentage of interneurons as compared to the rodent play a greater role in information processing.

Striatal Interneurons

The remaining neurons of the neostriatum are the interneurons. They are comprised of a heterogeneous population of mostly GABAergic interneurons (Bolam et al., 1983; Aoki and Pickel, 1989; Kawaguchi, 1993; Kita, 1993; Kawaguchi et al., 1997; Tepper and Bolam, 2004; Tepper et al., 2004; Wilson, 2007; Tepper et al., 2008; Tepper et al., 2010). Evidence for the existence of various types of striatal neurons dates back to the time of Ramon y Cajal,

when he first reported, in addition to the existence of a great number of small to medium-sized neurons, a significantly smaller population of large-sized neurons (Ramon y Cajal, 1911). We now recognize that these small to medium sized neurons comprise not just the spiny projection neurons but also the GABAergic interneurons and a smaller number of large somatic sized neurons, which are the cholinergic interneurons (Kawaguchi, 1992, 1993; Kita, 1993; Kawaguchi et al., 1997).

The morphological, neurochemical, and electrophysiological heterogeneity of some of the striatal interneurons was reported in a now widely recognized landmark study by Kawaguchi, who showed there were three broad classes of interneurons in the neostriatum of the rat (Kawaguchi, 1993). This study also characterized the medium spiny projection neurons, which has a highly hyperpolarized resting membrane potential in vitro (≈ -80 mV) and a low input resistance (≈ 200 M Ω). In general, interneurons were found having larger somata.

Evidence of neostriatal GABAergic interneurons was based on Golgi-staining, autoradiography, and electron microscopy (Bolam et al., 1983). One of the first electrophysiologically characterized GABAergic neostriatal interneurons was a parvalbumin (PV) expressing fast-spiking (FS) neuron with short-duration afterhyperpolarizations, low resting membrane potential, and low-input resistance, which fired rapidly and repetitively during depolarization (Kawaguchi, 1993). The landmark study by Kawaguchi (1993) initially found three classes of neostriatal interneurons. The spike width at half amplitude for FS cells was the most narrow, being roughly a third of the other cell types or (≈ 0.3 ms). FS cells were also found to express GABA, establishing

that they were inhibitory neurons. FS cells were further characterized morphologically as having either a localized dendritic field or a more extended dendritic arbor, which suggests two functionally distinct subclasses of FS neuron.

In contrast, the second class of neostriatal interneuron identified was an NADPH diaphorase-expressing cell termed PLTS: persistent low-threshold spike cells. In comparison to FS cells, PLTS cells have a higher input-resistance and fire Na^{2+} -dependent persistent depolarized spikes and Ca^{2+} -dependent low-threshold spikes, which could be initiated from hyperpolarizing potentials. Compared to FS and SPNs, PLTS interneurons have a markedly more depolarized resting membrane potential of (≈ -55 mV), and a high input resistance (≈ 600 M Ω). In addition, PLTS cells were neurochemically distinguishable by being immunoreactive for nitric oxide synthase (NOS).

The last encountered neostriatal cell type was a large aspiny interneuron with highly dendrites that was immunoreactive for choline acetyltransferase (ChAT). It was termed LA cell for “long-lasting afterhyperpolarization.” Its electrophysiology was marked by a Ca^{2+} -dependent long-lasting afterhyperpolarization and a pronounced time-dependent hyperpolarizing anomalous rectification, owed to I_h . Compared to other striatal neurons, LA cells have much larger somata (≈ 25 μm). Like the PLTS cells, LA cells have a less negative resting membrane potential (≈ -55 mV) and a high input resistance (≈ 400 M Ω). Today, these interneurons are better known as ChAT interneurons (CINs) (Martone et al., 1994; Holt et al., 1997; Salin et al., 2009; English et al., 2012) and are widely regarded as the tonically active

interneurons (TANs) readily recorded in the primate striatum (Aosaki et al., 1994b; Aosaki et al., 1995; Kimura et al., 2003).

In rodents, the cholinergic interneurons comprise somewhere between 0.5-1.0 % of the neostriatal interneurons and GABAergic interneurons represent 3-4% of the remaining population (Bolam et al., 1983; Kawaguchi, 1992, 1993; Tepper et al., 2004; Wilson, 2004; Tepper et al., 2010). While interneurons account for a small proportion of striatal cells, they nonetheless play a significant role in sculpting striatal output (Koos and Tepper, 2002; Zhou et al., 2002; Tepper et al., 2004; Wilson, 2007; Tepper et al., 2008; Chuhma et al., 2011) and serve specialized roles in processing behaviorally relevant information (Aosaki et al., 1994b; Kimura et al., 2003; English et al., 2012). Evidence for this specialization goes back many decades, where histological studies alone suggested that the striatum was highly organized and evolved in particular for specialized cortical information processing (Gerfen, 1992; Graybiel et al., 1994).

Striatal interneuron processing of output neurons

The SPNs serve as integrators of cortical and thalamic information. The major of their excitatory inputs comes from the cerebral cortex and secondly from the midline and intralaminar thalamic nuclei (Wilson, 2004; Tepper, 2006). These excitatory afferents also demonstrate synaptic specificity with nearly 90% of them targeting spine heads¹ (Bolam and Bennett., 1995; Tepper et al., 2004; Wilson, 2004). These excitatory inputs drive the so-called “UP” and “DOWN”

¹ The exception to this is that the parafascicular thalamic nucleus predominantly targets the dendritic shafts of SPNs

states of SPNs, which have been seen *in vivo* and characterized by rhythmic fluctuations in membrane potential that oscillate between a hyperpolarized potential of near -80 mV (the “DOWN” state) and a depolarized “UP” state potential of around -50 mV (Wilson and Kawaguchi, 1996; Plenz and Kitai, 1998; Wilson, 2004; Tepper, 2006). These UP and DOWN states are now known to arise from interactions between a fast inward rectifier and outward rectifier driven by synchronous excitatory input from large ensembles of cortical and thalamic glutamatergic neurons (Gerfen C. R., 1996; Wilson, 2004). Striatal GABAergic interneurons, however, also play an important role in sculpting these oscillations as well and determining when an SPN can fire during an “UP” state (Plenz, 2003). As described below, GABAergic interneurons determine the timing of SPN firing (Koos and Tepper, 1999; Tepper and Bolam, 2004) and serve a permissive roles for spike-timing dependent plasticity (Centonze et al., 1999). In contrast, cholinergic interneurons serve to modulate the sub- and suprathreshold responses of SPNs to cortical and thalamic inputs, especially during circuit activation encoding reward-relevant information (Bennett and Wilson, 1999; Centonze et al., 1999; Bennett et al., 2000; Apicella, 2002; Tepper and Bolam, 2004; Aosaki et al., 2010; Ding et al., 2010).

Cholinergic (ChAT) interneurons (CINs) are the most abundant interneuronal types of the striatum, accounting for 1% of the total striatal population. They not only innervate SPNs but other striatal interneurons, particularly the FS cells (Gerfen C. R., 1996; Koos and Tepper, 2002; Tepper and Bolam, 2004; Wilson, 2004). A striking feature of these cells is their spontaneous firing of about 3 Hz (Kawaguchi, 1993; Aosaki et al., 1995). CINs undergo a stereotypical 500 ms pause in their ongoing firing during

reinforcement learning and involved with the nigrostriatal reward prediction error signal (Schultz, 1998; Goldberg and Reynolds, 2011; Chuhma et al., 2014). For example, in rats that have undergone operant conditioning, the spontaneous firing of CINs pause in response to reward expectation (Aosaki et al., 1994b; Apicella, 2002; Kimura et al., 2003). The spontaneous activity of ChAT interneurons is due to an interplay between a hyperpolarization-activated conductance non-specific cation (HCH) and a persistent sodium conductance (Wilson, 2005; Tepper, 2006). In addition, a potassium inward rectifier (K_{IR}) regeneratively amplifying hyperpolarization onsets and produces stereotyped responses to hyperpolarizing inputs. This gives rise to pauses whose duration is determined by the endogenous properties of the ChAT interneurons themselves, not the nature of the triggering input (Wilson, 2005).

Whereas the ChAT interneurons can mediate complex, mixed excitatory and inhibitory inputs (Zhou et al., 2002; Oldenburg and Ding, 2011), the fast-spiking and PLTS cells, serve distinct inhibitory roles (Koos and Tepper, 1999; Koos et al., 2004; Tepper and Bolam, 2004; Gittis et al., 2010). Moreover, although these three broad classes of interneurons have been best studied to date, many other types of striatal interneurons exist.

Diversity of striatal interneurons

Evidence for other interneuronal cell types comes from the original work by Ramon y Cajal (1911) and from more recent Golgi studies. Together, they show that there are at least five distinct medium-sized and several smaller

sized interneurons that have (Chang et al., 1982). For instance, we now know that there is at least one other NPY+ subtype (Ibanez-Sandoval et al., 2011), the neurogliaform cell, which interacts with the cholinergic interneurons to mediate reinforcement-related signaling (English et al., 2012). In addition, there are the calretinin-expressing interneurons, which we know very little (Bennett and Bolam, 1993; Schlosser et al., 1999; Rymar et al., 2004; Tepper et al., 2010) and the serotonin 5-HT(3A) receptor-expressing interneurons of the striatum, which are among the least studied to date. Finally, there are the tyrosine hydroxylase (TH) expressing interneurons, whose characterization has just begun (Ibanez-Sandoval et al., 2010; Tepper et al., 2010; Unal et al., 2011; Unal et al., 2013).

Striatal tyrosine hydroxylase interneurons (THINS)

Immunocytochemical evidence for striatal TH+ neurons

Until recently, a traditional view based on neurochemical markers has held that there are three basic subtypes of striatal GABAergic interneurons: one class expressing the peptides somatostatin (SOM), neuropeptide Y (NPY), NADPH diaphorase and nitric oxide synthase (NOS), and the remaining classes expressing either the calcium binding proteins parvalbumin (PV) or calretinin (CR) (Kawaguchi, 1993; Kawaguchi et al., 1995). Collectively, these GABAergic interneurons have been shown to account for $\approx 2\%$ of neostriatal cells (Rymar et al., 2004).

In 1987, however, a study reported the existence in the adult monkeys a population of striatal neurons that expressed tyrosine hydroxylase (TH), the rate-limiting enzyme required for catecholamine synthesis (Dubach et al., 1987). Since then, TH⁺ striatal neurons have been shown existent mice (Mao et al., 2001; Petroske et al., 2001; Ibanez-Sandoval et al., 2010), rats (Tashiro et al., 1989a; Meredith et al., 1999), and in other primates (Betarbet et al., 1997; Mazloom and Smith, 2006), including humans (Porritt et al., 2000; Cossette et al., 2005).

Evidence that striatal TH⁺ neurons are “dopaminergic”

This discovery prompted further interest and investigation by many research groups, which found that besides TH, other traditional neurochemical makers used to identify DAergic neurons of the mesencephalon were also found in the striatum. These included aromatic L-amino acid decarboxylase (AADC) (Tashiro et al., 1989a; Mura et al., 1995; Meredith et al., 1999; Lopez-Real et al., 2003) and the dopamine transporter (DAT) (Porritt et al., 2000; Palfi et al., 2002; Cossette et al., 2005; Porritt et al., 2006; Huot et al., 2007; Huot and Parent, 2007), thus further supporting the view that TH⁺ neurons as being DAergic. These finding however were controversial. There were even reports that concluded TH⁺ neurons not only had the intrinsic capacity to express DA (Mura et al., 1995) but also were DAergic and serving a compensating role for the loss of nigrostriatal DA (Betarbet et al., 1997). One study reported existence of DAergic striatal somata (Meredith et al., 1999). However this same study also reported that the same striatal cells did not express TH and DA.

In general, until recently, the early literature concerning TH⁺ striatal neurons was confusing and contradictory. Even the most basic parameters such as soma size and morphology did not agree between studies, even within a given species (Tashiro et al., 1989a; Meredith et al., 1999). Still more, there was no agreement as to whether these newly discovered striatal cell types were interneurons or projection neurons, as Darmopil, et al. (2008) had reported.

However, a rare instance of near universal agreement and reporting was that TH⁺ striatal neurons increase in number in Parkinson's patients or following experimental depletion of striatal dopamine (Betarbet et al., 1997; Meredith et al., 1999; Porritt et al., 2000; Mao et al., 2001; Petroske et al., 2001; Palfi et al., 2002; Jollivet et al., 2004; Mazloom and Smith, 2006; Darmopil et al., 2008). Yet, the reason for this increase was debated. Was it due to neurogenesis or to an upregulation of TH expression in preexisting neurons (Lopez-Real et al., 2003; Mazloom and Smith, 2006)?

Until recently, the evidence for TH⁺ neurons being DAergic has been based entirely on immunocytochemistry. These have included the markers used to detect the presence of DAergic neurons of the midbrain, such as TH, AADC, and DAT, and dopamine itself (Dubach et al., 1987; Tashiro et al., 1989b; Mura et al., 1995; Betarbet et al., 1997; Meredith et al., 1999; Lopez-Real et al., 2003; Jollivet et al., 2004; Cossette et al., 2005; Huot and Parent, 2007; Darmopil et al., 2008). These studies, however, have proven inconclusive in two major ways. First, there has been much disagreement regarding the expression of these markers, even within the same species, suggesting that non-specific antibody staining generated false positives (Tashiro et al., 1989a; Komori et al., 1991; Mura et al., 1995; Nagatsu et al., 1997; Meredith et al., 1999).

Second, and more significantly, even if TH⁺ striatal interneurons do indeed possess and colocalize these markers, it would not prove that these cells in fact would release dopamine.

Striatal TH⁺ neurons increase in number following nigrostriatal deletion

One of the main reasons that striatal TH⁺ neurons have been thought to be dopaminergic, aside from them expressing a requisite enzyme for catecholamine synthesis, is that their numbers dramatically increase following nigrostriatal depletion. Many labs have now independently found that the number of TH⁺ interneurons increase 3 to 6 fold after experimentally-induced lesions of the SNc (Betarbet et al., 1997; Meredith et al., 1999; Porritt et al., 2000; Mao et al., 2001; Petroske et al., 2001; Palfi et al., 2002; Jollivet et al., 2004; Mazloom and Smith, 2006; Darmopil et al., 2008). This observation lead some to conclude the striatal TH⁺ neurons were DAergic and functionally serving to compensate for the decrease of extracellular DA in the striatum (Betarbet et al., 1997; Huot and Parent, 2007). The therapeutic implications of this increase, if indeed these cells have the capacity to naturally release DA, are then obvious.

Interestingly, it has been reported that TH⁺ striatal interneurons increase in numbers in human Parkinson's disease sufferers (Porritt et al., 2000), thus further suggesting that striatal TH⁺ neurons serve a compensating function. However, these striatal cells appear to be vulnerable to the disease progression of Parkinson's, being gradually lost over time (Porritt et al., 2006).

Yet another study reported the same observations in Huntington's disease (Huot et al., 2007)².

How tyrosine hydroxylase levels are regulated after DA depletion is still unclear. This is especially true of the host of regulatory transcriptional factors that are activated in a tissue specific-manner, where secondary messenger interactions including cAMP and Ca²⁺ also participate in regulating TH levels (Lenartowski and Goc, 2011), as well as post-transcriptional regulation in response to metabolic stress (Tank et al., 2008). It is evident that intrinsic sensing and post-transcriptional regulatory mechanisms have evolved to homeostatically maintain catecholamine levels. For instance, the insertion of the human copy of TH in transgenic mice, which results in a transcriptional output 50 times higher compared to wild type mice, catecholamine levels are not altered (Kaneda et al., 1991).

One important transcriptional activator of TH however is the nuclear orphan receptor Nurr1, which transactivates TH transcription production (Sakurada et al., 1999) in a cell-specific fashion (Kim et al., 2003). In mice from embryonic day E0 – E14, in midbrain neurons developmentally fated for a dopaminergic phenotype, Nurr1 expression has been shown to be D2R-mediated via an extracellular signal-regulated kinase (ERK) pathway (Sakurada et al., 1999). In contrast, for adult midbrain neurons, a host of short and long term mechanisms are at play, particularly a cAMP-mediated post-transcriptional one that is sensitive to external stimuli (Chen et al., 2008). Such sensing mechanisms, which serve to homeostatically regulate dopamine

² This later study however involved L-DOPA treatment, and the authors suggest a possible explanation of the eventual cell loss as a result of a compensating negative-feedback mechanism in reducing tyrosine hydroxylase expression in these cells.

output, might specifically find a special role in striatal TH⁺ interneurons, which could have evolved as a possible standby source of dopamine for the striatum during any decreased output from the nigrostriatal pathway. Indeed, such a compensating mechanism has been previously suggested (Bezard and Gross, 1998) and has experimental support in several studies. For example, it has been shown that during dopamine depletion, particularly in the arcuate nucleus, otherwise non-dopaminergic neurons begin a *de novo* synthesis of dopaminergic markers (Ugrumov et al., 2004; Ershov et al., 2005; Ugrumov, 2009).

Striatal TH⁺ neurons detected after nigrostriatal DA loss are from pre-existing neurons

There is some agreement among a few studies however that help place these numerous discrepant findings in perspective by suggesting a needed conditional induction of the “dopaminergic” phenotype. Meredith et al., (1999) reports that in unilateral 6-hydroxydopamine lesioned rats, there arises a small population of TH⁺ cells, which appear to be projection neurons located in the ventral striatum as well as the central and dorsal areas of the caudate-putamen. The same study also reported that there are striatal cells that are immunoreactive for AADC and DA, located in the dorsal medial subcallosal area of the caudate-putamen, but whose smaller size and morphology is indicative of local neurons. This finding agrees with Mura et al., (2000), who report that after exogenous application of L-DOPA, there arises a small population of AADC⁺ cells that overlap with DA⁺ cells found in the dorsal

medial striatum, directly under the corpus callosum, along the ventricles. Moreover, these cells were similarly small and aspiny, and appeared to be of the same size and morphology that resembled the local neurons reported by Meredith et al. (1999).

Two distinct populations of TH+ cells appear to exist. One consists of a large number of TH+ only cells found throughout the striatum and recently have been shown to be a class of GABAergic interneuron. The other population overlaps with cells expressing AADC and DA and anatomically restricted beneath the subcallosal area and appear capable of synthesizing DA directly following nigrostriatal deletion or posses the capacity to convert L-DOPA into DA through AADC (as suggested by the Mura et al. finding).

Moreover, in macaques that underwent MPTP-induced nigrostriatal deletion, Tandé et al. (2006) found striatal cells immunoreactive for TH+ that also expressed DAT but did not incorporate bromodeoxyuridine (BrdU), a marker of proliferating cells. This suggested that the striatal TH+ neurons detected following depletion of nigrostriatal dopamine do not arise from neurogenesis but rather from a preexisting pool that undergoes a phenotypic shift towards becoming catecholaminergic, most likely due to an upregulation of TH expression.

Lastly, this result agrees well with the study by Cossette, et al. (2005), which found that only approximately 30% of TH+ striatal interneurons expressed TuJ1, an indicator of proliferating neural progenitors (Zhang et al., 2003; Park et al., 2005), supporting the conclusion reached in the Tandé et al. (2006).

There remained however many unresolved questions concerning striatal TH+ neurons. Whether these cells were projection neurons as reported by Meredith et al. (1999) or interneurons was unclear and only recently determined to be the latter (Ibanez-Sandoval et al., 2010). In addition, there are many inconsistencies between colocalization studies (Tashiro et al., 1989a; Komori et al., 1991; Mura et al., 1995; Nagatsu et al., 1997; Meredith et al., 1999), suggesting that non-specific antibody staining possibly generated false positives. Most of the evidence for TH+ neurons being DAergic has however come from these studies and no definitive and detailed study to look for colocalization of DAergic markers in TH+ cells has been made.

This is not the first time controversy concerning the neurocytological nature of neostriatal neurons of the neostriatum. Although the large neurons of the striatum having been historically first properly identified as interneurons (Kölliker, 1896), Ramon y Cajal erroneously identified them as projection cells and the medium sized striatal neurons as interneurons (Ramon y Cajal, 1911). This mistake was further repeated by a later publication (Vogt and Vogt, 1920). For many decades, the view of the striatum as being comprised of a vast majority of interneurons and a minority of projection neurons remained until being finally corrected Grofova (1979). In part, this controversy was owed to limitations of the technology of the time. The studies of Ramon y Cajal were based on the Golgi silver impregnation method (Spacek, 1992), which famously led to the Neuronal Doctrine (De Carlos and Borrell, 2007). It was not until nearly 6 decades later with retrograde labeling from the globus pallidus and substantia nigra, pars reticulata that the medium sized neurons incorrectly

identified as interneurons were definitively identified as projection neurons and the large aspiny neurons as interneurons (Grofova, 1979).

Striatal TH+ neurons are GABAergic interneurons with four distinct subtypes

Much of the controversy surrounding the nature of striatal TH+ neurons has been settled and reported in a relatively recent publication (Ibanez-Sandoval et al., 2010), which characterized the morphology, anatomy, and electrophysiology of these cells. This study used EGFP-TH BAC transgenic mice that expressed the enhanced green fluorescent protein (EGFP) under the control of the regulatory elements of TH, allowing for fluorescent identification of striatal TH+ neurons. This in turn allowed for them to be patched and electrophysiologically recorded and filled with biocytin for later anatomical analysis. Such analyses along with retrograde labeling revealed these cells to be medium sized interneurons that form GABAergic synapses onto SPNs interneurons.

The finding that these cells were GABAergic were keeping with earlier studies, which reported that these cells are immunoreactive for glutamic acid decarboxylase (GAD) (Betarbet et al., 1997; Mura et al., 2000; Cossette et al., 2005; Mazloom and Smith, 2006; Tande et al., 2006; Huot and Parent, 2007). Both isoforms of GAD were also found in primates, with GAD₆₅ in humans and monkeys (Huot and Parent, 2007) and GAD₆₇ in monkeys (Betarbet et al., 1997; Tande et al., 2006).

In the 2010 Ibañez-Sandoval study, cluster analysis of the electrophysiological parameters (resting membrane potential, input resistance, and maximum frequency, and the number of action potentials elicited) revealed four distinct groups of TH+ interneurons (THINs). This same study showed that these cells are striatal interneurons and not projection neurons, as claimed in an earlier study (Darmopil et al., 2008). Injection of rhodamine beads into the substantia nigra and globus pallidus, did not retrogradely label EGFP-TH cells. Additionally, biocytin reconstruction revealed that these cells have medium size cell bodies that contribute varicose axonal collaterals and varicose dendritic processes. It was also determined in this same study that there were at least 3,000 of these cells per mouse striatal hemisphere. This estimate however was based on non-lesioned mice. In Parkinsonian states, such as following 6-OHDA-induced degeneration of the nigrostriatal pathway, the number of THINs markedly increases. This increase is again not owed to neurogenesis but to an upregulation of TH. EGFP-TH mice that are non-lesioned underestimate the number of THINs, since the transcriptional activity of TH in EGFP-TH mice is low compared to the Parkinsonian state. In subsequent studies where unilateral lesions of the midbrain were made in EGFP-TH mice, the estimates of striatal THINs becomes as high as 4,500, indicating that THINs represent a significantly higher number than previously reported in the Ibañez-Sandoval et al. study.

Electrophysiologically, these diverse interneuronal subtypes, designated Type I-IV TH interneurons or THINs, are well integrated into the striatal microcircuitry, receiving cortical input and forming GABAergic synapses onto SPNs. Cortical and local electric stimulation elicited an EPSP-IPSP sequence in

THINs. The EPSP was abolished by bath application of DNQX, where the residual IPSP was blocked by bicuculline, thus demonstrating that it is GABA_A-mediated (Ibanez-Sandoval et al., 2010).

Moreover, Type I and Type III striatal THINs make highly reliable GABAergic inputs onto SPNs (100% probability that a presynaptic spike will generate a post-synaptic IPSP/IPSC). Type II cells also make GABAergic synapses onto SPNs but have a lower release probability ($\approx 40\%$) and exhibit short-term depression. Type III cells elicit a sufficiently strong IPSP to delay induced spiking in MSN cells.

Lastly, Ibañez-Sandoval et al. (2010) reported THINs have a large dendritic arbor ($\approx 200 \mu\text{m}$) and axonal field ($\approx 300 \mu\text{m}$). A typical Type I THIN, for example, has around 5 primary aspiny dendrites, which will become invested with numerous spines approximately $20 \mu\text{m}$ from the soma as higher order dendrites begin to branch (see Figure 18C for a sense of the widespread arborization of THIN processes). The morphology of these cells is such to suggest a widespread connectivity, further impressing their well-established integration into the striatal microcircuitry playing a local inhibitory role, where most likely their distinct subtypes are functionally diverse.

Subtype specific electrophysiology of THINs

In terms of their subtype distribution, Type I THINs are the most frequently encountered, accounting for roughly 75-80% of the population, followed by IV THINs (Unal et al., 2013). Type II and Type III THINs comprise a small minority of THINs.

Type I THINs have a very high input resistance ($\approx 700 \text{ M}\Omega$). Like cholinergic interneurons, these cells are spontaneously active *in vitro*. A further characteristic feature is their inability to fire continuously during strong depolarizations. Instead, they exhibit a depolarization-block-like state and an intrinsically driven prolonged plateau potential (see Figure 29), which is dependent upon a nimodipine sensitive L-type Ca^{2+} channel conductance and the non-selective cationic conductance, I_{CAN} . During this plateau potential, they generated subthreshold membrane potential oscillations over a broad spectrum of frequencies and amplitudes (Fig. 29B). Type I THINs also exhibit a time-dependent sag during hyperpolarizing current injections, which is due to activation of I_h . Finally, Type I interneurons also frequently generate rebound bursting at the offset of a hyperpolarizing current injection, especially if held at depolarized potentials.

Similarly to Type I THINs, Type II THINs are spontaneously active, have a lower mean input resistance ($\approx 400 \text{ M}\Omega$), do not exhibit depolarization-block, and can sustain a mean maximal firing rate of $\approx 200 \text{ Hz}$. Compared to Type I THINs, a lower proportion of Type II THINs exhibit plateau potentials ($\sim 25\%$ of the time). In addition, like Type I THINs, Type II THINs also exhibit a similar sag response to hyperpolarizing current injection mediated by I_h .

Type III THINs have the most negative resting potential of all the THINs (-89 mV) and the lowest mean input resistance ($\approx 180 \text{ M}\Omega$), owed to a strong inward rectification activated at membrane potentials below -80 mV (Ibanez-Sandoval et al., 2010). Similarly to Type I THINs, Type III THINs cannot fire in a sustained manner during strong depolarization and exhibit nimodipine sensitive plateau potentials that proved to be nimodipine sensitive as well.

Lastly, Type IV THINs had a similar mean input resistance and range as that of Type I THINs, $471 \pm 8 \text{ M}\Omega$ (235 – 831 $\text{M}\Omega$). Similar to Type I and Type II interneurons, Type IV THINs also exhibited a HCN-dependent sag. Their striking characteristic, however, is their presentation of a low-threshold spike (LTS), which was typically followed by a short barrage of action potentials at frequency of $\approx 300 \text{ Hz}$. These LTS spikes could be either elicited from rest in response to depolarization or at the offset of negative current pulses.

Striatal THINs distribution obey a striosome-matrix-based cytoarchitecture

In terms of their neuroanatomical organization, THINs exhibit no gross distinguishing organization along the dorsal-ventral axis and appear to be sparsely distributed throughout the striatum in general (Unal et al., 2011). There is, however, an underlying subtle organization of THINs that speaks to a possible role in regulating information exchange between the striosomal and matrix compartments of the striatum.

Aside from a dorsal-ventral division, the striatum is also divided in patches (or striosomes) and matrix regions that are distinct neurochemically and in terms of connectivity (Graybiel et al., 1981; Graybiel et al., 1987; Gerfen et al., 1990; Gerfen, 1992). In the striosomes, there is marked immunoreactivity for substance P, enkephalin, μ -opioid receptor (MOR) (Mikula et al., 2009), and limbic associated membrane protein (Graybiel et al., 1981; Gerfen et al., 1985; Bolam et al., 1988; Holt et al., 1997). In comparison, the matrix exhibits high immunoreactivity for acetylcholinesterase and calbindin. In terms of cytoarchitectural organization, the dendritic and axonal arborizations of SPNs

respect the striosome-matrix boundaries. In contrast, GABAergic and cholinergic interneuronal processes do not obey such boundary divisions (Chesselet and Graybiel, 1986; Kawaguchi, 1992). More specifically, the somata of both cholinergic and NPY interneurons reside between the striosome-matrix boundaries (Kubota and Kawaguchi, 1993; Martone et al., 1994; Saka et al., 2002). Such an striosome-matrix organizational principle is also true for EGFP-TH interneurons (Unal et al., 2011).

While there is no overall difference in the distribution of THIN interneuronal subtypes along the dorsal-ventral axis, an interesting separation of where EGFP-THINs are chiefly distributed in terms of the matrix versus striosome does exist along the dorsal-ventral axis. In the dorsal striatum, THINs were preferentially situated in the matrix regions. In contrast, in the ventral striatum, THINs were mostly found in the μ -opioid receptor regions of the striosomes. Unal et al. (2011) argue that this difference suggests that THINs process information differently in the dorsal and ventral striatum in terms of striosome-matrix boundaries, similarly to how cholinergic and NPY interneurons differentially process information between such compartments, where neurites cross patch-matrix boundaries (Kawaguchi, 1992; Kubota and Kawaguchi, 1993). In particular, Type IV THINs (20%) were situated on the patch-matrix boundary, and Type I THINs (80%) were within DA-rich islands of the patch (Unal et al., 2011). Additionally, Unal et al. (2011) found that the neurites of both subtypes cross the patch-matrix compartments. Interestingly, in a more recent study by Ibañez-Sandoval et al. (2014, in revision), Type I THINs are found to potently respond to DA, which elicits long-lasting plateau potentials and an accompaniment of action potentials.

Neuromodulation of striatal THINs

The fact that during conditions when nigrostriatal DA is depleted there is an upregulation of TH in striatal THINs and an accompanying increase in the number of TH+ somata in the striatum (Darmopil et al., 2008; Espadas et al., 2012; Unal et al., 2013), would suggest that striatal THINs can both sense and respond to changes in extracellular DA. For example, it was that following nigrostriatal depletion, THINs undergo morphological and electrophysiological changes, including increases in the density of proximal dendritic spines and an increase in the frequency of spontaneous EPSCs and IPSCs (Unal et al., 2013). Both DA and acetylcholine, the two major modulatory neurotransmitters of the striatum (Calabresi et al., 2000; Calabresi et al., 2007; Gerfen and Surmeier, 2011; Oldenburg and Ding, 2011; Ericsson et al., 2013b), are candidates for modulating the electrophysiological properties of striatal THINs.

Ibañez-Sandoval et al. (2014, in revision) studied the neuromodulatory effects of DA and ACh on plateau potentials (PP). It was found in this same study that both DA and ACh evoke long-lasting PPs in THINs. In the case of DA, this effect is D1/D5 receptor-mediated and often accompanied by firing on the PP. With ACh, Type I and Type IV THINs, generate spike bursts, followed by a prolonged PP, which is also often accompanied by spiking.

Striatal THINs: Are they DAergic?

As mentioned, until the late 1980's there was no indication of an intrinsic striatal source of DA. Dubach's 1987 publication, showed in monkeys that there were striatal interneurons immunoreactive for tyrosine hydroxylase (TH), the rate-limiting enzyme for catecholamine synthesis (Graybiel et al., 1987). It has

remained unclear however if the striatal THINs, a sizable population of the TH+ neurons, are indeed DAergic.

To date, what is best and clearly understood about THINs is their electrophysiology. The variety of striatal THIN subtype electrophysiology and their distribution in terms of a patch-matrix cytoarchitecture, strongly suggest THINs have segregated roles for processing information in either the patch or matrix along the dorsal-ventral axis. This complexity of both subtype electrophysiological diversity and THINs respecting a patch-matrix boundary are analogous to observations made decades earlier of a patch-matrix based compartmental organization of the striatum and its likely significance of processing cortical information (Bolam et al., 1988; Gerfen, 1992). Moreover, the fact that THINs make GABAergic synapses onto SPNs directly suggests that their function is to regulate striatal output.

Despite no direct evidence of THINs being DAergic, recent publications continue to present THINs as DAergic and compensating for a decrease in striatal dopamine (Espadas et al., 2012) or present THINs as releasing DA during action potential firing and modulating the striatal microcircuitry (Gittis and Kreitzer, 2012). To date, however, no selective targeting and activation of THINs has been done during simultaneous voltammetry to unambiguously determine if THINs release DA. Moreover, it is not known if THINs colocalize other DAergic markers, such as AADC, the enzyme required to convert L-DOPA made from TH into DA (Lopez-Real et al., 2003; Shen et al., 2003; Ugrumov et al., 2004). As mentioned previously, the literature regarding colocalization studies has been contradictory and no systematic method to look for colocalization of TH with other markers has been undertaken.

Moreover, it is important to define precisely the term “dopaminergic.” The use of the term in the literature has been made in the immunocytochemical sense of markers indicative of a cell containing dopamine. The “ergic” suffix, however, has an additional and important meaning that speaks to the defining criteria that establishes a substance as a neurotransmitter. Among other criteria, this includes that the substance must be present in the presynaptic neuron and released in a Ca^{2+} -mediated manner in response to synaptic depolarization. Even if a cell contains the full repertoire of the traditional neurochemical markers found in midbrain DAergic neurons, THINs would not be DAergic unless they release DA.

This thesis addresses these unresolved issues and is chiefly concerned with determining whether striatal THINs are DAergic. A careful immunocytochemical colocalization study of EGFP-TH with AADC, VMAT2, and DAT were made to determine if these traditional DAergic markers colocalize with striatal THINs. More importantly, an immunofluorescent protocol that successfully labels DA itself in the dopaminergic neurons of the midbrain has been used to directly test if indeed THINs colocalize dopamine. For these series of colocalization experiments, an EGFP-TH mouse line was used and combined with immunofluorescence to test for EGFP-TH colocalization with DA, AADC, VMAT2, or DAT.

Some EGFP-TH mice used in these experiments were unilaterally lesioned with 6-hydroxydopamine (6-OHDA), a compound highly effective in producing a neurotoxic lesion of the nigrostriatal pathway and frequently used in mouse models of Parkinson’s disease (Stott and Barker, 2013). As mentioned, there has been near universal reporting of striatal TH⁺ neurons

increasing in number following progressive loss of striatal dopamine, observed both in Parkinson's patients (Porritt et al., 2000; Porritt et al., 2006) and in models of Parkinson's disease (Betarbet et al., 1997; Meredith et al., 1999; Petroske et al., 2001; Mazloom and Smith, 2006). In particular, it has been reported that TH⁺ neurons become DAergic following depletion of nigrostriatal DA (Betarbet et al., 1997; Cossette et al., 2005). Having a control striatum with an intact nigrostriatal pathway and a striatum whose nigrostriatal pathway was degenerated by unilateral 6-OHDA of the midbrain thus allowed for testing whether THINs become DAergic during loss of DA.

In addition, TH-Cre mice were used in combination with optogenetics and voltammetry to determine if striatal THINs can release DA during optogenetic activation of THINs and simultaneous voltammetric recordings³. Using this same mouse line, SPNs were also patched while THINs were optogenetically activated. This was motivated by the original 2010 study by Ibañez-Sandoval, which was based on a limited number of paired recordings between THINs and SPNs. While this study showed that THINs made GABAergic synapses onto SPNs that could regulate timing of SPN firing, an outstanding question that remained was how widespread and significant as a population the inhibitory synapses of THINs onto SPNs were. Lastly, the SMOs of THINs were studied to test if their dynamics are modulated by DA and what ions contribute to the oscillations.

³ See Methods section for a description of how THINs were selectively targeted and activated using Cre-dependent virus.

CHAPTER II

METHODS

Subjects

Striatal TH interneurons (THINs) were studied using a mouse BAC transgenic TH-Cre [Tg(TH-Cre)12Gsat; Gene Expression Nervous System Atlas] and Tg(Th-EGFP)1Gsat/MNmc transgenic mice, simply referred hereafter as TH-cre and EGFP-TH mice, respectively. All EGFP-TH mice were initially acquired from the Mutant Mouse Regional Resource Center at UCLA, derived from GENSAT (<http://www.mmrrc.org/strains/292/0292.html>). Mice were bred at our AAALAC-accredited animal colony and genotyped from tail samples. All surgical procedures were performed in accordance with the National Institutes of Health Guide to the Care and Use of Laboratory Animals and with the approval of the Rutgers University Institutional Animal Care and Use Committee.

Optogenetics

The microbial-type rhodopsins, or photosensitive G-protein-coupled receptors originated from the Archae, Bacteria, and Eukarya. Some of these rhodopsins have evolved into membrane ion transport proteins (Power and Sah, 2008). One of these proteins is a light-gated cation channel found in the green algae *Chlamydomonas reinhardtii* called channelrhodopsin-2 (ChR2), which generates photocurrents in response to exposure to light over a select spectrum (Fenno et al., 2011) and can be used to activate diverse types of mammalian neurons (Power and Sah, 2008; Deisseroth et al., 2009). This method of expressing ChR2 into neurons is called optogenetics (Knopfel et al., 2010; Liu and Tonegawa, 2010; Deisseroth, 2011; Fenno et al., 2011) and has

matured tremendously in recent years (Han, 2012). Optogenetics has revolutionized neuroscience research, allowing detailed analyses of the underlying neural circuitry of the brain (Zhang et al., 2010; Kravitz and Kreitzer, 2011; Yizhar et al., 2011). It has allowed for understanding changes of the neural circuitry in diseased states such as Parkinson's disease (Gradinaru et al., 2009), mapping excitatory inputs (Stuber et al., 2011), and even manipulating diseased conditions such as schizophrenia (Peled, 2011) or Parkinson's disease (Kravitz et al., 2010). The true power of optogenetics lies in its ability to selectively target specific cell-types of interest. This is accomplished by combining a cre recombinase-dependent viral vector (Gradinaru et al., 2010) with cre-expressing transgenic rodent lines (Gong et al., 2007) to transfer and express the gene encoding ChR2 in specific cell-types.

Viral mediated gene transfer

Cre-based optogenetic tools and methods were initially developed by Karl Deisseroth (Deisseroth et al., 2006; Zhang et al., 2006; Gradinaru et al., 2007; Gradinaru et al., 2009) and adopted by our lab (Tecuapetla et al., 2010; English et al., 2012) to express ChR2 in either mesencephalic TH+ dopaminergic neurons or in striatal THINs. Transduction of the opsin gene encoding ChR2 fused to the enhanced yellow fluorescent protein (EYFP) was achieved via the cre-dependent adeno-associated virus AAV5-EF1a-DIO-hChR2(H134R)-EYFP (University of North Carolina, Vector Core Services, Chapel Hill, NC), which from here on is simply referred to as AAV-ChR2-

EYFP. AAV5 was chosen for its relatively low seroprevalence and transduction efficiency (Sen et al., 2013). Other serotypes were observed to cause greater cytotoxicity in THINs of TH-Cre mice. A pair of incompatible loxP recombination sites oriented in an inverted open reading frame flanks the ChR2-EYFP fusion gene. Upon Cre recombination, the fusion gene is properly oriented and translated into ChR2-EYFP. When this viral construct is injected into the striatum or midbrain of TH-Cre mice, cre recombination results in the selective expression of ChR2-EYFP in cells that normally express the TH gene.

Stereotaxic intracerebral viral and 6-hydroxydopamine injections

Mice were anesthetized with isoflurane and affixed to a stereotaxic frame. After subcutaneous administration of bupivacaine, the scalp was reflected. Small burr holes were drilled bilaterally over the striatum (AP: 0.5 mm from bregma, L: 1.85 mm from midline) for viral injections and over the midbrain (AP: -3.3 mm from bregma, L: 0.8 mm from the midline) for the injection of 6-OHDA. Injections were done within a Biosafety Level-2 (BSL-2) rated isolation cabinet using a Nanoject II Auto-Nanoliter Injector (Cat. No. 3-000-204, Drummond Scientific Company, Broomall, PA) mounted on a MP-285 micromanipulator (Sutter Instruments, Novato, California). Glass capillaries (Cat. No. 3-000-203-G/X, Drummond Scientific Company, Broomall, PA; (O.D.) 1.14 diameter, (ID = 0.53 mm) were pulled on a Narishige PE-2 glass microelectrode puller (Narishige International USA,

Inc., East Meadow, NY). Pipette tips were back cut to an O.D. of ~40–50 μ m. Virus was bilaterally injected at a rate of 23 nl/s at -2.25 mm (0.5 μ l) and -3.0 mm (0.83 μ l) from the surface of the brain. 6-OHDA was prepared in 0.9% NaCl and 0.2% ascorbic acid at a concentration of 3.6 mg/ml. 6-OHDA (0.8 μ l) of was injected into the midbrain unilaterally at a depth of 4.3 mm from cortical surface. After completion of each injection the pipette was kept in place for 10 minutes to prevent spread back along the pipette track and then gradually withdrawn. Injected animals were housed for a 7-10 day period under BSL-2 quarantine and experiments performed 14-21 days later.

Preparation of brain slices

Mice were deeply anesthetized with 150 mg/kg ketamine and 30 mg/kg xylazine i.p. and transcardially perfused with an ice cold modified Ringer's solution containing the following (in mM): 248 sucrose, 2.5 KCl, 7 MgCl₂, 23 NaHCO₃ 1.2 NaH₂PO₄, 7 glucose, 1 ascorbic acid, and 3 sodium pyruvate. The solution was bubbled before use with 95% O₂ and 5% CO₂. Brains were quickly removed, blocked and cut into 300 μ m coronal or parahorizontal slices on a Vibratome 3000. Slices were immediately transferred to a holding chamber containing normal Ringer's solution containing (in mM): 124 NaCl, 2.5 KCl, 1.2 NaH₂PO₄, 26 NaHCO₃, 1.3 MgCl₂, 2 CaCl₂, 10 glucose, 1 ascorbic acid, 3 pyruvate, 0.4 myo-inositol at ~33°C and continuously bubbled with 95% O₂ and 5% CO₂.

Imaging of slices

Slices were transferred into the recording chamber, perfused with the same modified Ringer's solution at $\sim 32\text{-}33^{\circ}\text{C}$. Using a high-sensitivity digital frame transfer camera (Cooke SensiCam, PCO-Tech, Inc., Romulus, Michigan) mounted on a BX-50WI Olympus fixed stage upright microscope, slices were initially examined under epifluorescence. For whole-cell recordings, ChR2-EYFP cells were identified and patching was then performed with infrared visualization using an oblique condenser, yielding a DIC-like image. Regions rich with fluorescent ChR2-EYFP somata and/or processes were selected for voltammetric recordings and the carbon fiber electrodes (CFE) were positioned within these regions under visual guidance.

In vitro electrophysiology

Whole-cell patch recording

Whole-cell recordings were obtained with a Multiclamp 700B amplifier (Molecular Devices) and an ITC-1600 digitizer (HEKA Instruments, Inc., Bellmore, NY). Data were acquired on a PowerMac G5 with Axograph (www.Axographx.com) at a digitization rate of 20 kHz. Micropipettes for patch-clamp recordings were made using thin-wall borosilicate pipettes with an outer diameter of 1.2 mm and 0.94 mm inner diameter (Cat. No. GC120T-7.5, Harvard Apparatus, Holliston, MA), and pulled on a Sutter P-97 micropipette puller (Sutter Instruments). Patch pipette resistances were typically 3 M Ω . Whole-cell current-clamp recordings were performed using

an internal solution containing the following (in mM): 130 K-gluconate, 10 NaCl, 2 MgCl₂, 10 HEPES, 3 Na₂-ATP, 0.3 GTP, 1 EGTA, 0.1 CaCl₂, and either 0.5% biocytin or 25 mM of Alexa Fluor 594 (Invitrogen, cat. no. A-10438), pH 7.3-7.4.

Subthreshold membrane oscillation induction

Subthreshold membrane oscillations (SMOs) were generated in striatal THINs of EGFP-TH mice via strong depolarizing current injection, done during whole cell patch recording in current mode. A sufficiently high current injection level was selected that assured persistence generation of SMOs in a strongly depolarized regime when a depolarization block-like state occurred (see Fig. 29B). SMOs were cropped from these regions to then be analyzed, as detailed below in the statistic section.

In vitro voltammetry

To determine whether striatal THINs can electrophysiologically release DA, in vitro fast-scan cyclic voltammetry (FSCV; (John and Jones, 2007)) was used during simultaneous optogenetic activation of striatal THINs in TH-Cre mice. This electroanalytical technique works by rapidly applying a cyclic changing potential over a carbon fiber electrode (CFE). DA is first oxidized during a positive ramping of the applied potential into dopamine-o-quinone, donating 2 electrons in the process (Fig. 2A). This oxidized form is then reduced back to DA during a negative

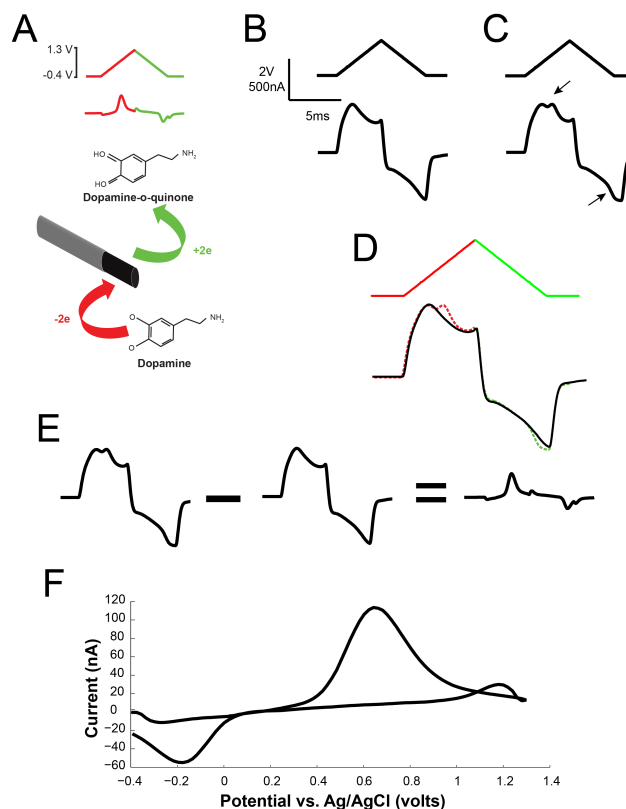


Figure 2. Fast scan cyclic voltammetry (FSCV). A. Schematic representation of a carbon-fiber micro electrode undergoing a cyclic applied voltage ramp from -0.4 V to 1.3 V and back to -0.4 V, in which dopamine is first oxidized during the anodic increasing voltage phase (red) to dopamine-o-quinone and then reduced back to dopamine during the cathodic decreasing voltage phase (green). B. In the absence of dopamine, an electrode generates a capacitive-resistant background profile during each cyclic scan, which is non-Faradaic and involves no current changes. C. In contrast, during the oxidation and reduction of dopamine, Faradaic currents are produced at the respective oxidative and reductive potentials (black arrows). D. Raw voltammetric overlapping data of the non-Faradaic profile (black trace) and Faradaic profiles (dashed red and green traces, respectively showing the oxidative and reductive generated currents). E. Background subtraction of the non-Faradaic profile from the Faradaic profile, producing a current versus applied potential trace. F. Standard cyclic voltammogram representation of trace in E.

rate of change in potential, and these oxidation and reduction events are detected by subtracting the non-Faradaic component of the CFE in the absence of DA from the CFE current profile vs. applied potential when oxidation and reduction on the CFE surface occur (Fig. 2 B-D). This subtraction then gives the so-called Faradaic changes of current vs. applied potential, owed to the oxidative and reductive current components (Fig. 2E). Traditionally, this profile is represented as depicted in Figure 2F, called a cyclic voltammogram.

An Ensmann EI-400 biopotentiostat (Cypress Systems, Inc., Lawrence, KS) was used for all voltammetric recordings. Scans were performed at 10 Hz over a potential range from -0.4 V to +1.3 V (vs. Ag/AgCl) at a rate of 400 V/s. Data were digitalized at 1000 points per scan and transferred to a PC via a NI PCI-6052E PC board (National Instruments, Austin, TX). Raw data were analyzed and processed for graphical output by custom programs written in MATLAB (www.mathworks.com). CFEs were constructed from borosilicate glass capillaries (cat. no. GC200-10, Harvard Apparatus, Holliston, MA) and 7-8 μm diameter carbon fiber (Goodfellow Corporation, PA) using standard techniques (Wiedemann et al., 1991; Millar and Pelling, 2001; Patel and Rice, 2006). Each CFE was fashioned by threading a carbon fiber into a glass capillary, which was then pulled on a Narishige PE-2 glass microelectrode puller (Narishige International USA, Inc., East Meadow, NY), forming a tight glass seal around the carbon fiber. The exposed fiber was cut 30-70 μm from the end of the glass seal with a scalpel mounted on a Narishige MX-1 micromanipulator (Narishige International USA, Inc., East Meadow, NY). The internal carbon fiber was connected to a thin caliber wire

with Woods metal (Goodfellow). DA was identified by its characteristic single oxidation and reduction peak potentials, at approximately 0.7 V and -0.3 V respectively (Wiedemann et al., 1991). The CFE was positioned under visual control with an MP-225 micromanipulator (Sutter Instruments, Novato, CA) and positioned $\sim 80\ \mu\text{m}$ beneath the surface of the slice. Electrical or optical stimuli were delivered every 30 seconds (see below for protocols). Extracellular concentrations of evoked DA ($[\text{DA}]_e$) were post-calibrated in the bath at 32-33°C with a 1 μM DA standard for both control and drug containing solutions. In addition, for some voltammetric experiments, L-DOPA treated TH-cre mice were used, following the same L-DOPA treatment protocol used for DA immunocytochemistry (see below).

Stimulation protocols

Electrical stimulation

Local electrical stimulation consisted of single 250 μA , 50 μs square wave current pulses delivered through a concentric bipolar tungsten metal microelectrode (Harvard Apparatus, Holliston, MA), generated by a SC-100 constant-current stimulus isolation unit controlled through the digitizer and acquisition software. The stimulating microelectrode was positioned 100 μm from the inserted tip of the CFE and at a depth of $\sim 50\text{-}80\ \mu\text{m}$ beneath the surface of the slice. Single stimuli were delivered every 30 seconds between 10 second FSCV recordings.

Optical stimulation

Neurons transduced with ChR2-EYFP were activated by single 2.5 ms pulses of blue light emitted by a 750 mW blue LED (www.cree.com) positioned just below the condenser with the iris and sector stops fully opened. Timing was controlled through the digitizer by the data acquisition software. In some experiments, epifluorescence illumination was delivered by a xenon lamp and passed through a filter to deliver blue light of wavelength 470 ± 20 nm (Chroma Technology Corp., Bellows Falls, VT). The duration of the epifluorescence stimulation was controlled with a Uniblitz shutter (Vincent Associates, Rochester, NY) controlled by the acquisition software through the digitizer. Light pulses were delivered every 30 seconds between 10 second FSCV recordings.

Biocytin histochemistry

Slices containing biocytin-filled neurons were transferred into a scintillation vial containing ~2 ml 4% PFA and microwave-fixed and left in the fixative overnight. Slices were then washed 3x in 0.1 M PBS and typically resectioned into 3-4 60 μ m thick sections. After washing 3x for 10 minutes in 0.1 M PBS, sections were then washed in 10% methanol and 3% H₂O₂ for 15 minutes, and incubated in avidin-biotin-peroxidase complex (1:200; Vector Labs) with 0.1% Triton-X overnight at 4°C. Sections were then washed 6x for ten minutes in 0.1 M PBS and then reacted with 0.025% 3,3'-diaminobenzidine (DAB) and 0.0008% H₂O₂. Typically, nickel intensification (Adams, 1981) was carried out with 2.5 mM nickel ammonium sulfate and 7

mM ammonium chloride during the DAB/H₂O₂ incubation. Sections were then post-fixed in osmium tetroxide (0.1% in PB) for 30 minutes and then dehydrated through an increasing series of ethanols. Lastly, sections were infiltrated overnight with a 50%/50% propylene oxide and epoxy resin mixture (Durcupan; Fluka) and then placed in a fresh 100% resin for several hours, and finally flat embedded between glass slides and coverslips and allowed to polymerize for 24 hours in an oven at 60°C.

Fluorescent immunocytochemistry

Immunocytochemistry for TH and DA

To assess the efficacy of 6-OHDA lesions, the midbrains and striata of TH-Cre mice used for in vitro studies were retained and kept in 4% paraformaldehyde (PFA) and 15% saturated picric acid (vol/vol) and later processed for TH immunoreactivity. 50-60 μ m coronal sections were cut in cold 0.15 M phosphate buffer solution (PBS) using a Vibratome 1500 (The Vibratome Company, St. Louis, MO). Sections were cleared in 10% methanol and 3% hydrogen peroxide in PBS. Blocking was done overnight at 4°C with 10% normal donkey serum (NDS) and 3% bovine serum albumin (BSA) with 0.5% Triton-X in PBS. Sections were then incubated in the same blocking solution at 4°C for 48 hours containing rabbit anti-TH IgG (1:1500; Millipore Corp., cat. no. AB152). Sections were then washed 3x in PBS and incubated overnight at 4°C in donkey anti-rabbit IgG conjugated to Alexa-594 (1:500; Invitrogen, cat. no. A-21207) in PBS. Sections were then washed 3x in PBS,

mounted on slides and coverslipped with Vectashield hardset mounting medium (Vector Labs, Burlingame, CA).

Slices that contained biocytin filled neurons were transferred into a scintillation tube containing ~ 2ml of 4% PFA and microwaved to ~ 60°C for 8-10 seconds and fixed overnight. Slices were washed in PBS, gel embedded, and re-sectioned on a vibratome into 60 μ m sections. The sections were then either immunocytochemically processed for TH as detailed above or histochemically processed for biocytin (see below).

The colocalization study for DA immunoreactivity was performed in EGFP-TH mice and used a modified glutaraldehyde-based immunocytochemistry protocol (McRae-Degueurce and Geffard, 1986) following L-DOPA treatment. To inhibit peripheral metabolism of L-DOPA, the aromatic l-amino acid decarboxylase (AADC) inhibitor benserazide (15 mg/kg, i.p.), was administered 30 minutes prior to L-DOPA injection (30 mg/kg, i.p.). Previous studies have shown that L-DOPA has a maximal effect on extracellular DA levels 60 minutes after i.p. administration (Zigmond et al., 1992; Miller and Abercrombie, 1999).

60 minutes after L-DOPA injection, heparin (4000 units/kg) was administered i.p. followed by ketamine/xylazine (160/30 mg/kg, i.p.). Mice were then transcardially perfused with 20 ml of ice cold buffer containing 0.1 M sodium cacodylate and 1% (w/v) sodium meta-bisulfate in ddH₂O (pH between 6.2 – 6.5), followed by 100 ml of fixative containing 5% glutaraldehyde, 1% sodium meta-bisulfate, and 0.1 M sodium cacodylate in ddH₂O (pH between 7.0 – 7.5). The brain was then removed and left in the same fixative for 15-30 minutes and then washed 3 times with a 0.05 M Tris

buffer solution containing 0.85% sodium meta-bisulfate (Tris-SMB) and sectioned at 50 μ m in the same solution with a vibratome. Sections were incubated in 0.1 M sodium borohydrate for 20 minutes. Blocking of non-specific antibody binding was done at room temperature for 2 hours with 5% NDS and 0.5% Triton-X solution in Tris-SMB solution. Sections were incubated for 16 hours in 4°C using a polyclonal rabbit antibody against DA (ABcam, cat. no. AB8888) at a 1:2000 dilution in Tris-SMB solution containing 0.1% Triton-X and 2% NDS. Sections were washed 3 times for 10 minutes with Tris-SMB and incubated for 6 hours in RT with donkey anti-rabbit secondary conjugated to Alexa-594 (1:200). Following 3x ten minute washes with Tris-SMB, sections were mounted on non-gelatin coated slides and coverslipped with Vectashield hardest anti-fade mounting medium and sealed with clear nail polish (VWR, cat. #: 100491-940) to prevent drying.

Immunocytochemistry for AADC

Heparin (4000 units/kg) was injected intraperitoneal (i.p.) into EGFP-TH mice, which were then anesthetized 5 minutes later by ketamine/xylazine (160/30 mg/kg, i.p.) The mice were then transcardially perfused with 20 ml of ice cold artificial CSF, followed by 100 ml of fixative containing 4% paraformaldehyde and 15% picric acid. The brains were then extracted and post-fixed overnight with again 4% paraformaldehyde and 15% picric acid and then washed 3x the next day for 10 minutes each time in 0.15 M phosphate buffer solution (PBS). The brains were then blocked and 50-60 mm coronal sections were cut in cold 0.15 M PBS using a Vibratome 1500 (The Vibratome Company, St. Louis, MO). Sections were collected in 6

well plates and cleared in 10% methanol and 3% hydrogen peroxide in PBS for 15-20 minutes. Blocking was done overnight at 4°C with 3% bovine serum albumin (BSA) and 10% normal donkey serum (NDS) with 0.5% Triton-X in PBS. The sections were then incubated with 1% BSA and 1% NDS plus 0.1% Triton-X solution containing 1:2000 primary rabbit anti-DOPA decarboxylase (AADC) IgG (ABcam #ab3905) in PBS for 1.5 days at room temperature. The sections were then washed 3x for ten minutes each time in PBS and incubated with 1:400 secondary donkey anti-rabbit IgG-Alexa 594 (Invitrogen, cat. no. A-21207) in PBS overnight at 4°C in the dark. Finally, sections were then washed 3x in PBS, mounted on slides and coverslipped with Vectashield hardset mounting medium (Vector Labs, Burlingame, CA) and sealed with clear nail polish (VWR, cat. #: 100491-940) to prevent drying.

Immunocytochemistry for VMAT2

EGFP-TH mice were anesthetized by ketamine/xylazine (160/30 mg/kg, i.p.) following a five-minute wait period after heparin (4000 unites/kg) was injected intraperitoneal (i.p.). The mice were then transcardially perfused with 20 ml of ice cold artificial CSF, followed by 100 ml of fixative containing 4% paraformaldehyde and 15% picric acid. Brains were extracted and post-fixed overnight with again 4% paraformaldehyde and 15% picric acid and then washed 3x the next day for 10 minutes each time in 0.15 M phosphate buffer solution (PBS). 50-60 mm coronal sections were cut in cold 0.15 M PBS using a Vibratome 1500 (The Vibratome Company, St. Louis, MO). Sections were once again collected in 6 well plates

and then treated with 1% sodium borohydrate in PBS for 15 minutes. The sections were then washed 3x PBS for ten minutes each wash. Sections were then treated with PBS containing 10% methanol plus 3% H₂O₂ (Sigma #216763) for 15 minutes and then washed in PBS for 3x ten minutes each wash cycle. Blocking was done overnight at 4°C with 3% bovine serum albumin (BSA) and 10% normal donkey serum (NDS) with 0.5% Triton-X in PBS. The sections were then incubated with 1:2000 primary rabbit anti-VMAT2 IgG (Immunostar, Inc. #20042) in PBS for 1.5 days at room temperature and then washed for 3x in PBS, ten minutes for each wash cycle. The sections were then incubated with 1:400 secondary donkey anti-rabbit IgG-Alexa 594 (Invitrogen, cat. no. A-21207) in PBS for 4-6 hours at room temperature in the dark and washed for a final time 4x in PBS, again ten minutes each wash cycle. Sections were finally mounted on plain (non-gelatin coated) slides and coverslipped with Vectashield HardSet mounting medium (Vector Labs, Burlingame, CA) and sealed with clear nail polish (VWR, cat. #: 100491-940) to prevent drying.

Immunocytochemistry for DAT

EGFP-TH mice were similarly anesthetized by ketamine/xylazine (160/30 mg/kg, i.p.) following a five-minute wait period after heparin (4000 unites/kg) was injected intraperitoneal (i.p.). The mice were then transcardially perfused with 20 ml of ice cold artificial CSF, followed by 100 ml of fixative containing 4% paraformaldehyde and 15% picric acid. Brains were extracted and post-fixed overnight with again 4% paraformaldehyde and 15% picric acid and then washed 3x the next day for 10 minutes each

time in 0.15 M phosphate buffer solution (PBS). 50-60 mm coronal sections were cut in cold 0.15 M PBS using a Vibratome 1500 (The Vibratome Company, St. Louis, MO). Sections were once again collected in 6 well plates and then treated with 1% sodium borohydrate in PBS for 15-20 minutes. The sections were then washed in PBS containing 10% methanol plus 3% H₂O₂ (Sigma #216763) for 15-20 minutes and then washed in PBS for 3x ten minutes each wash cycle. Blocking was done overnight at 4°C with 3% bovine serum albumin (BSA) and 10% normal donkey serum (NDS) with 0.5% Triton-X in PBS. The sections were then incubated with 1:1000 primary rat anti-DAT IgG (Chemicon MAB369) in PBS for 1.5 days at room temperature and then washed for 3x in PBS, ten minutes for each wash cycle. The sections were then incubated with 1:400 secondary donkey anti-rat IgG-Alexa 594 (Invitrogen, cat. no. A-21207) in PBS for 4-6 hours at room temperature in the dark and washed for a final time 3x in PBS, again ten minutes each wash cycle. Sections were finally mounted on plain (non-gelatin coated) slides and coverslipped with Vectashield HardSet mounting medium (Vector Labs, Burlingame, CA) and sealed with clear nail polish (VWR, cat. #: 100491-940) to prevent drying.

Statistical analysis and graphical representations

Numerical values for evoked [DA]_e or inhibitory postsynaptic currents (IPSCs) were reported as the mean ± SEM. Significance differences between group data were determined by either two-sample t-tests or one-way ANOVA followed by Bonferroni's post hoc tests. Differences were

considered to be significant if p-values were less than 0.05.

All heat maps and other graphical representations were created using either custom programs written by me in MATLAB (www.mathworks.com) or using the graphical statistics package OriginLab (www.originlab.com).

Significant differences in changes of oscillatory power for the cropped segments of subthreshold membrane oscillations (SMOs) were analyzed by custom software written in MATLAB, using both fast-Fourier transform (FFT) and Lomb-Scargle analysis (Lomb, 1976; Scargle, 1982; Ruf, 1999). As further discussed in the results section, to maintain a consistent definition of the frequency domains corresponding to the “theta,” “beta,” and “gamma” frequency bands, the following frequency range conventions were adopted: 5-10 Hz for theta (DeCoteau et al., 2007; Hawes et al., 2013), 10-30 Hz for beta (Bibbig et al., 2001; Hammond et al., 2007; Leventhal et al., 2012), 30-70 Hz for “low” gamma, and 70 Hz and above for “high gamma” (Bibbig et al., 2001; Berke et al., 2009; Leventhal et al., 2012).

CHAPTER III

RESULTS

Immunofluorescent characterization of striatal THINs

Other than reports of TH immunoreactivity in striatal cells, inconsistent findings were obtained with other DAergic markers such as aromatic L-amino acid decarboxylase (AADC) or the dopamine transporter (DAT). For instance, it was reported that in rats there are striatal neurons immunoreactive for AADC (Tashiro et al., 1989a; Mura et al., 1995; Meredith et al., 1999; Mura et al., 2000). Mura et al. (1995) further reported that it appeared striatal neurons were able to synthesize DA from exogenously applied L-DOPA. It was however also reported in this study that none of these cells appeared to be immunoreactive for TH. In addition, Meredith et al. (1999) also reported the immunoreactive presence of DA in striatal neurons, suggesting that at least some striatal cells are DAergic. There was however no study done to show if these cells co-expressed TH. Still more, there were reports of DAT expression in striatal neurons in primates (Betarbet et al., 1997; Cossette et al., 2005; Tande et al., 2006), further suggesting the existence of DAergic cells in the striatum.

To date, however, there has been no systemized study to investigate if TH colocalizes with DA in striatal THINs. The question if any of the striatal cells reported immunoreactive for either AADC or DA are also expressing TH still remains an open question, and more importantly if any of these reported cells correspond with those previously characterized by our lab and unambiguously determined to be striatal interneurons. To therefore test if striatal THINs contain AADC, DA, and DAT and colocalize with TH in striatal THINs, immunofluorescent cytochemistry was performed for these respective DAergic markers in the striatum of EGFP-TH mice.

DA immunofluorescence

Characterization of DA in the midbrains of unilaterally lesioned EGFP-TH mice

As a positive control for the specificity and efficacy of the DA antigen used, fluorescent immunocytochemistry was first performed on the unilaterally lesioned midbrains of EGFP-TH mice ($n = 3$).

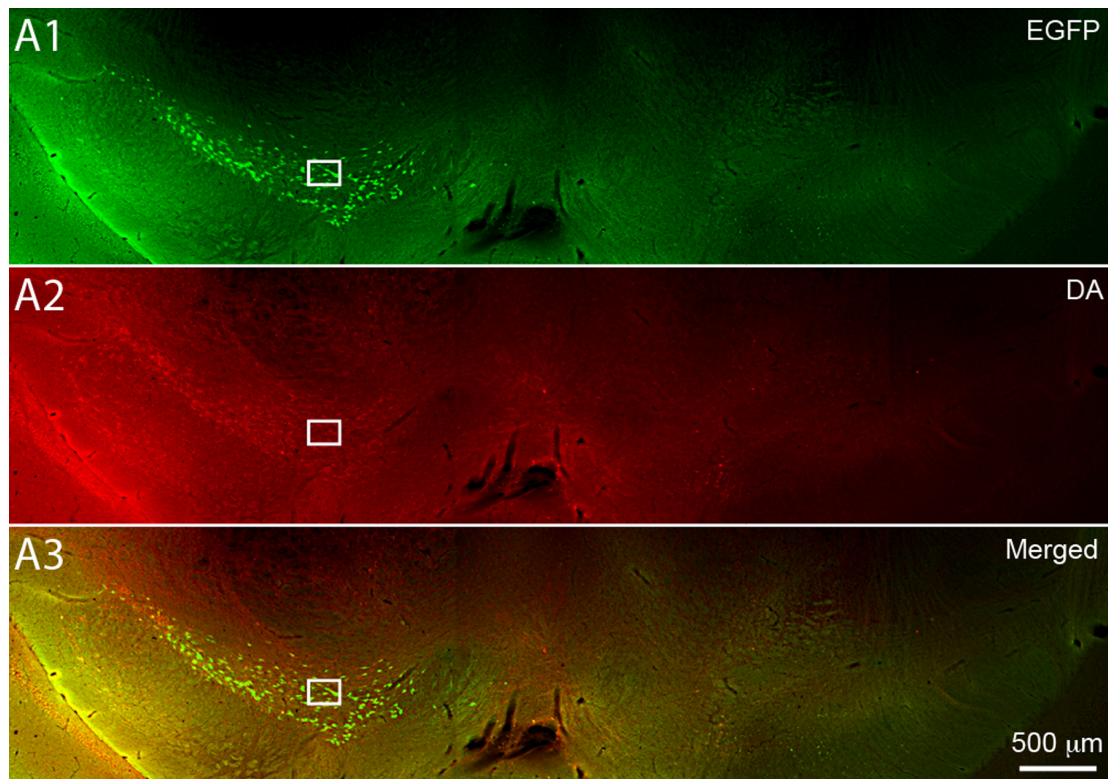


Figure 3. DA immunofluorescence of the midbrain of unilaterally 6-OHDA lesioned EGFP-TH mice. A. Coronal section of the midbrain section of a unilateral 6-OHDA lesioned EGFP-TH mouse, showing absence of EGFP-TH fluorescence on the 6-OHDA treated side but a complete preservation of EGFP-TH somata, as well as axonal and dendritic fibers on the contralateral side. B. Similarly, there is no expression of DA immunofluorescence on the 6-OHDA treated side, but ample DA immunofluorescence again on the contralateral side. C. Merged image of EGFP fluorescence and DA immunofluorescence shows abundant colocalization of EGFP with DA.

The rationale for the unilateral lesioning was based on the reported observations of an increase of TH expression in striatal cells following lesioning (Tashiro et al., 1989a; Betarbet et al., 1997; Meredith et al., 1999; Mao et al., 2001; Petroske et al., 2001; Palfi et al., 2002; Jollivet et al., 2004; Mazloom and Smith, 2006; Tande et al., 2006; Darmopil et al., 2008). After a two week post-injection wait period following 6-OHDA unilateral lesioning of the midbrains, the substantia nigra (SNc)/ventral tegmental area (VTA) regions were examined for colocalization of DA with EGFP-TH.

There was a complete absence of EGFP-TH+ cells on the side of the lesioning, as shown in Figure 3 (right side). In contrast, there was abundant expression of EGFP-TH+ cells in the SNc/VTA on the non-lesioned side (Fig. 3, left), revealing the restriction of the 6-OHDA midbrain lesioning was to only one side.

In addition, examination for DA fluorescent immunocytochemistry revealed ample DA+ expression throughout the SNc/VTA region (Fig. 3, left). There was no immunofluorescence for DA on the lesioned side. Moreover, at

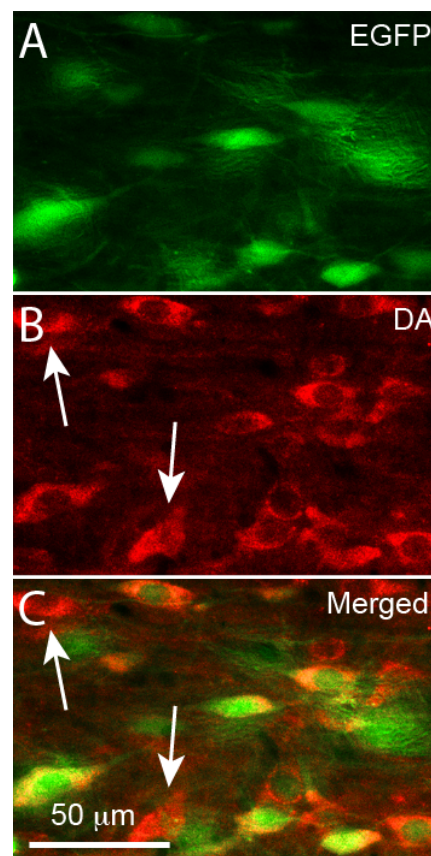


Figure 4. High magnification of corresponding box regions in Figure 1. A. High magnified view of EGFP-TH soma, reveals densely packed somata and their associated axonal and dendritic processes. B. Similarly, DA immunofluorescence reveals likewise densely packed somata, as well as labeling of their associated axonal and dendritic processes. C. While there was abundant overlap of EGFP fluorescence with DA immunofluorescence, some cells expressed one but not the other marker. For example, some cells immunofluorescent for DA did not colocalize with EGFP (white arrows).

higher magnification of the boxed regions in Figure 3, there was robust expression of EGFP-TH⁺ and DA⁺ in dense packed soma, as well as axonal and dendritic processes, as seen in Figure 4. There was also considerable colocalization of EGFP fluorescence and DA immunofluorescence, but there were also a few somata that fluorescently expressed one or the other DAergic markers (Fig. 4, arrows). This demonstrates that the 6-OHDA unilateral midbrain lesions performed preserved the contralateral midbrain and that the DA antigen used for this immunofluorescent study worked and that in EGFP-TH mice, there is colocalization of EGFP with DA.

Characterization of DA in the striatum of unilaterally lesioned EGFP-TH mice

The striata of the same mice whose midbrains were unilaterally lesioned with 6-OHDA, colocalization for EGFP fluorescence and DA immunofluorescence were next examined (n = 3). First examining for DA immunofluorescence and then switching the filters settings to check for any EGFP fluorescence in each field examined, a systematic 20x magnification grid-by-grid search for such colocalization was performed. In neither the contralateral nor ipsilateral side, where presumably there is a compensating expression of DA following DA depletion, no EGFP⁺ fluorescent somata were found colocalizing with DA. In keeping with previous reports of increased expression of TH in striatal neurons following DA depletion, there was a small increase in the detectable number of EGFP-TH⁺ interneurons compared to the contralateral side. This increase was noted in both the dorsal (Figure 5) and ventral (Figure 6) striata and was previously reported by our lab (Unal et al., 2013) and owed to an upregulation of TH and not an induced neurogenesis

(Tande et al., 2006). There was also a decrease in the background fluorescence in the ipsilateral side compared to the contralateral side, which is a reflection of the loss of nigrostriatal fibers.

In addition, putative DAergic afferents surrounding the perisomatic regions of THINs were observed in the control side, but only infrequently and weakly in the lesioned side, a further reflection of the effective nigrostriatal lesion (cf. the high-magnification photomicrographs of A and B for DA Immunofluorescence, separately within each of Fig. 5 and Fig. 6).

Lastly, in three additional unilaterally lesioned mice, L-DOPA was administered prior to sacrifice, as described in the methods section. As L-DOPA is directly converted to DA via AADC, pretreatment of L-DOPA was done to maximize any intrinsic capacity of striatal THINs to manufacture DA. Despite this L-DOPA pre-treatment, no DA expression was evident on either side of the unilaterally 6-OHDA lesioned EGFP-TH mice examined (not shown).

Although none of the striatal EGFP-TH neurons examined evidenced immunofluorescence for DA, there were, however, a very few number of small-sized, faintly DA⁺ immunofluorescent somata encountered. While no stereological count or detailed study of them was made, they typically averaged ~3-8 cells per 60 μ m thick section, and were of similar size (~6-8 μ m) and morphology indicative of the ones reported by Meredith et al., and moreover were similarly located along the subcallosal region of the dorsal and medial striatum as also similarly observed by Meredith et al. (data not shown). Compared to the striatal THINs, these cells were not EGFP⁺ however and were neuroanatomically very confined, had smaller soma, no evident dendritic

branching, and accounted for no more than 20 cells per entire mouse hemisphere, which typically laid within 2-4 consecutive 60 μm thick sections.

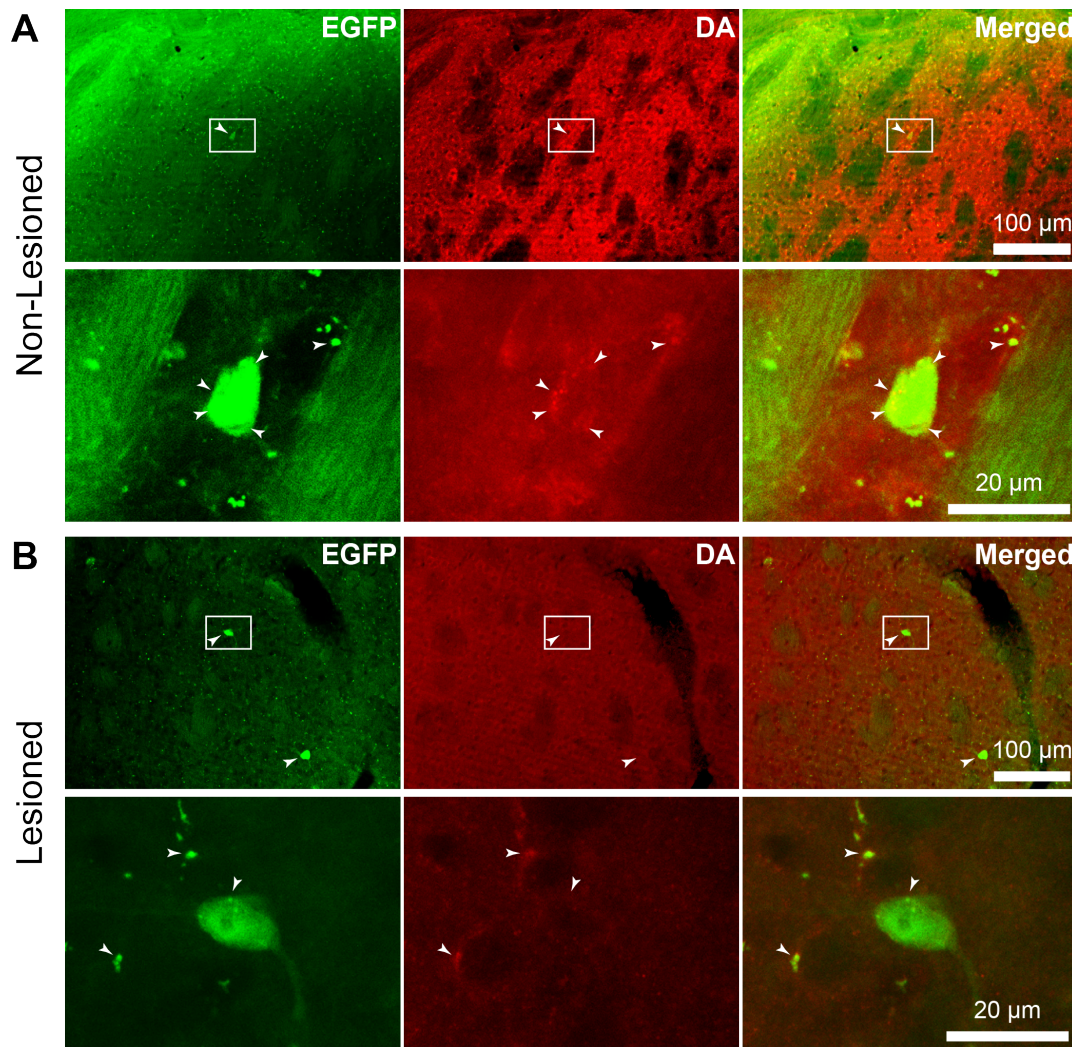


Figure 5. Photomicrographs of coronal sections of the *dorsal* striatum of a representative EGFP-TH mouse processed for DA immunofluorescence after unilateral 6-OHDA lesioning of the midbrain. A. Control side, showing an EGFP-TH+ striatal cell, which does not colocalize with DA immunofluorescence. *Bottom row*: higher magnified view of corresponding boxed regions in top row. Note the DA+ puncta surrounding the perisoma (white arrows). B. Lesioned side, showing no change in typical morphology but slight increase in EGFP-TH striatal interneuron numbers and no expression of DA with EGFP. Note the slight decrease in DA immunofluorescence, indicative of the destruction of nigrostriatal fibers following 6-OHDA treatment. No somatic colocalization of DA with EGFP was seen in any of the sections examined ($n = 3$ brains), but compare the DA immunofluorescent puncta surrounding the perisomatic territory of the THIN in the control side with the much weaker seen and less numerous puncta for the THIN in the lesioned side.

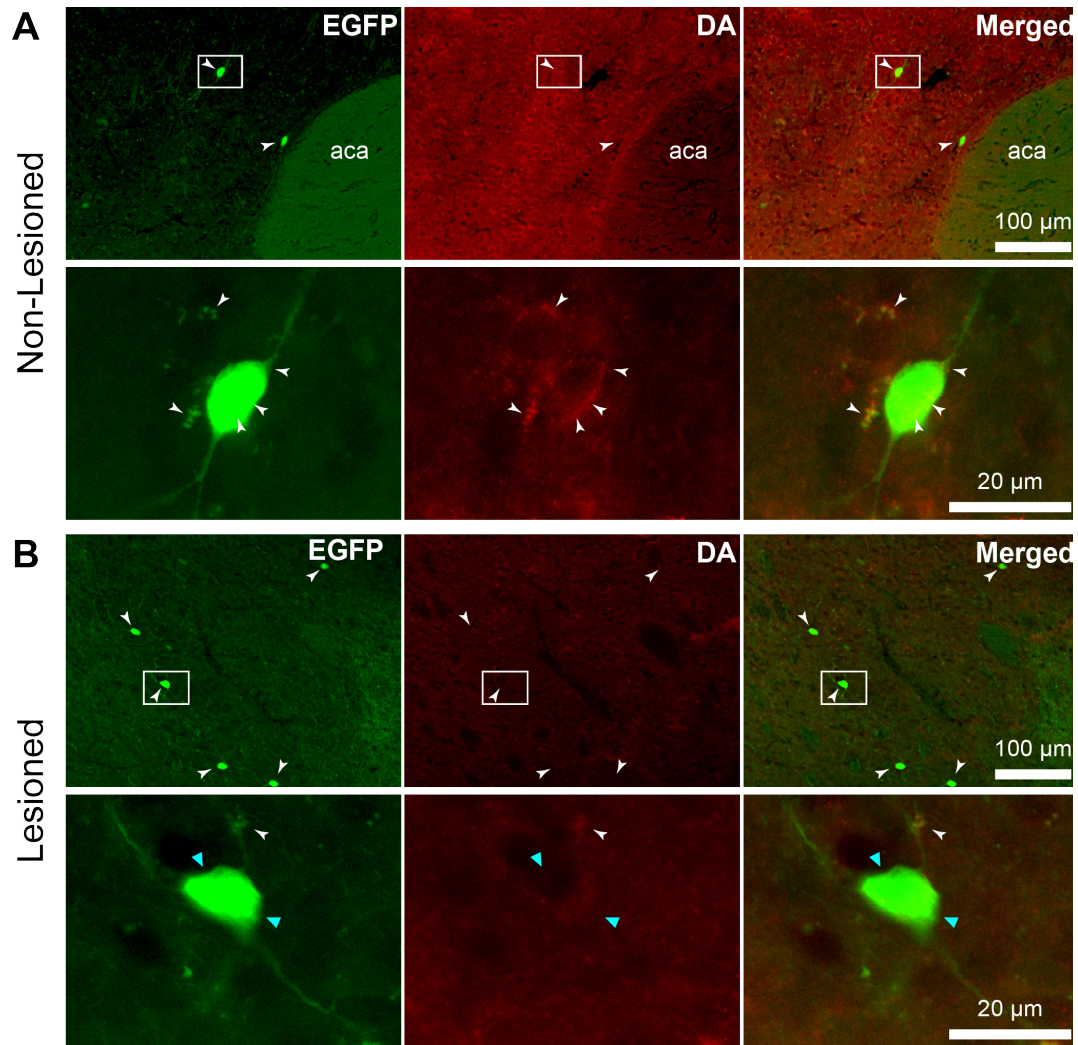


Figure 6. Photomicrographs of coronal sections of the *ventral* striatum of a representative EGFP-TH mouse processed for DA immunofluorescence after unilateral 6-OHDA lesioning of the midbrain. A. Control side, showing an EGFP-TH+ striatal cell, which does not colocalize with DA immunofluorescence. *Bottom row*: higher magnified view of corresponding boxed regions in top row. B. Lesioned side, showing no change in typical morphology but again as with the dorsal striatum, there was a slight increase in EGFP-TH striatal interneuron numbers and again no expression of DA with EGFP. Note again the slight decrease in DA immunofluorescence, indicative of the destruction of nigrostriatal fibers following 6-OHDA treatment. No somatic colocalization of DA with EGFP was seen in any of the sections examined ($n = 3$ brains), but note the DA immunofluorescent puncta surrounding the perisomatic territory of the THIN in the control side (white arrows), which is absent for the THIN in the lesioned side. *Cyan triangles* mark the outer edge of the THIN in the lesioned side.

AADC immunofluorescence

Control characterization of AADC in the midbrains of EGFP-TH mice

Although the lack of DA expression in striatal EGFP-TH interneurons, even after L-DOPA pretreatment, would suggest the absence of AADC, the required enzyme that directly converts L-DOPA into DA, AADC was still directly examined in EGFP-TH mice. 3-4 month old adult EGFP-TH mice ($n = 3$) were sacrificed, perfused, and processed for immuno labeling for AADC, as outlined in the methods section.

As a control for the specificity and efficacy of the antibody used for AADC detection, the midbrains of EGFP-TH mice were first examined. As shown in Figure 7, there was ample expression and overlap for both EGFP fluorescence and AADC immunofluorescence, demonstrating that the antibody was efficient in detecting AADC and colocalized with TH+ neurons in EGFP-TH mice.

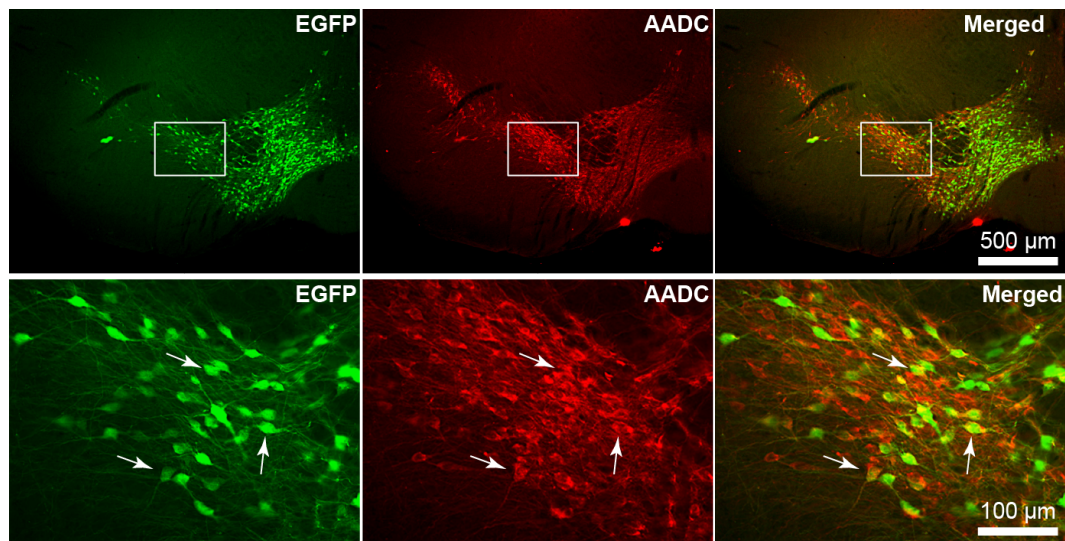


Figure 7. AADC immunofluorescence of the midbrain in EGFP-TH mice. A representative midbrain coronal section reveals densely packed somata of the SNc and VTA, as well as their associated axonal and dendritic fibers. The merged image of EGFP fluorescence and AADC immunofluorescence shows widespread colocalization of EGFP and AADC throughout the midbrain (white arrows). *Bottom row*: magnified view of box regions in the above row.

Characterization of AADC in the striatum of EGFP-TH mice

Next, the striata of the same mice processed for AADC in the midbrain were then inspected, specifically examining whether any EGFP-TH+ striatal interneurons co-expressed AADC. A systematic grid-by-grid search under 20x magnification was conducted under the filter setting for AADC immunofluorescence and then switched to the EGFP filter to determine if there was any colocalization with EGFP-TH+ striatal cells. In none of the cells examined were any striatal EGFP+ THINs found to colocalize AADC (n = 3 mice). Figure 8 shows high-magnified fluorescent photomicrographs of representative EGFP+ striatal THINs, which do not colocalize AADC. Despite the lack of AADC colocalization with EGFP+ THINs, there was abundant AADC+ immunofluorescent nigrostriatal fibers heavily innervating the surrounding area, demonstrating a high efficacy of the AADC antibody and that the likelihood of a false negative was very low (high magnified inset, Fig. 8A).

The EGFP+ fluorescent processes of the THINs are evident in both the non-lesioned and lesioned sides, as is the EGFP+ fluorescence from the accompanying intact nigrostriatal fibers. Only in the nigrostriatal fibers was there AADC expression colocalizing with EGFP. The detection of AADC in nigrostriatal fibers therefore gives a high confidence that the lack of AADC expression in striatal THINs was because of the absence of AADC in THINs and is in agreement with the lack of colocalization of DA and EGFP-TH in striatal THINs.

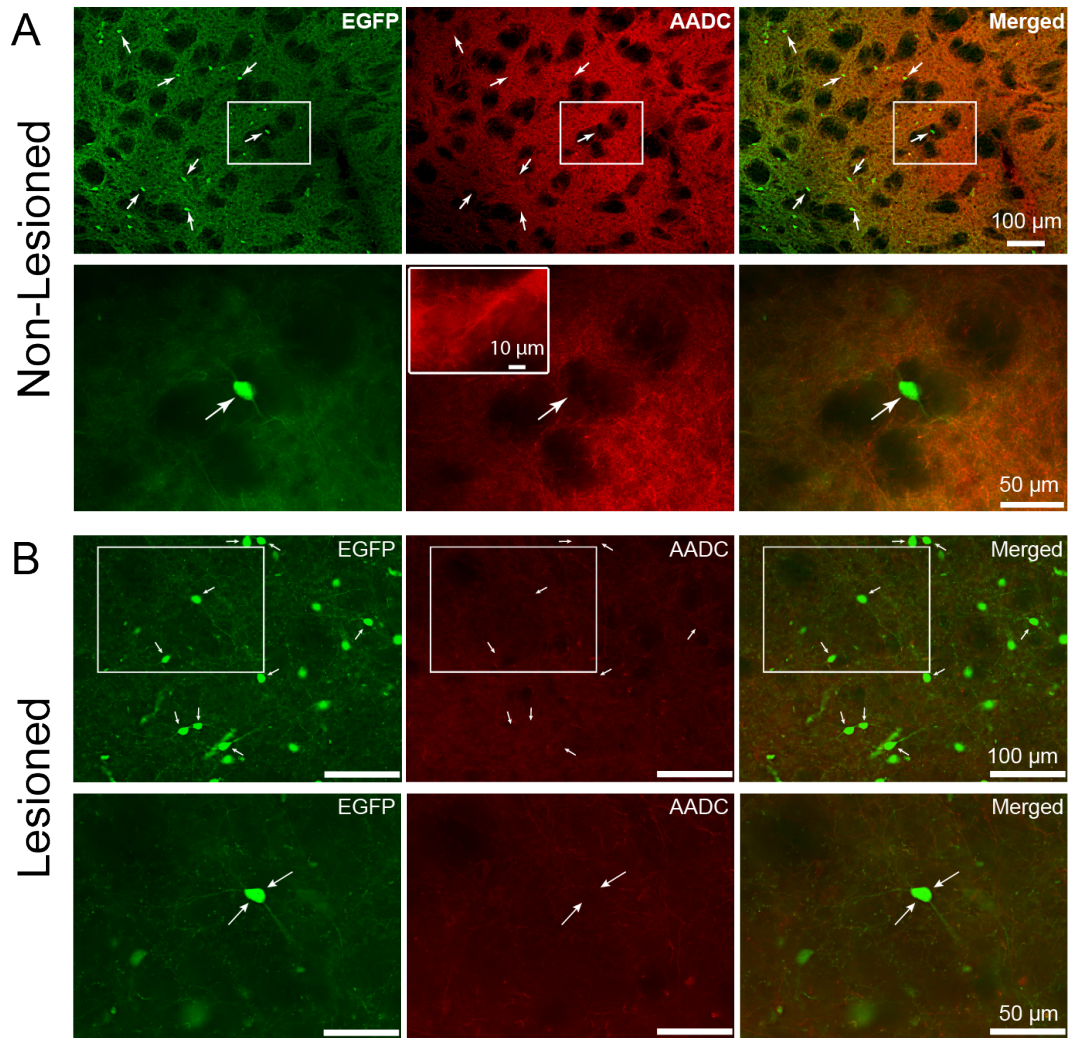


Figure 8. Photomicrographs of striatal coronal sections of the same representative EGFP-TH mouse in fig. 7. A. EGFP fluorescence of a striatal THIN with typical morphology shows dendritic and axonal processes from the striatal THIN as well as abundant axonal fibers from the intact nigrostriatal pathway. In contrast, there is no AADC immunofluorescence from the same neuron, even though there is extensive AADC labeling of nigrostriatal fibers (shown in high-magnified inset). The merged image of these respective fluorescent reporters reveals widespread colocalization of AADC and EGFP in nigrostriatal fibers but none for the EGFP+ soma. None of the striatal THINs examined evidenced colocalization with AADC ($n = 3$ mice).

There was however a very few number of AADC+ striatal cells that were found and of a clear differing morphology that were not indicative of striatal THINs, and which more importantly did not express EGFP fluorescence. Although no stereological analysis of them was made, they were roughly found to be of the same number and size ($\sim 6\text{-}8\ \mu\text{m}$) as the striatal DA+ fluorescent cells encountered and also similarly neuroanatomically confined to the subcallosal region of the dorsal medial striatum and indicative of the cells reported by Meredith et al. (1999).

Figure 9 shows two cells, one which is TH+ and has a similar size and morphology of a striatal THIN, and another non-EGFP+ but AADC+ immunofluorescent cell body, whose size and morphology are markedly different than a striatal THIN. Each cell does not express the complementary neurochemical marker of the other to complete DA synthesis alone. An average of 4 cells for each of the $n = 3$ EGFP-TH mice examined for AADC immunofluorescence were found to be AADC+ only expressing cells. All of them had a monopolar, unbranched morphology, which was markedly different

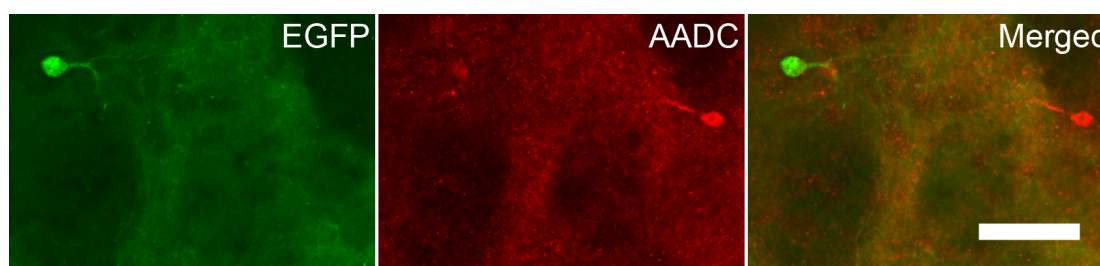


Figure 9. Mutually exclusive expression of EGFP-TH and AADC in the striatum of EGFP-TH mice. A representative example of two striatal cells, in which one was EGFP+ and the other AADC+, were each marker is mutually exclusively expressed in one another. The EGFP-TH+ cell has a morphology indicative of a striatal THIN, including a somatic width of $\sim 15\ \mu\text{m}$ and a prominent primary dendrite. In comparison, the AADC+ only cell has a smaller somatic size and morphology. The merged image of each separate fluorescent channel shows no overlap of expression. Scale bar, $50\ \mu\text{m}$.

compared to THINs, revealing them to be a separate class of striatal cell type than that of the striatal THINs.

VMAT2 immunofluorescence

Control characterization of VMAT2 in the midbrains of EGFP-TH mice

THINs were also examined to determine whether they express the vesicular monoamine transporter-2 (VMAT2). Unilaterally lesioned EGFP-TH mice were examined (n = 4). Immunofluorescence for VMAT2 was first performed in the midbrain as a positive control. Figure 10 reveals beautiful and abundant colocalization of VMAT2 with EGFP⁺ somata throughout the VTA of the midbrain in a representative coronal section, thus demonstrating the efficacy of the VMAT2 antibody employed.

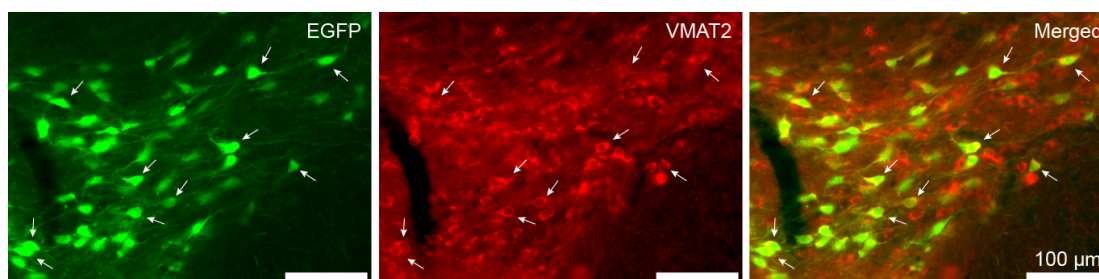


Figure 10. Photomicrograph of VMAT2 immunofluorescence in the midbrain of a representative EGFP-TH mouse. VMAT2 can be found abundantly colocalizing EGFP throughout the VTA (white arrows).

Characterization of VMAT2 in the striatum of EGFP-TH mice

Next, striatal THINs were examined for expression of VMAT2. EGFP-TH mice were once again used and had their midbrains unilaterally lesioned with 6-OHDA. Although there was abundant co-expression of VMAT2 with EGFP⁺

nigrostriatal fibers (Fig. 11A), no striatal THIN expressed VMAT2. VMAT2 expression was similarly not found in THINs in striata that had their nigrostriatal pathway degenerated (Fig. 11B).

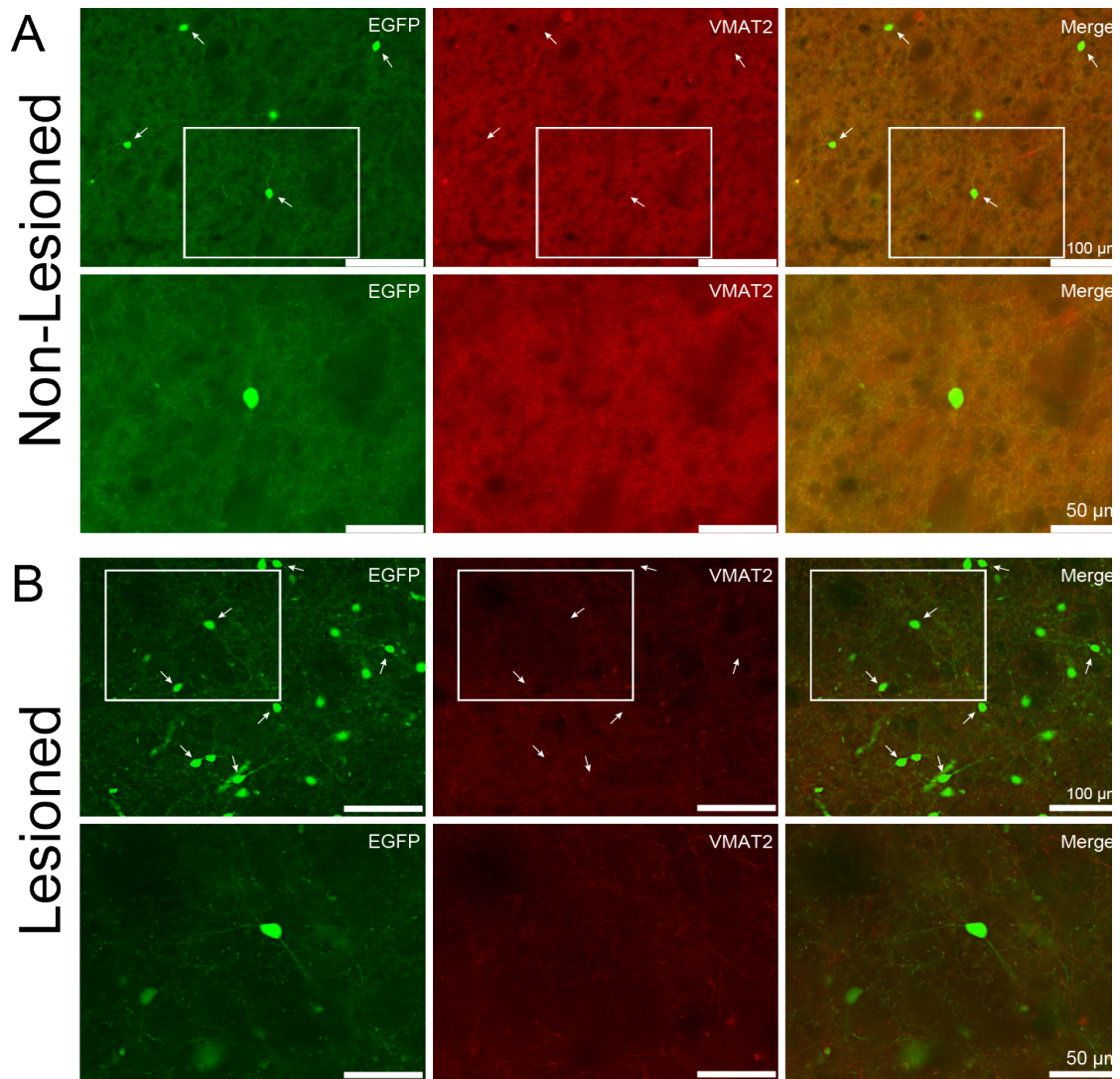


Figure 11. Immunofluorescent photomicrographs of striatal coronal sections of EGFP-TH mice examined for VMAT2. A. The non-lesioned striatum evidenced abundant VMAT2 staining, which colocalized with nigrostriatal fibers. No striatal EGFP+ THIN however colocalized VMAT2. B. Examination of the striatum where the nigrostriatal pathway was depleted similarly lack colocalization of VMAT2 with EGFP in any of the THINs examined. Note the increase expression of TH in THINS and the lower VMAT2 background compared to the non-lesioned side. Magnified views of the boxed regions are shown in the corresponding panels directly below.

DAT immunofluorescence

Although the absence of DA and AADC expression in striatal THINs, even following L-DOPA pretreatment would strongly indicate they have no intrinsic capacity to directly manufacture DA, this does not exclude the possibility that they could have the capacity to uptake DA from the DAT. In particular, Tande et al. (2006) argues that striatal TH⁺ neurons in the primate undergo a phenotypic shift and express DAT following MPTP treatment that is not owed to neurogenesis. To test the hypothesis that DA depletion can cause a phenotypic shift of DAT expression in the mouse, 6-OHDA unilaterally lesioned EGFP-TH mice were sacrificed, perfused, and processed for DAT immunoreactivity following a two-week post-injection period, as described in detail in the methods sections.

Control characterization of DAT in the midbrains of EGFP-TH mice

First, as a positive control used to characterize the efficacy of the DAT antibody, midbrain coronal sections of 6-OHDA unilaterally lesioned EGFP-TH were examined. Figure 12 shows a representative coronal section of the midbrain of a 6-OHDA unilaterally lesioned EGFP-TH mouse. Unlike TH, which is found throughout the cytosol, the DAT is localized at the cell membrane. This cell membrane localization of the DAT was reflected in the immunofluorescent detection of DAT seen at the perisomatic territories of EGFP⁺ cells.

There is both ample EGFP fluorescence and DAT immunofluorescence of dense somata and their related axonal and dendritic processes in the SNc/VTA.

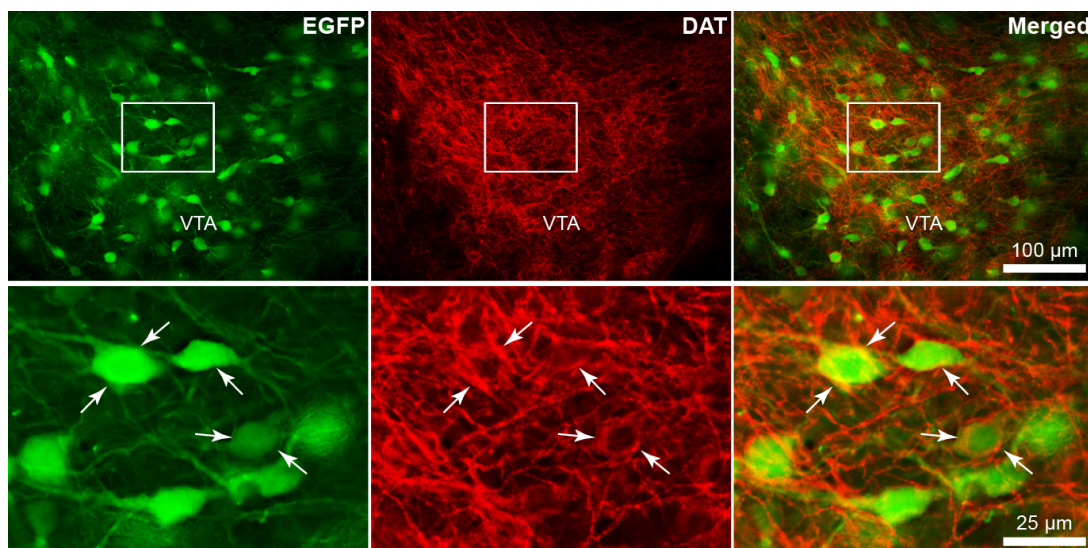


Figure 12. Photomicrographs of coronal sections through the midbrain of EGFP-TH mice processed for DAT immunofluorescence. A representative section of the VTA region reveals widespread colocalization of EGFP fluorescence with DAT immunofluorescence in densely packed somata and their accompanying axonal and dendritic fibers. Note the particularly denser perisomatic labeling of DAT immunofluorescence in numerous large, dense soma and their stronger colocalization with EGFP (white arrows).

Moreover there is abundant colocalization of EGFP-TH⁺ somata with DAT immunofluorescence, thus demonstrating the DAT antibody not only works but also colocalizes with TH expressing cells in EGFP-TH mice

Characterization of DAT in the striatum of EGFP-TH mice

Next, in the same 6-OHDA unilaterally lesioned mice, the striata were examined to determine if EGFP fluorescent striatal THINs colocalizes with DAT immunofluorescence ($n = 3$ mice). Figure 13A are photomicrographs of coronal sections of the control striatum of a representative EGFP-TH mouse. There was a clear background of DAT immunoreactive nigrostriatal fibers but no colocalization of EGFP with DAT immunofluorescence. On the ipsilateral side, the effectiveness the 6-OHDA induced degeneration of the nigrostriatal pathway can be readily seen by the marked background reduction in both EGFP

fluorescence and DAT immunoreactivity (Fig. 13B). This reduction of the nigrostriatal fibers and its associated fluorescence were to such an extent that it unmasked the EGFP+ axonal and dendritic processes of the THINs, allowing them to be more readily seen. There was also an increase in the number of EGFP+ cells in the lesioned side. Lastly, there was no colocalization of DAT with EGFP immunofluorescence on the lesioned side of the striatum where there was clearly a substantial depletion of nigrostriatal DA, presumed to be a state in which DAT expression would occur.

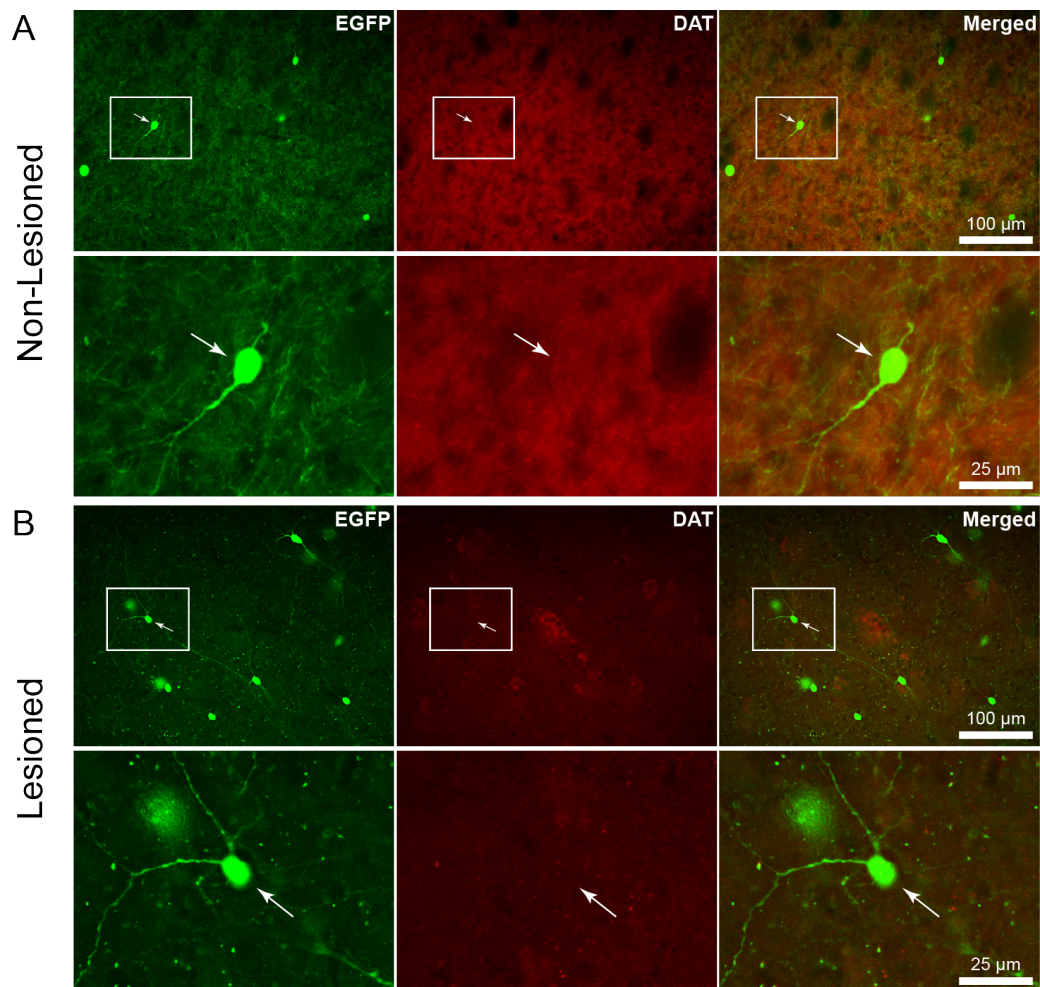


Figure 13. Immunofluorescent photomicrographs of striatal coronal sections processed for DAT. A. Unlesioned, control side of striatum shows no colocalization of DAT with EGFP. B. Lesioned side similarly had no EGFP+ THINs that colocalized DAT. Note the darker background of DAT in the lesioned side, indicative of a loss of nigrostriatal fibers.

Voltammetry

The absence of DAergic neurochemical markers in striatal THINs strongly suggests that striatal THINs are not DAergic. Nonetheless, as both an independent, alternative experimental approach to determine if THINs are DAergic and directly test if striatal THINs contain and can release DA, fast-scan cyclic voltammetry (FSCV) was used to selectively target and activate striatal THINs with optogenetics in a TH-Cre mouse line, as described in the methods section. Moreover, the TH-Cre mice used for these experiments were again unilaterally lesioned with 6-OHDA for several reasons. First, as previously stated, DA depletion has been argued to confer a DAergic phenotype in striatal THINs, and hence unilaterally lesioned mice allows this claim to be directly tested. In addition, in having a striatum whose nigrostriatal fibers are left intact (the contralateral side), a positive control is also afforded to examine the sensitivity and effectiveness of our DA detection setup using FSCV.

Characterization of in vitro fast-scan cyclic voltammetric detection of DA

Carbon fiber electrodes (CFE) were manufactured as outlined in the methods sections and used for FSCV by directly inserting the tip of the CFE into striatal slices for the detection of DA. To quantify the amount of detected DA released within striatal tissue, a calibration of each electrode was first performed using a 1 μ M DA standard concentration that was bath applied into the recording chamber, where the CFE was held during FSCV. Figure 14 is representative of a typical calibration. The heat map representation of the oxidation and reduction events of evoked DA (Fig. 14A) are clearly seen, revealing the detection of DA occurs at around 5 seconds into the scan. Fig. 14B

gives the more traditional cyclic voltammogram representation of DA detection and identification, in which the oxidative peak is situated at around 0.6 V and the reductive peak at around negative 0.2 V. The peak oxidative current was then used to calibrate the CFEs used in subsequent measurements to determine evoked DA concentrations during either electrical or optical stimulation.

Next, to determine the effectiveness of the FSCV setup employed for in vitro detection of DA, CFEs were inserted approximately 100 μm into striatal tissues and FSCV was performed during presentation of a single 50

μs current pulse of 250 μA , delivered from a concentric bipolar stimulating electrode. Figure 15A shows the typical experimental setup of a CFE (left side) inserted into a parahorizontal striatal slice. The bipolar stimulating electrode (bottom) is inserted just beneath the surface of the slice to a depth typically no more than 50 μm . The heat map representation of the FSCV is depicted in Fig. 15B (note the electrical stimulation artifact as indicative by the black arrow). The

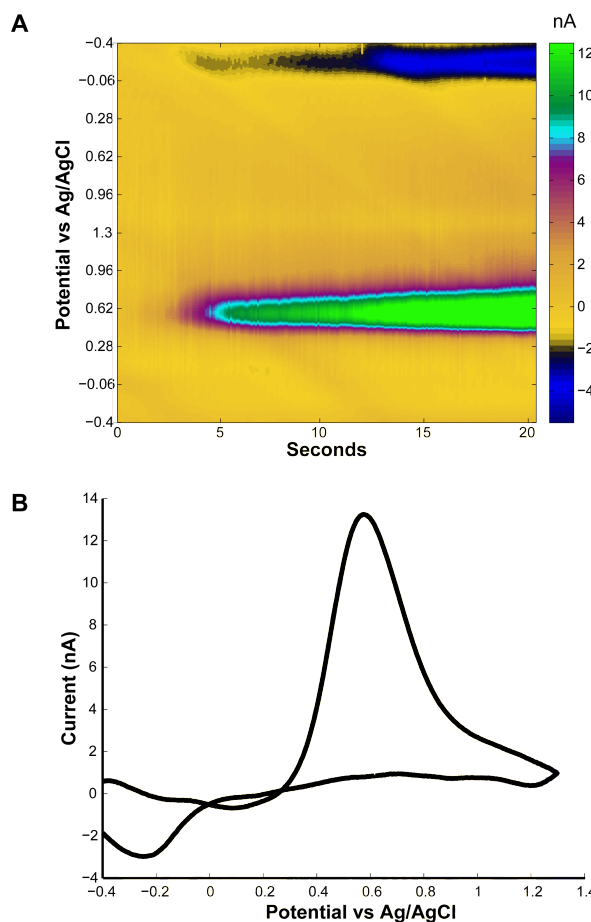


Figure 14. Calibration of carbon fiber electrodes using a DA standard concentration. A. heat map representation of a FSCV scan, showing the detected oxidative and reductive events of a bath application of a 1 μM DA standard. B. Typical cyclic voltammogram of the same detection as in A, showing the distances of the oxidative and reductive peaks and their respective centers identify the detected analyte as DA.

current changes through the potential scan at the time point where the maximum oxidative current occurs (blue line in Fig. 15B) then gives a more traditional cyclic voltammogram representation of the scan, as depicted in Fig. 15C. Moreover, using a standard calibration, the concentration of release through time could be quantified. In particular, the change of current during time through this maximum current peak (red line in Fig. 15B) then gives the change of evoked $[DA]_e$ over time, as depicted in Fig. 15D. Finally, an alternative means of

visualizing this typical FSCV scan is depicted in the “landscape” representation of the heat map representation in Fig. 15E, in which the oxidative “mountains” and reductive “valleys” are more readily seen.

To increase DA detection, the DA reuptake inhibitor nomifensine was used to determine the effect on DA detection. Figure 16 shows the $[DA]_e$ vs. time

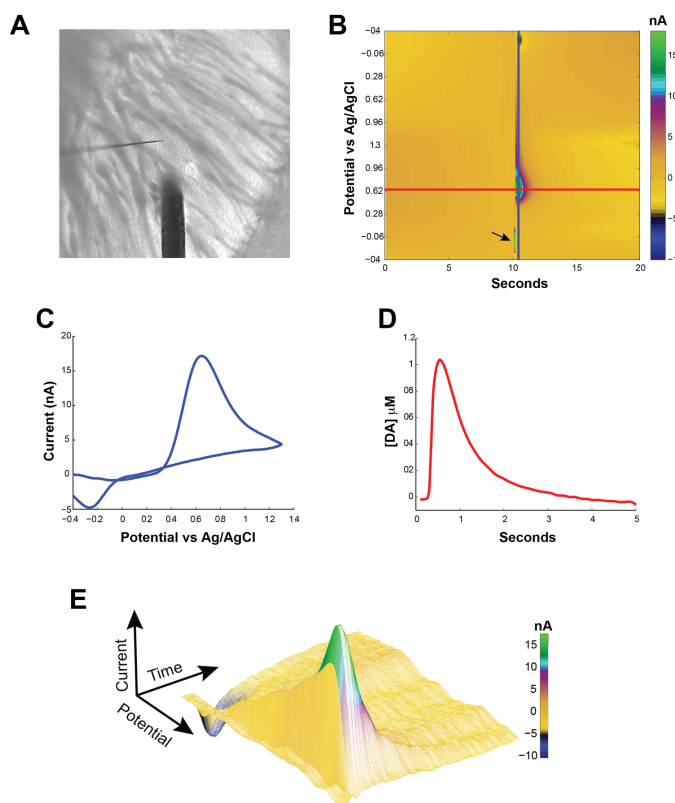


Figure 15. In vitro FSCV detection of evoked DA release. A. Typical experimental set up of a parahorizontal slice, in which a 7 μm thin CFE (right) is inserted to a depth of approximately 100 μm , while a concentric bipolar stimulating electrode (bottom) is inserted just beneath the surface of the tissue. B. Heat map representation of an electrically evoked detection of DA during after a single 50 μs long 250 μA current pulse. Note the electrical stimulation artifact (arrow). C. Derived cyclic voltammogram from B (as explained in the text). D. Time course of evoked DA release after back calibrating from a standard DA concentration. E. Alternative landscape visualization of the FSCV data, showing the oxidative “mountain” and reductive “valley” of the scan.

plots and corresponding cyclic voltammograms of evoked DA following a single 50 μ s, 250 μ A current pulse.

The control (Fig. 16A) FSCV recording was followed by a second FSCV recording after a 10 μ M bath application of nomifensine (Fig. 16B). As seen in Fig. 16C, there was a significant increase in detected $[DA]_e$ (1.6 ± 0.44 fold increase; $p = 0.0366$, paired t-test, $n = 4$ samples, $n = 4$ electrodes, $n = 4$ slices in $n = 2$ mice).

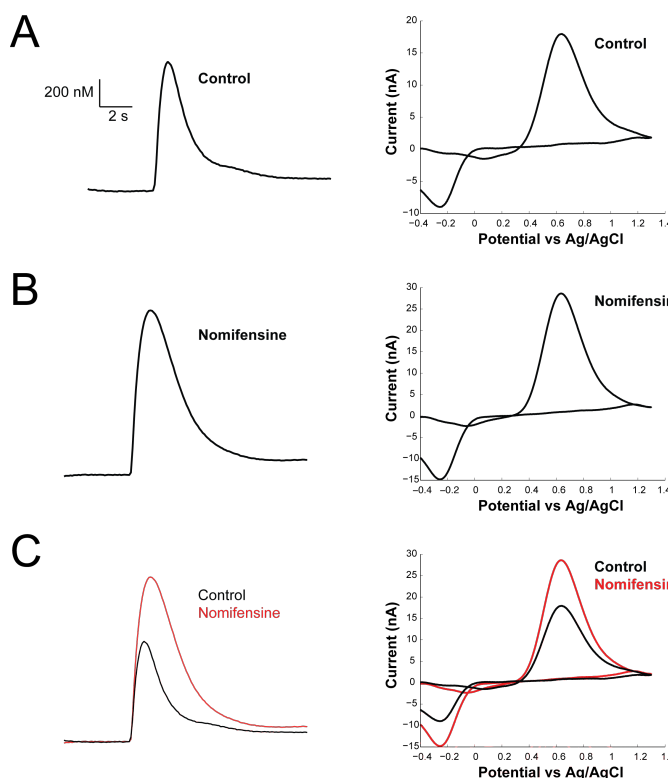


Figure 16. Pharmacological enhancement of FSCV detection of DA. A. Evoke $[DA]_e$ vs. time plot and corresponding cyclic voltammogram during a control FSCV recording. B. In the same slice preparation as that in A, another FSCV recording after a 10 μ M bath application of nomifensine, a DA reuptake inhibitor. C. Overlapped $[DA]_e$ vs. time and corresponding cyclic voltammograms, showing a significant 60% increase in detected evoked DA.

Lastly, to further quantify the sensitivity of CFE sensitivity, a concentric bipolar electrode was again used to locally stimulate the striatum during FSCV with a series of bath applications of the D2 auto-receptor agonist quinpirole (Fig. 17A, left). The percentage of inhibition of evoked $[DA]_e$ over the range of quinpirole concentrations were fitted to a sigmoidal response curve (Fig. 17B), as described in the methods section. The IC_{50} for quinpirole was determined to be near 100 nM. As seen in Fig. 17B, even at nearly 90% inhibition, corresponding to roughly a 1 μ M concentration of quinpirole, there is still sufficient signal-to-noise ratio to discern not only evoked $[DA]_e$ vs. time but also its corresponding

cyclic voltammogram (yellow traces). For this 1 μM application of quinpirole, the average $[\text{DA}]_e$ was 176.7 nM. In contrast, the average level of detection for dopamine release during a 10 μM application of quinpirole was 28.1 nM. Lastly, while no discernable voltammogram could be produced at this concentration for quinpirole, the current generated is beyond the level of noise, which for a well-fashioned

carbon-fiber microelectrode is 0.1 nA peak-to-peak, translating to a detection limit of 10 nM (where ~10 nA is typical for a 1 μM DA standard response calibration). Furthermore, it should be noted that during electrically evoked release, stimulus artifacts could mask this theoretical detection. With photostimulation this is not a concern however, and moreover, pharmacological reagents such as nomifensine would further enhance FSCV detection.

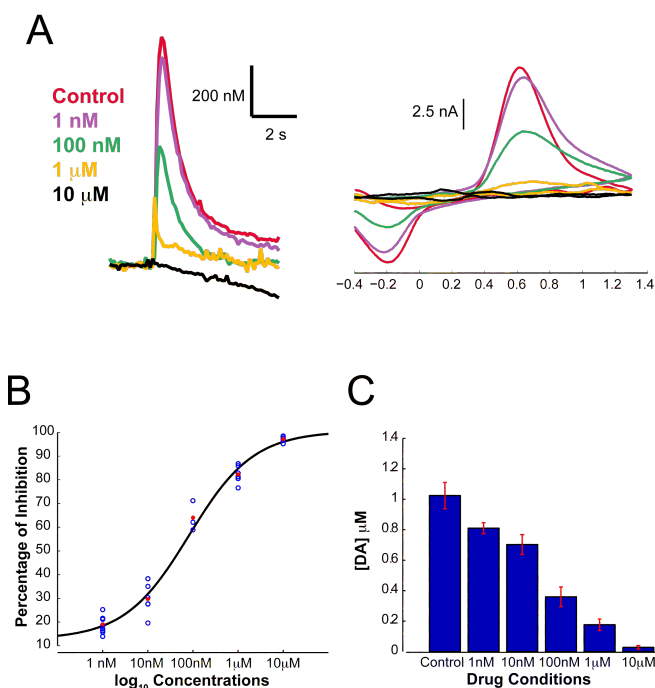


Figure 17. CFE detection of evoked DA sensitive to the tens of nM range. A. $[\text{DA}]_e$ vs. time plots and corresponding cyclic voltammograms for a series of bath applications of quinpirole, a select D2 agonist. B. The percentage of inhibition of evoked $[\text{DA}]_e$ for a series of repeated measures ($n = 6$) for each concentration of quinpirole, fitted to a sigmoidal curve. C. Average evoked $[\text{DA}]_e$ responses for each concentration of quinpirole used.

Optogenetics with simultaneous voltammetry

Selective targeting and optogenetic activation of striatal THINs

Next, to directly target striatal THINs, a cre-dependent virus was used in a TH-Cre BAC transgenic mouse line that expresses the Cre recombinase enzyme under the control of the regulatory elements of TH. This transgenic mouse line was used in combination with a recombinant adeno-associated virus that employs a double floxed strategy and contains an inverted open reading frame sequence for the fusion protein encoding channelrhodopsin-2 (ChR2) and the enhanced yellow fluorescent protein (EYFP). AAV-ChR2-EYFP (~1.3 μ L) virus was intracerebrally injected into the striata of TH-Cre mice (2-4 months old). After a two-week wait period, striatal THINs were transduced to express ChR2-EYFP and examined for both expression level and transduction efficiency. Figure 18 depicts a representative example of a TH-Cre mouse whose striata was injected with AAV-

ChR2-EYFP. Figure 18B shows that there was a widespread transduction of striatal THINs, in which not only numerous somata from striatal THINs but also their associated axonal and

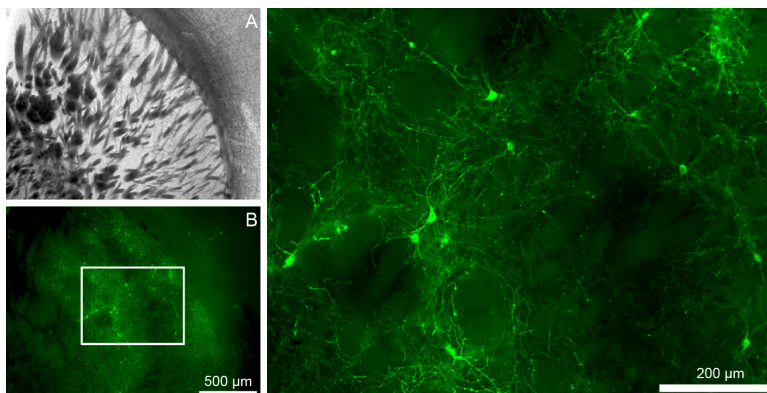


Figure 18. Selective optogenetic targeting of striatal THINs in TH-Cre mice. A. Bright field photomicrograph of a coronal striatal section of a TH-Cre mouse that was intracerebrally injected with cre-dependent AAV-DIO-ChR2-EYFP virus. B. Fluorescent photomicrograph of the same field as in A, showing widespread transduction of striatal THINs, expressing the fusion ChR2-EYFP protein. C. Magnified view of the box region in B, showing numerous EYFP+ striatal soma and their associated axonal and dendritic arborization.

dendritic processes were EYFP+ fluorescent (Fig, 18C). Lastly, the processes of a given striatal THIN overlapped extensively with the axonal arborizations of numerous neighboring striatal THINs, giving rise to a widespread coverage of the striatum.

To verify whether the virally transduced striatal THINs were capable of being optogenetically activated, transduced EYFP+ fluorescent striatal THINs were patched and recorded in current clamp mode during a presentation of a single 2.5 ms pulse of blue light (Figure 19B). A series of hyperpolarizing and depolarizing injections (Fig. 19A) of one such recorded cell, identified it as a Type I THIN, which electrophysiologically verified the efficiency of the viral targeting strategy of striatal THINs.

Moreover, virally transduced striatal THINs were reliable optogenetically activated in response to 2.5 ms blue light pulses (Fig. 19B). Every recorded striatal THIN that was transduced to express ChR2-EYFP was found to fire an action potential. As seen in figure 19B, a striatal THIN is optically stimulated (blue ticks) by 2.5 ms pulsed of blue light, each time firing an action potential. Optogenetic activation of striatal THINs proceeds with first a large depolarization followed by an immediate action potential and then by a very modest afterdepolarization potential (ADP) due to the slower inactivating kinetics of ChR2 compared to voltage-gated sodium channels.

This therefore demonstrated that the combination of viral targeting of striatal THINs using cre-dependent virus in a Cre mouse transgenic works and striatal THINs could be reliably activated.

Lastly, it should be noted also that in none of the EYFP+ fluorescent striatal neurons that were patched and recorded was there any difference in the

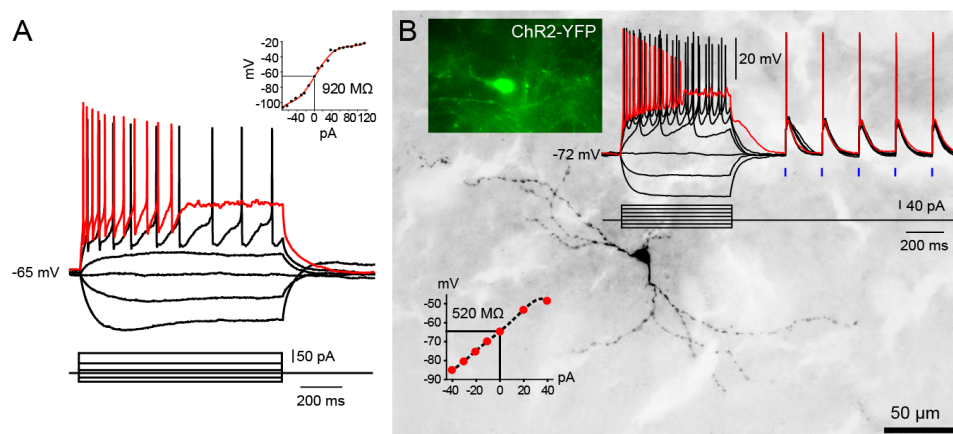


Figure 19. Selective optogenetic activation of striatal THINs in TH-Cre mice. A. Representative whole-cell current-clamp recording of a Type I striatal THIN from an EGFP-TH mouse, exhibiting typical high input resistance and the characteristic depolarization block at moderate depolarizing current injections typical of Type I THINs reported previously. B. A whole-cell recording of a virally transduced ChR2-EYFP striatal TH interneuron (upper right inset) from a coronal striatal section from a TH-Cre mouse. Both the electrophysiology and anatomy were typical of Type I striatal THINs as previously seen in EGFP-TH mice (compare to A). 2.5 ms optical stimuli from a blue LED (blue ticks) evoke large depolarizations followed by spiking.

electrophysiology previously encountered and described in TH-GFP transgenic mice (Ibanez-Sandoval et al., 2010).

Electrophysiology with simultaneous FSCV

With this ability to target TH⁺ neurons in a TH-Cre mouse line, focus on showing simultaneous fast-scan cyclic voltammetry (FSCV) with electrophysiology was undertaken to demonstrate that THINs were activated during voltammetric recording sweeps. Using TH-Cre mice that were injected in the striatum with AAV5-ChR2-EYFP virus, THINs were whole cell patched in current mode and first local electrical stimulation was applied near the recording carbon fiber electrode (CFE). A schematic representation of this setup is depicted in Figure 20A. Current-clamp recordings of a representative Type-I THIN in response to increasing current injections are shown in Figure 20B. This same

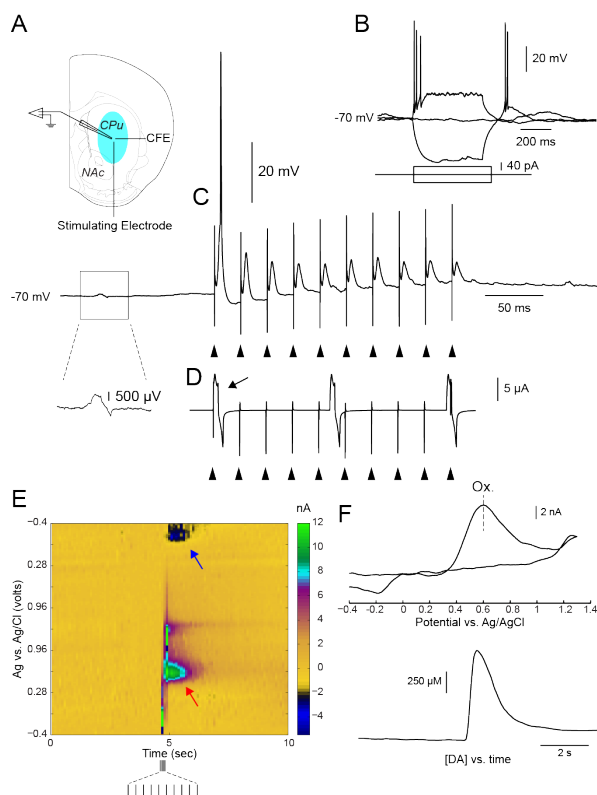


Figure 20. Simultaneous FSCV with electrophysiology. A. Schematic of experimental set-up. B. Current-clamp recording of a Type I THIN. C. Same THIN as in B stimulated with a train of 450 μ A electrical pulses (10 pulses, 50 μ s in duration and 25 ms ISI). Note the induced current change mirroring the resistive-capacitive CFE profile during FSCV scanning (boxed region). D. FSCV sweep. Heat map (E) and cyclic voltammogram and concentration vs. time of evoked DA (F). *Black arrows*: time points of applied pulses.

THIN was then recorded while 10 electric square pulses of 450 μ A were applied for 50 μ s with an interstimulus interval of 25 ms (Fig. 20 C, black triangles). This train stimulus elicited a single action potential during the first pulse, followed by a gradual depression of EPSPs. The inductive resistive-capacitive profile of the CFE during the voltammetric scan can be seen in the current clamp sweep (blow up of boxed region in Fig. 20C), demonstrating that FSCV was simultaneously with electrophysiological recording.

This voltammetric sweep can be seen in sync with these induced current changes in the current clamp sweeps (Fig. 20D). A heat map representation of the FSCV sweep reveals the detection of DA at its characteristic oxidation and reduction potentials (red and blue arrow, respectively) and an approximately 1 μ M release of DA (Fig. 20E-F).

Next, striatal THINs of TH-Cre transduced to express ChR2-EYFP were whole-cell recorded in current clamp mode during optical stimulation and simultaneous optogenetic activation (Fig. 21). A modest current injection of 50

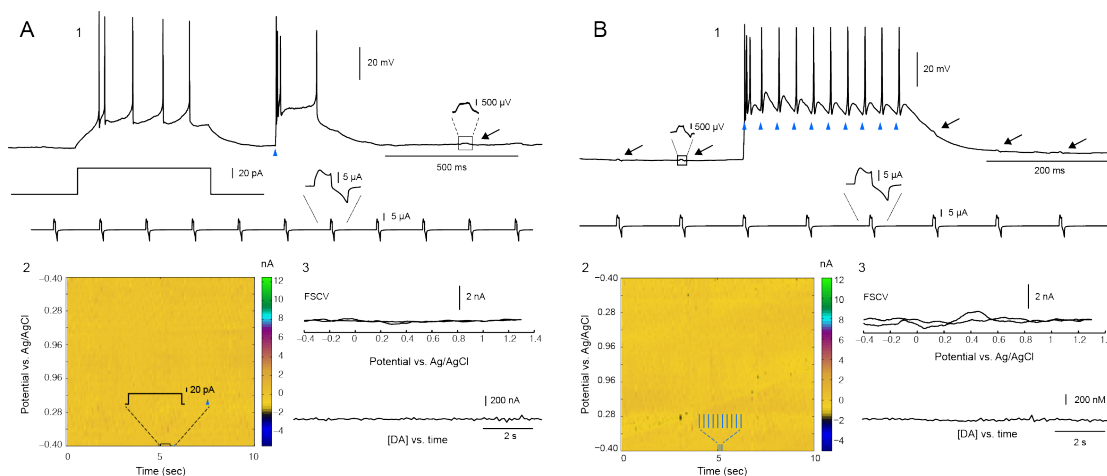


Figure 21. Optogenetic activation of striatal THINs during simultaneous FSCV. A. Neither current injection (50 pA for 500 ms) nor optical stimulation (single 5 ms light pulse, blue triangle) elicited detectable amounts of DA. No oxidation or reduction events occurred in the voltammetric heat map data (A3) or in the cyclic voltammogram (top) nor any detected evoked [DA] release over a several second long recording period. B. Neither did strong optical stimulation evoked release of DA (10, 5 ms blue light pulse with an ISI of 25 ms). Blue triangles: light pulses; black arrows, inductive current changes of FSCV sweep in traces below current clamp recordings.

pA for 500 ms was first applied followed by a single 5 ms pulse of blue light (Fig. 21A, blue triangle). The current injection first elicited a doublet of action potentials, followed by several other spikes. The single pulse of blue light evoked first a triplet of action potentials and a plateau potential, on which another spike occurred (Fig. 21, A1). This mixed protocol of electrical and optical stimulation was to determine if THINs could release DA, and if activation of a single THIN by current injection was sufficient. As seen in Figure 21, A2-A3, no evoked DA release was detected. A train of 10 optical pulses of blue light (5 ms in duration, 25 ms ISI) was then applied (blue triangles). Despite each pulse eliciting firing, no evoked DA was detected (Fig. 21, B1-B3).

Attention was then turned to targeting TH⁺ projection neurons in the midbrain, so as to transduce nigrostriatal terminals to express ChR2-EYFP. This in turn would allow optogenetic activation of nigrostriatal terminals during

simultaneous fast scan cycle voltammetry in the striatum to be used as a positive control.

The midbrain of TH-Cre mice were injected with AAV-ChR2-EYFP (~1.2 μ L) and allowed a 3-4 week wait period, a sufficient time to transduce the nigrostriatal pathway. As seen in Figure 22 B1, a fluorescent photomicrograph of a striatal coronal section of a TH-Cre mouse whose midbrain was injected with AAV-ChR2-EYFP reveals widespread EYFP+ fluorescence of the nigrostriatal terminals in the striatum. High-magnified examination (Fig. 22 B2) shows abundant individual nigrostriatal axons densely innervating the striatum.

Optogenetic evoked release of nigrostriatal DA during FSCV in the striatum

As a positive control for the optogenetic and voltammetric procedures, the midbrain of a TH-Cre mouse was injected with AAV-ChR2-EYFP and allowed to have adequate transduction of ChR2. The mouse was then sacrificed and perfused for in vitro voltammetry. As previously described, this procedure efficiently transduced both mesencephalic DAergic neurons and their nigrostriatal fibers (Tecuapetla et al., 2010). Figure 22C depicts a bright field photomicrograph of a coronal striatal section, in which a carbon fiber electrode (CFE) and bipolar stimulating electrode have been inserted into the tissue. To compare the release of $[DA]_e$ evoked by optical versus local electrical stimulation, either a single 2.5 ms pulse of blue light or a single 250 μ A, 50 μ s square electrical pulse was presented during simultaneous FSCV (Fig. 22D). Large DA transient releases were reliably evoked by either stimulus and produced very similar cyclic voltammograms. The mean peak $[DA]_e$ concentration evoked by local electrical stimulation ($853.6 \text{ nM} \pm 36.1$; range 743 nM – 937 nM) was slightly but

not significantly greater than the peak DA concentration evoked by optical stimulation ($808.5 \text{ nM} \pm 40.7$; range $687 \text{ nM} - 893 \text{ nM}$) (Fig. 22 E1). Additionally, there was no significant difference between the mean voltages at which the oxidation and reduction peaks of DA was evoked by either of the two stimuli (two-sample t-test, $p > 0.1$). Lastly, there was no difference between the release kinetics of DA evoked by electrical or optical stimulation (Fig. 22 E2). Together

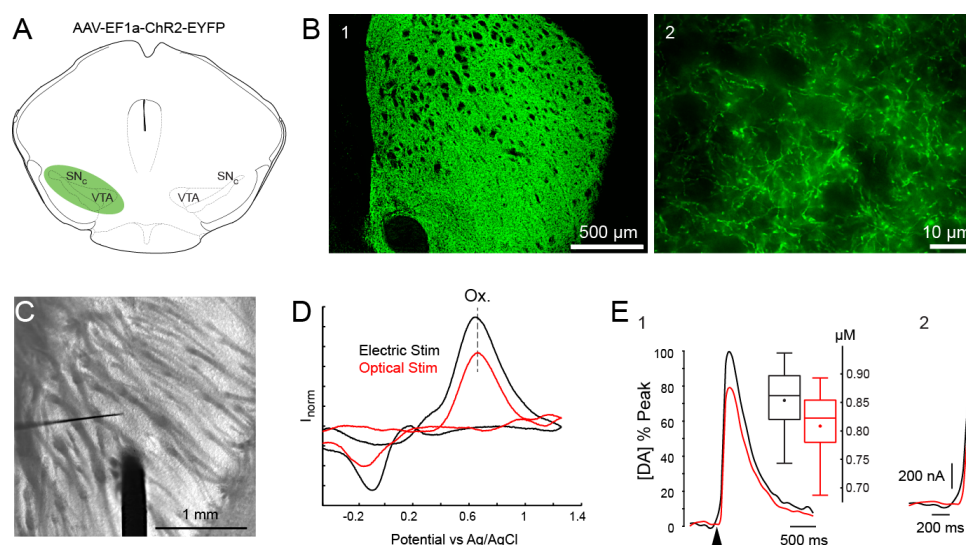


Figure 22. Voltammetric detection of optogenetically evoked nigrostriatal DA release in a TH-cre mouse. A. Schematic illustration of a midbrain unilateral injection of AAV-ChR2-EYFP ($1.2 \mu\text{l}$). B1. Coronal section of striatum of a TH-Cre mouse following a two week post unilateral midbrain injection of AAV-ChR2-EYFP, showing an extremely dense distribution of fluorescent virally transduced nigrostriatal fibers throughout the striatum. B2, High magnification photomicrograph of the same striatum shown in B1, illustrates individual nigrostriatal fibers. C. Bright field micrograph taken through the recording microscope shows the placement of the concentric bipolar stimulating electrode (thick dark structure) and the much thinner carbon fiber electrode. D. Both electrical and optical stimulation protocols produce nearly identical cyclic voltammograms, whose peak oxidation and reduction potentials identify them as resulting from DA. *Note the nearly identical oxidation potentials for the two peaks (dashed line).* E1. The concentration versus time plots of evoked DA release following electrical (black) or optical (red) stimulation. E1 is normalized to the maximum peak oxidation current. Box plot summaries of evoked $[\text{DA}]_e$ from electrical (black) and optical (red) stimuli show no significant difference ($n = 5$ slices; $n = 2$ animals). E2, a magnified view of the initial time profile of E1, illustrating identical release kinetics for both stimulation protocols. *Arrowhead denotes onset for either electrical or optical stimulation.*

these experiments show that TH+ DAergic neurons can be reliably targeted and activated during simultaneous voltammetry.

Optogenetic activation of striatal THINs during FSCV in the striatum

To determine if striatal THINs can release DA, AAV-ChR2-EYFP was intracerebrally injected into the striata of TH-Cre mice whose midbrains were unilaterally lesioned with 6-OHDA. This procedure again allowed a selective expression of ChR2-EYFP only in striatal THINs. After a two-week post-injection wait period to ensure adequate viral transduction, in vitro FSCV was performed in the striatum contralateral or ipsilateral to the lesion. A single 250 μ A, 50 μ s electrical square pulse local or a 2.5 ms blue light pulse stimulus was used during simultaneous in vitro FSCV recording.

In all cases (n = 6 mice; n = 11 slices), the 6-OHDA lesions were highly effective in eliminating TH+ mesencephalic neurons and their nigrostriatal projections on the ipsilateral side, while leaving the TH+ neurons and their nigrostriatal input to the contralateral side unaffected (Fig. 23 A2). This procedure was performed for two reasons. One, by lesioning the nigrostriatal pathway on one side, false positive results due to retrograde transduction of mesencephalic DAergic neurons via nigrostriatal terminals are eliminated. Second, numerous studies report an increase in the number of TH+ somata following DA depletion, owed to an up-regulation of TH expression (Betarbet et al., 1997; Meredith et al., 1999; Cossette et al., 2005; Tande et al., 2006; Huot and Parent, 2007; Darmopil et al., 2008). Moreover, in addition to studies showing that striatal THINs undergo neurochemical and electrophysiological changes following nigrostriatal depletion (Mazloom and Smith, 2006; Unal et al., 2013), it

has been argued that the increase of TH expression in striatal THINs serve to compensate for a decrease in nigrostriatal DA (Betarbet et al., 1997; Darmopil et al., 2008). Therefore, 6-OHDA lesioning provides a physiological state in which, supposedly, striatal THINs are either induced into a DAergic phenotype or have that already existent capacity enhanced. Lastly, this strategy also provided both positive and negative controls for DA release in the striatum of the same slice, thereby verifying the effectiveness of the CFEs used during FSCV recordings.

Placement of the recording CFE was aided by the fluorescent EYFP reporter in the transduced axons of striatal THINs. CFEs were placed directly within regions containing the densest collection of striatal THINs and their associated axonal arborizations, as shown in Figure 23 B2. Before selecting such areas for FSCV recorded, typically a few striatal THINs were recorded in whole-cell current clamp mode to verify whether they could be reliably optogenetically activated. A 2.5 ms blue light pulse reliably activated striatal THINs in all cases. A typical example is shown in Fig. 23 B2, where a single light pulse is sufficient to elicit a large depolarization, which in turn triggers an action potential (inset).

Despite the optogenetic activation of striatal THINs, optical stimulation of THINs did not elicit detectable striatal DA release in either the intact or lesioned side. In contrast, a single local 250 μ A, 50 μ s electrical stimulus reliably elicited DA release in the intact striatum ($850 \text{ nM} \pm 60.2$; range, 560.3 nM - 1.2624 μ M), but not in the lesioned striatum, as illustrated for a representative experiment in Figure 23 C.

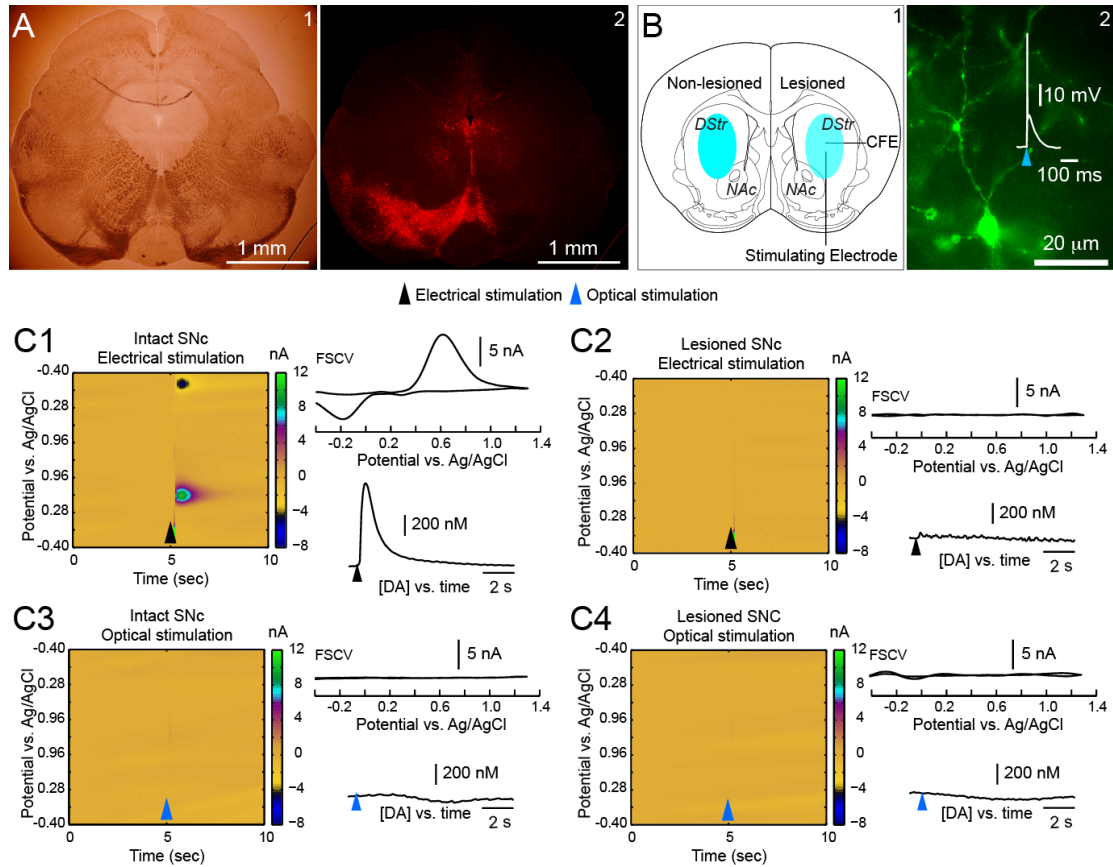


Figure 23. Voltammetry in striatum during optogenetic activation of striatal THINs. A1. Bright field photomicrograph of a midbrain coronal section of a TH-cre mouse following a unilateral 6-OHDA injection into the midbrain and bilateral injections of AAV-ChR2-EYFP (1.33 μ l) into the striatum. A2. Fluorescent photomicrograph of the same field as in A1, processed for TH immunofluorescence showing a complete absence of TH on the 6-OHDA treated side but densely packed TH immunoreactive somata and processes in substantia nigra and the ventral tegmental area on the contralateral side. B1. Schematic depiction of bilateral striatal injections of AAV-ChR2-EYFP. B2. Whole cell current clamp recording of a striatal THIN transduced to express ChR2-EYFP. The neuron reliably fires an action potential upon a single 2.5 ms pulse of blue light. The voltammetric electrode was placed under visual guidance into a region of dense fluorescent labeling. C. Voltammetric heat maps, fast scan cyclic voltammograms (FSCVs), and [DA] vs. time plots. Electrical stimulation elicits DA from the non-lesioned striatum (C1) but not the lesioned side (C2). In contrast, optical stimulation failed to elicit any detectable amounts of DA from either the non-lesioned or lesioned striata (C3-C4). *Black and red arrowheads, respectively, denote onset of electrical and optical stimulation.*

Next, to further maximize the detection of evoked DA from striatal THINs, FSCV was again simultaneously performed during either local electrical or optical stimulation with a bath application of the DA reuptake inhibitor nomifensine (10 μ M) and the D₂ autoreceptor antagonist raclopride (10 μ M). Both drugs are known to significantly increase the extracellular concentration of evoked DA release from mesencephalic DAergic neurons (Ogren et al., 1986; Earl et al., 1998; Robinson and Wightman, 2004).

As compared to the peak [DA]_e under control conditions, nomifensine plus raclopride significantly increased both the amplitude and duration of the DA transient, as illustrated in Figure 24 A (1.7020 ± 0.1232 μ M; range, 1.5808 - 1.7917 μ M; two-sample t-test, $p < 0.001$). Despite this increase in electrically

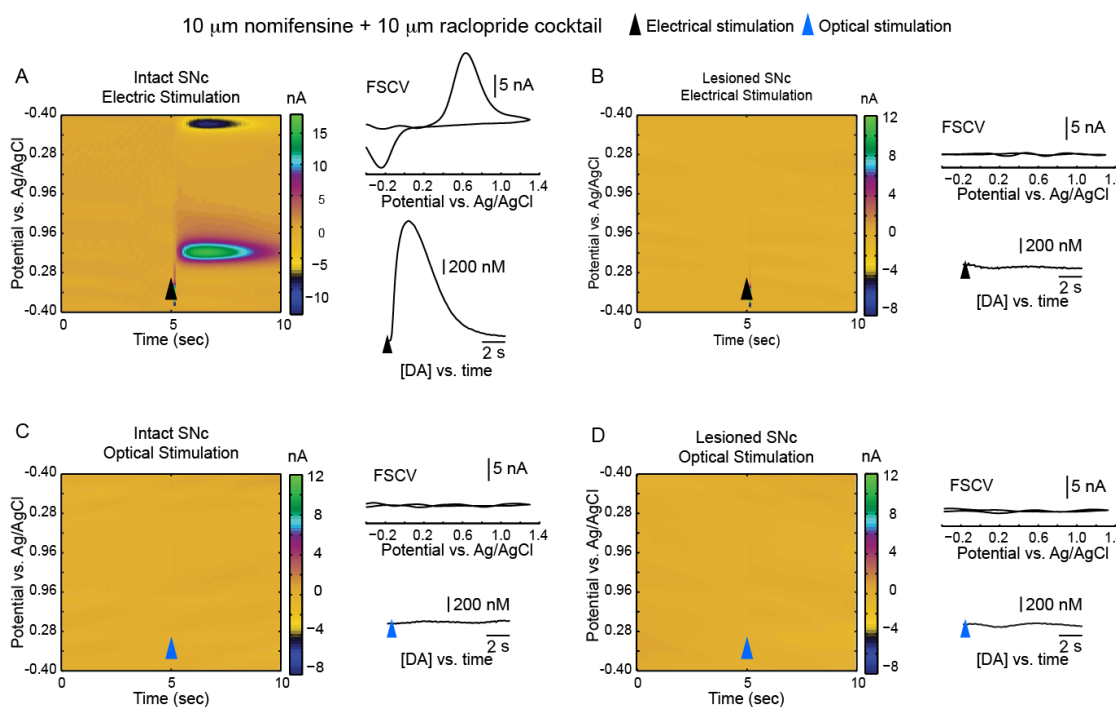


Figure 24. Effects of DA uptake and autoreceptor blockade on striatal DA release following optogenetic activation of striatal THINs. Nomifensine (10 μ M) plus raclopride (10 μ M) were present for all experiments. A. Nomifensine plus raclopride greatly enhanced the release of DA in response to local electrical stimulation in the intact striatum, but failed to yield any detectable release of DA on the lesioned side (B). C-D, Optical stimulation failed to elicit detectable levels of DA from either the lesioned or control side.

evoked $[DA]_e$ in the intact striatum, no electrically evoked DA release was observed in the striatal side ipsilateral to the midbrain 6-OHDA lesion (Fig. 24 B). Furthermore, as was the case in the voltammetric recordings performed in the absence of DA uptake inhibition and autoreceptor blockade (cf. Fig. 23 C3-C4), optical stimulation failed to elicit DA release in either striatum (Fig 24 C-D).

These experiments were also repeated on TH-cre mice that were treated with L-DOPA (30 kg/mg i.p., n=2) for one hour before making our slice preparations and recorded 40 minutes later. Electrically evoked DA release was unaltered on the contralateral side to where the 6-OHDA lesion. As before, detectable DA release was not observed during optical stimulation for either side of the striatum was observed. This was despite the significant increase in evoked DA as compared to control conditions even in the presence of nomifensine (Fig.

25

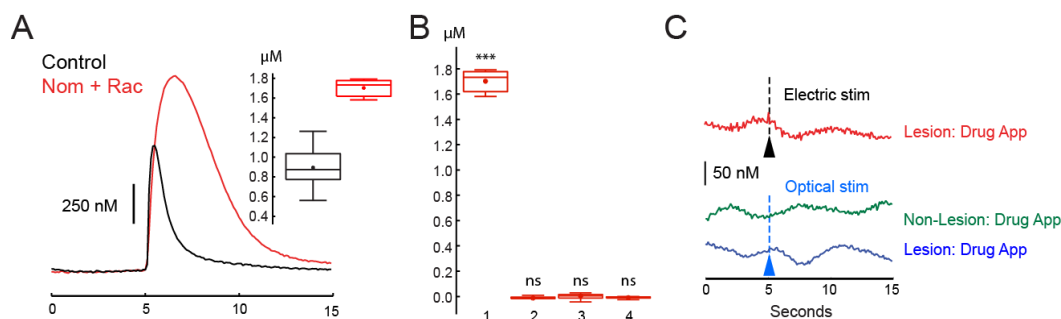


Figure 25. Summary statistics of pharmacological effects during optogenetic activation of striatal THINs. A. Overlay of evoked $[DA]_e$ following electrical stimulation in the absence (black) and presence (red) of nomifensine plus raclopride. Peak $[DA]_e$ in the presence ($1702 \text{ nM} \pm 123 \text{ nM}$) of the drugs was significantly greater than in their absence ($895 \text{ nM} \pm 60.2 \text{ nM}$; $p < 0.001$). B. Box plot summaries of evoked peak $[DA]_e$ in nomifensine plus raclopride for the following groups: electrical stimulation in striata contralateral to lesion (group 1), electrical stimulation ipsilateral to lesion (group 2), optical stimulation in contralateral side (group 3), and optical stimulation ipsilateral to lesion (group 4). While there was a significant difference between the data for electrical stimulation in the contralateral side (group 1) and the other groups ($p < 0.001$, one-way ANOVA, followed by Bonferroni's *post hoc* tests), there was none for the other groups. C. Magnified scale of $[DA]_e$ versus time plots of A2-A4, showing no detection of DA for group 2 (red trace), group 3 (green trace), and group 4 (blue trace), even down at the level of CFE noise. *** $p < 0.001$.

A). Only during local electrical stimulation of the contralateral side then was there any detected release of DA (summary plot in Fig. 25 B). Lastly, for all these experiments, the typical noise level of our voltammetric recordings was < 25 nM $[DA]_e$ (Fig. 25 C).

Electrophysiology and modulation of striatal THINs

Inhibitory effects of striatal THINs on SPNs

In previous studies, striatal THINs were found to number roughly ~4500 per striatal hemisphere (Unal et al., 2013) and exert GABAergic inhibition onto SPNs (Ibanez-Sandoval et al., 2010). As a continuation to these earlier studies, which was based on a limited number of paired recordings, optogenetics was used to further characterize the inhibitory effect of striatal THINs on SPNs.

THINs alter the spike timing of SPNs

It was previously shown that striatal THINs form powerful synaptic GABAergic connections onto SPNs (Ibanez-Sandoval et al., 2010). As mentioned, this study was based on a relatively small number of paired recordings, in which THINs were found to evoke monosynaptic GABA_A IPSP/Cs in postsynaptic SPNs capable of delaying or blocking evoked spikes. To determine the effects of the synchronous activation of a large population of striatal THINs on SPNs, we performed whole cell recordings of SPNs located within striatal regions that were densely innervated by the axons of virally transduced ChR2-EYFP striatal THINs, which were abundant throughout the striatum (c.f., Figure 16 C). In all cases ($n = 4$ mice; $n = 8$ slices; $n = 12$ SPNs), optogenetic activation of striatal

THINs elicited inhibitory postsynaptic potentials (IPSPs) that were sufficient to either delay or veto action potentials altogether.

Unilaterally lesioned TH-cre mice were also bilaterally injected in the striatum with AAV-ChR2-EYFP, as described in the methods section. Medium spiny projection neurons (SPNs) were then patched in current mode and a depolarizing current injection was applied during the recordings either in the absence or presence of optical stimulation (Fig.

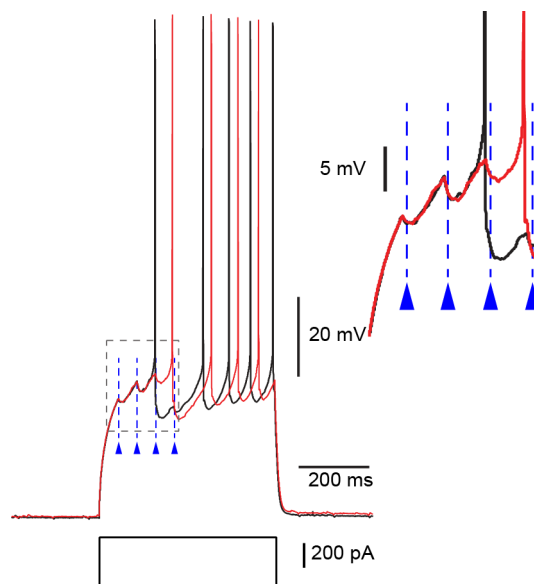


Figure 26. Striatal THINs exert widespread GABAergic inhibition onto SPNs. A. *In vitro* whole cell current clamp recording of a SPN in a TH-Cre mouse bilaterally injected with AAV-ChR2-EYFP in the striatum. Presentation of 2.5 ms blue light stimuli elicits IPSPs (red traces). The IPSP are sufficient to either delay the arrival of action potential firing or abolish firing altogether.

26). As can be seen in the blow-up inset in Figure 26, single 2.5 ms pulses of blue light elicited strong IPSPs in SPNs. As compared to control recordings (black traces), the recordings during optical stimulation (blue arrows) exhibited sufficiently strong IPSPs to either abolish action potential firing, especially during the early rise phase of current-injection-induced depolarization, or delay arrival of an action potential (red traces). The same results were obtained on both sides of the striatum, thus showing the IPSCs did not result from GABA release by nigrostriatal terminals (Tritsch et al., 2012).

THINs elicit robust GABA_A-mediated IPSCs into SPNs

As Figure 27 illustrates in a representative recording from another SPN in

a TH-Cre mouse, these IPSPs were GABA_A-mediated, as demonstrated when the IPSCs were abolished after a bath application of 10 μ M bicuculline, a GABA_A agonist (Fig. 27, bottom recording). In every SPN recorded, there was always an elicited IPSP during optical stimulation of striatal THINs, regardless of the striatal area recorded from, including both the dorsal and ventral areas.

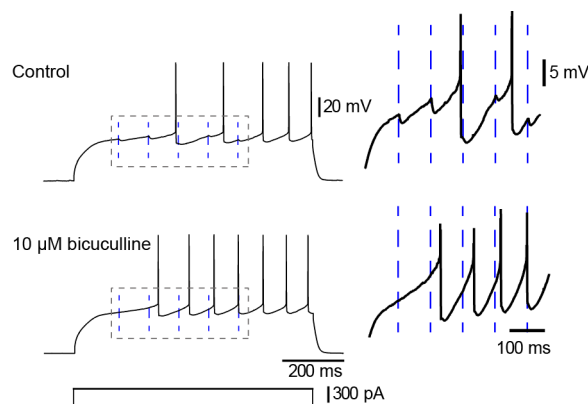


Figure 27. Striatal THIN inhibition onto SPNs are GABAergic. IPSPs in another SPN evoked by optical stimulation of THINs (dashed lines) are blocked by bicuculline, a GABA_A antagonist. Insets to the right of recording traces are magnified views of corresponding boxed regions on the left.

Next, to attempt to quantify the average TH-to-SPN convergence, voltage clamp data from previously published reports (Ibanez-Sandoval et al., 2010) were pooled with new recordings to show that the mean amplitude of the unitary IPSC responses in SPNs (held at -45 to -50 mV) following single action potentials evoked in THINs is 11.5 pA ($n = 3$ pairs) (Fig. 28 A). In contrast, for the synchronous optogenetic activation of an ensemble of virally transduced striatal THINs, the average IPSC on SPNs held at -45 mV is some three times larger than the unitary IPSC response (Fig. 28. B) (31.7 ± 4.9 pA; range 25.5 - 58.0 pA; $n = 12$ recordings). Comparing the ~ 12 pA mean unitary IPSC of a single THIN onto a SPN with that of the ~ 32 pA mean population response of synchronously activated THINs onto a single SPN, suggests an approximately 3:1 convergence of THINs onto a single SPN.

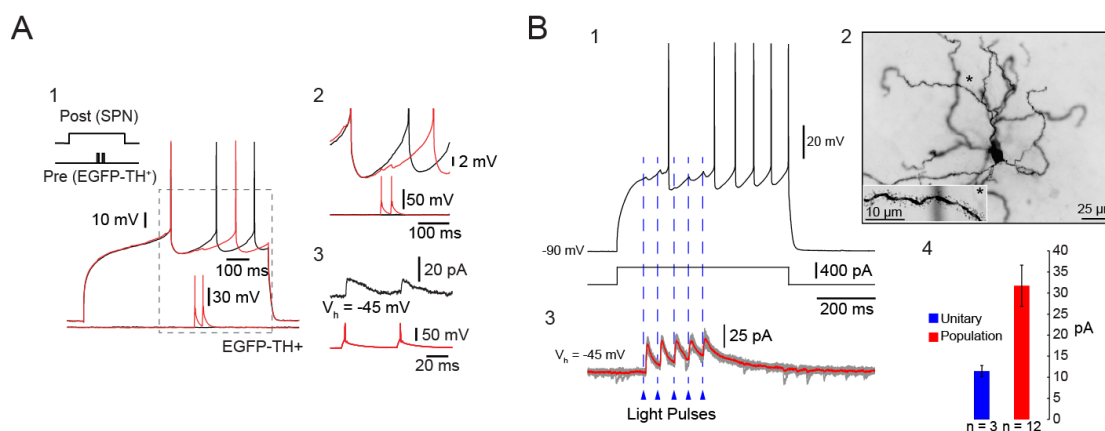


Figure 28. Characterization of unitary and population responses of striatal THINs onto SPNs. A1. Paired recording of a Type III THIN synaptically connected to a SPN during paired pulse current injections. A2. Magnified view of evoked unitary IPSPs of boxed region in 1. A3. Unitary IPSCs of ~16 pA (black trace) were evoked in the same pair at a holding potential of -45 mV. B1. Optogenetic activation of THINs during whole-cell recording of another SPN. B2. Photomicrograph of the SPN in B1. Inset at lower left is magnified view of the dendrite marked by asterisk. B3. Voltage clamp recording of same SPN during optogenetic activation of THINs reveals an average IPSC of ~32 pA at -45 mV. C4. Bar graphs of unitary and population IPSC responses.

Neuromodulation of striatal THINS

Although the immunocytochemical and voltammetric results indicate that THINs neither contain nor release DA, the fact that during conditions of DA depletion, there is an upregulation of TH in striatal THINs (Darmopil et al., 2008; Espadas et al., 2012; Unal et al., 2013), strongly suggests that striatal THINs can both sense and respond to changes in extracellular DA. Consistent with this, it was previously shown that following nigrostriatal depletion, THINs undergo both morphological and electrophysiological changes, which include increases in the density of proximal dendritic spines and an increase frequency of the spontaneous occurrences of both EPSCs and IPSCs (Unal et al., 2013). In addition, it was discovered that the PPs are enhanced by DA and D1/D5-like receptors. Moreover, during depolarizing current injections, a depolarization-

block occurs in striatal THINs, revealing subthreshold membrane oscillations (SMOs) over a wide range of frequencies and amplitudes (Fig. 29 B, yellow highlighted region).

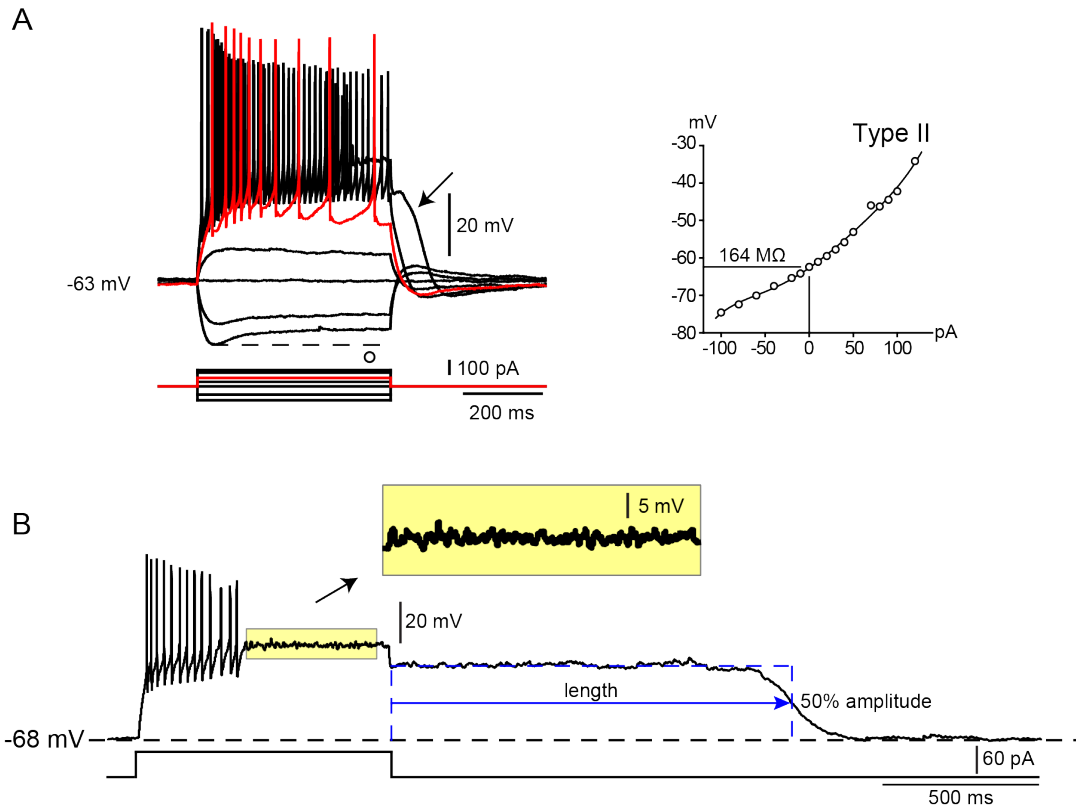


Figure 29. Plateau potentials and sub-threshold membrane oscillations in striatal THINs. A. A Type II striatal THIN with typical membrane resting potential and input resistance. Frequently, an afterdepolarization potential (ADP) occurs following the termination of current injection (black arrow). B. Sometimes, this ADP remains on well after the end of a depolarizing even, lasting a couple seconds or more. To distinguish this prolonged phenomenon from a far more transient ADP, the term plateau potential is used. In addition, while there are intrinsic oscillations evident throughout the plateau potential, there are also sub-threshold membrane potentials (SMO; yellow highlighted region) that occur during the depolarizing regime, which evident multiple oscillatory components and have a higher power of oscillation compared to the plateau potential oscillations.

SMOs and their modulation by DA

During the initial studies on striatal THINs, subthreshold membrane oscillations (SMOs) were observed during current injection, in the regime when a depolarization-block-like state occurred, and after action potential firing had ceased (see Fig. 30A). These oscillatory periods were quite distinct from PPs in that they displayed a broad spectrum of frequencies and amplitudes (see yellow highlighted region in Fig. 30A). To investigate further SMOs and whether, like PPs, they too were modulated by DA, we used fast-Fourier transform analysis (FFT) and a spectral analysis technique called Lomb-Scargle analysis (Lomb, 1976; Scargle, 1982; Ruf, 1999), which assigns significant values to the power spectrum and allows for statistical evaluation across pooled data and periodograms of that data to be made.

Striatal THINs were recorded in whole cell current mode, and injected with 125 pA of current for 2.5 seconds, giving rise to a prolonged SMO, which could be cropped for analysis (Fig. 30A, blowup cropped region from trace recording to the immediate left).

Cropped SMO regions were first inspected by FFT analysis and plotted as smoothed normalized

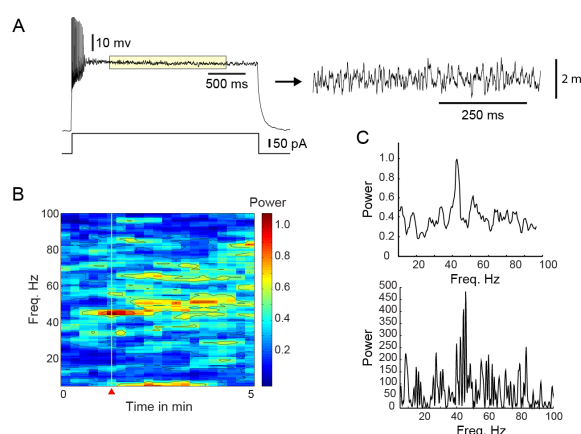


Figure 30. Striatal TH interneurons exhibit robust subthreshold membrane oscillations (modified from Ibañez-Sandoval and Xenias, et al., in revision). A, Whole-cell recording of a Type I THIN during prolonged current injection (125 pA for 2.5 seconds). SMOs were cropped and then processed by FFT analysis to produce a smoothed normalized heat map of the spectral power over time (B). C (top), a spectral power plot of the smoothed plot in B through the maximum value (yellow line) has a corresponding peak at the same frequency as that revealed by Lomb-Scargle analysis (C, bottom), showing the smoothed heat maps accurately reflect changes in spectral power.

heat maps of the power spectrum as a function of time and frequency, as shown in a representative example in Figure 30B. This heat map representation allowed for easy visualization of the data as a whole and identification of trends such as where peak changes in power occurred. A periodogram of the same raw FFT data through the peak power change is illustrated in Figure 30C (top) and illustrates that the heat map representation is in agreement with the FFT periodogram in showing a peak power change at around 40 Hz. A Lomb-Scargle periodogram gives the entire spectrum along with where significant values lie (Fig. 30C, bottom). This analysis also agrees with a significant difference in the power spectrum occurring at around 40 Hz. This shows that the analysis tools used are all in agreement with one another, and moreover that the heat map representations faithfully capture trends and allow for a global visualization of the entire data set.

DA or SKF 38393, a selective D1/D5-like agonist was bath applied during whole cell recordings and the respective SMOs for both the control (before start of drug application) and during bath application were analyzed and compared. Separate paired t-tests within the spectral bands corresponding to the theta, beta, and gamma range were performed to determine if there were any significant changes in modulation. The following frequency range conventions were adopted: 5-10 Hz for theta (DeCoteau et al., 2007; Hawes et al., 2013), 10-30 Hz for beta (Bibbig et al., 2001; Hammond et al., 2007; Leventhal et al., 2012), 30-70 Hz for “low” gamma, and 70 Hz and above for “high gamma” (Bibbig et al., 2001; Berke et al., 2009; Leventhal et al., 2012).

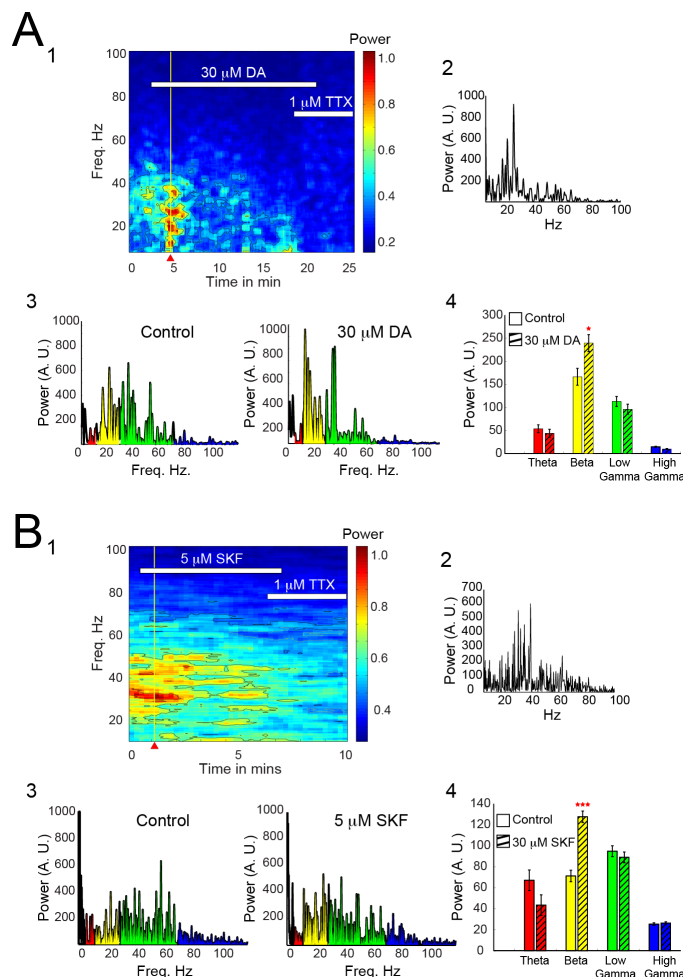
With these adopted conventions, analysis revealed that a bath application of DA (30 μ M) produced a transient increase of power in the 10-30 Hz or beta

frequency range of oscillation (Fig. 31 A1-A2). These transients were found to have a mean lifetime of 2.01 ± 0.07 minutes ($n = 3$) and a mean frequency of 21.9 ± 4.4 Hz (Fig. 31 A1). Moreover, DA induced a significant increase in the power in the beta range (mean power of control = 166.29 ± 18.33 ; mean power during drug application = 239.28 ± 27.73 ; $p < 0.05$, $df = 63$, Fig. 31 A3-A4).

Next, these experiments were repeated with SKF 38393, which exerted a similar but more prolonged modulatory effect that lasted throughout the duration of the drug application (compare Fig. 31 B1 with Fig. 31 A1). Furthermore, like DA, SKF 38393 significantly increased the power of the oscillations in the beta range (mean power of control = 71.12 ± 5.44 ; mean power during drug application = 127.52 ± 9.2 ; $p < 0.0001$, $df = 150$, $n = 3$, Fig. 31 B3-B4).

The observed differences in the lifetimes of the effects induced by DA and SKF 38393 are likely due to difference in their respective dissociation constants. The K_d of DA for the high-affinity state for D1R is 0.6 nM (Seeman, 1987). For SKF 38393, the K_d for D1R is 9.9 nM and the binding is readily reversible (Dubois et al., 1986). These differences in the affinities for the D1-like receptor suggest that the transient effect for DA compare to SKF 38393 is due to DA more readily desensitizing D1/D5 DA receptors, in which D1R is known to be variably desensitized in an agonist-dependent manner (Ng et al., 1994).

Lastly, a bath application of TTX ($1 \mu\text{M}$) significantly reduced the power in the beta frequency range ($p < 0.01$, $df = 63$) as well as the gamma frequency range (30 Hz and above; $p < 0.01$, $df = 150$) (Fig. 31 B1), demonstrating the SMO is in part generated by a sodium conductance.



show a significant increase in beta power during presence of DA ($n = 3$, $p < 0.05$, $df = 63$; mean power of control = 166.29 ± 18.33 ; mean power during drug application = 239.28 ± 27.73 ; A3-B4). B1, another Type-I THIN and its corresponding smoothed FFT heat map during bath application of 5 μ M of SKF 38393, a select D1/D5 class partial agonist and 1 μ M of TTX. B2, a Lomb-Scargle Periodogram of the spectrum at the time of maximum increase during the presence of SKF (yellow line in heat map of B1) shows for this example that again the peak power was in high beta range, as well as in the beginning range of the low gamma range. B3-B4, summary statistics of several recordings ($n = 3$), in which paired t-tests showed that power in beta however was the only spectral region that was significantly increased ($n = 3$, $p < 0.0001$, $df = 150$; mean power of control = 71.12 ± 5.44 ; mean power during drug application = 127.52 ± 9.20). * $p < 0.05$. *** $p < 0.001$.

Figure 31. D1/D5 receptor activation selectively and significantly increases beta power oscillations in THINs (modified from Ibañez-Sandoval and Xenias, et al., in revision). A1, whole cell recording of a Type-I THIN and its corresponding smoothed normalized FFT heat map during a bath application of 30 μ M of DA and 1 μ M of TTX reveals that DA produces a transient increase of power across the beta frequency range. TTX significantly abolishes the power in beta ($p < 0.01$, $df = 63$) and gamma ($p < 0.01$, $df = 150$) compared to the power of these ranges before start of drug application ($t=0$) as compared to the time during peak change in power (red triangle). A2, the Lomb-Scargle periodogram of the spectral power at the time of maximal power increase (yellow line in heat map of B1) reveals a sharp increase in power in the 15-25 Hz beta range. A3, Lomb-Scargle periodograms of pooled recordings ($n = 3$) of control and drug conditions, show clear increase of beta power during presence of DA. A4, paired t-tests for each of the separate mean frequency ranges of theta (5-10 Hz), beta (10-30 Hz), "low" gamma (30-70 Hz), and "high" gamma (70-100 Hz)

To further examine the ionic mechanism of the plateau potentials, TTX and cobalt-chloride (CoCl₂) was bath applied during whole cell recording of striatal EGFP-TH neurons when they were subjected a depolarizing current injection (Fig. 32, A2). A 250 pA current injection every 5 seconds evoked a depolarization block states and elicited broadband SMOs (Fig. 32B).

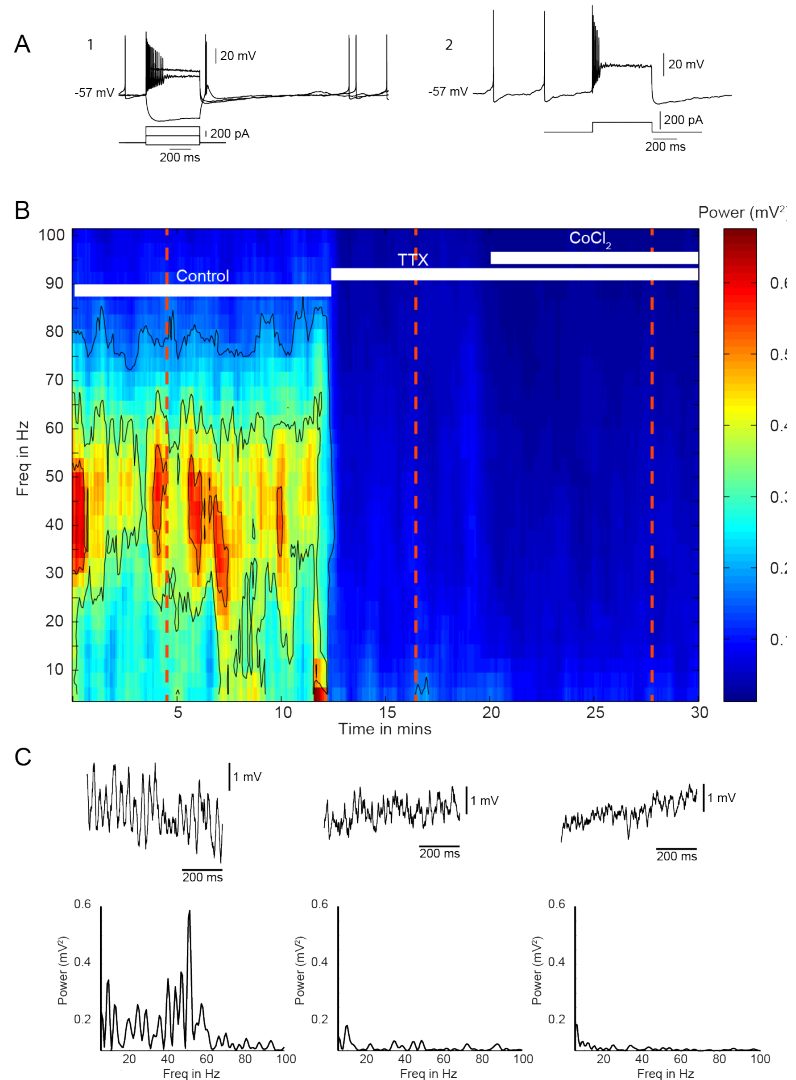


Figure 32. SMOs are TTX-sensitive sodium and calcium channel dependent. A current clamp recording traces (1) and injection protocol (2). B. Heat map of SMOs during applications of TTX and CoCl₂. C. Raw SMOs and their Lomb periodograms.

TTX and CoCl₂ significantly reduce the power of the SMOs across the frequency spectrum (Fig. 32, B-D). In response to depolarization, the SMOs of THINs typically have a broad spectrum around the high beta to low gamma frequency range (Fig. 33). TTX and CoCl₂ significantly lower the frequency of oscillation and the power across the spectrum (Fig. 32 A-B). The maximum

power for each regime (for the time traces shown through the dotted lines in Fig. 32B) was determined. The maximal power within the control region was 0.61 mV², corresponding to a dominant frequency of 48 Hz. The mean power of the control region was 0.47 ± 0.04 mV² (range, 0.08 - 0.61 mV²) and with a mean dominant frequency of 32 ± 5 Hz (range, 8 - 56 Hz). The maximal power during bath application of TTX was 0.19 mV² with a mean power of 0.15 ± 0.03 mV² (range, 0.02 - 0.19 mV²). The mean dominant frequency was 8 ± 0.6 Hz (range, 3 - 15 Hz). The maximal power during bath application of cobalt-chloride with TTX was 0.13 mV² with a mean of 0.11 ± 0.03 mV² (range, 0.01 - 0.11 mV²) and a mean dominant frequency of 7 ± 0.3 Hz (range 2 - 12 Hz). Both TTX and TTX with cobalt-chloride significantly reduced both the mean power and mean dominant frequency of the sub threshold membrane oscillations (unpaired t-test, $p < 0.0001$).

There was no significant change of the mean dominant frequency between any of the regimes for which there was a drug application. Although there was no significant change in the mean power of the SMOs between the cobalt-chloride and TTX applied regimes, there was a significant further reduction when both cobalt-chloride and TTX were applied ($p < 0.001$, $df = 97$ for cobalt vs. cobalt-chloride and TTX regimes, and $df = 121$ for TTX vs. cobalt-chloride and TTX regimes).

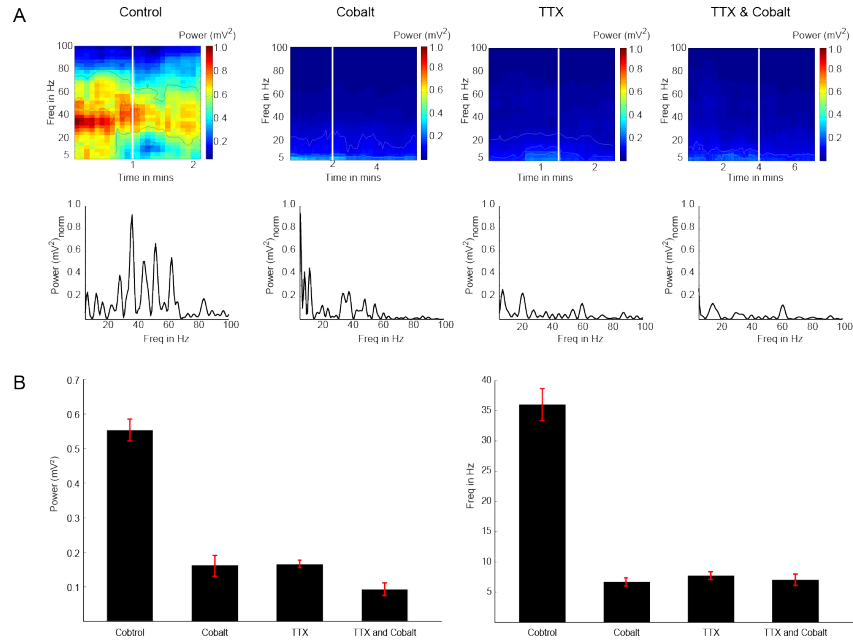


Figure 33. Both TTX-sensitive sodium channels and calcium influx are required to drive SMOs. A. Mean normalized heat maps of SMOs during control ($n = 7$) as well as during bath applications of cobalt ($n = 3$), TTX ($n = 3$), and TTX and cobalt-chloride ($n = 3$) (top row). The corresponding Lomb-Periodograms for each regime are shown below. The mean power and dominant frequency for the control regime was $0.55 \pm 0.03 \text{ mV}^2$ (range, $0.06 - 0.61 \text{ mV}^2$) and $36 \pm 3 \text{ Hz}$ (range, $24 - 52 \text{ Hz}$). For the cobalt alone regime, the mean power and mean dominant frequency was $0.15 \pm 0.7 \text{ mV}^2$ (range, $0.06 - 0.18 \text{ mV}^2$) and $6.8 \pm 0.6 \text{ Hz}$ (range, $2 - 14 \text{ Hz}$). Application of TTX gave a mean power and mean dominant frequency of $0.16 \pm 0.03 \text{ mV}^2$ (range $0.05 - 0.22 \text{ mV}^2$) and $7.7 \pm 0.6 \text{ Hz}$. The mean power and mean dominant frequency for the combine drug effects of TTX and cobalt-chloride was $0.09 \pm 0.04 \text{ mV}^2$ (range, $0.04 - 0.21 \text{ mV}^2$) and $7 \pm 0.9 \text{ Hz}$ (range, $2 - 10 \text{ Hz}$). Cobalt-chloride, TTX, and Cobalt-chloride with TTX all significantly reduced both the mean power and mean dominant frequency of the SMOs of the control regime ($p < 0.0001$, $df = 97$ for cobalt-chloride, $df = 119$ for TTX, and 175 for TTX and cobalt-chloride). B. Statistical bar graph summary.

CHAPTER IV

DISCUSSION

Dopaminergic neurons are a very small minority of striatal TH+ neurons

Since the discovery of striatal TH+ neurons in 1987 by Dubach, research has focused on two questions: whether they are dopaminergic neurons and whether they play a compensatory role for the loss of dopamine during the degeneration of the nigrostriatal system (Betarbet et al., 1997; Palfi et al., 2002; Huot et al., 2007). The unquestionable fact that these cells of the striatum were indeed expressing TH, the rate limiting enzyme for dopamine synthesis and a reliable neurochemical marker of mesencephalic dopaminergic neurons (Huot et al., 2007; Huot and Parent, 2007), immediately suggested that striatal TH+ neurons were dopaminergic. Additionally, this conclusion was further bolstered by the numerous reports of these cells increasing in number following loss of striatal dopamine, which was interpreted as a consequential induction of a dopaminergic phenotype by striatal TH neurons to balance reductions of nigrostriatal dopamine (Tashiro et al., 1989a; Tashiro et al., 1989b; Betarbet et al., 1997; Meredith et al., 1999; Mao et al., 2001; Petroske et al., 2001; Palfi et al., 2002; Jollivet et al., 2004; Mazloom and Smith, 2006; Tande et al., 2006; Darmopil et al., 2008).

Moreover, findings of inducible catecholaminergic phenotypes have been seen with cells in other brain regions, most notably in the arcuate nucleus (AN) of the hypothalamus following 6-OHDA induced destruction of the tuberoinfundibular dopaminergic system, where there is a consequential de novo expression of the requisite enzymes for dopamine synthesis, including TH and AADC (Ershov et al., 2005). Based on a double immunofluorescent examination, this study by Ershov et al. and previous ones (Ugrumov et al., 2002; Ugrumov et

al., 2004) found that in the AN of the hypothalamus, there are monoenzymatic neurons that express either TH+ or AADC+ but not both.

These findings of a mixed population of DAergic and non-DAergic neurons having common traditional neurochemical makers are also observed in the midbrain, where there are non-DAergic TH+ projections neurons that share nearly identical electrophysiologically profiles with DAergic neurons (Ungless and Grace, 2012), thus making clear identification of one type from the other difficult. The confusion among past reports concerning identifying dopaminergic neurons rests on the assumption that TH alone is a faithful DAergic indicator. The controversy of misidentifying neurons as DAergic often arises from using only a partial criteria, whether immunocytochemical or electrophysiological, which is customarily used to identify DAergic cells.

Such confusion in determining whether striatal TH+ neurons were DAergic was arguably evident in a report by Meredith et al. (1999), whose immunocytochemical-based study showed that there were very few AADC+ cells that were markedly different from striatal TH+ neurons in three major ways. First, neurochemically, it was clear that there were cells that were immunoreactive for dopamine or AADC and distinct from a separate cell population that were monoenzymatic TH+ neurons. Second, neuroanatomically, the cells that were AADC+ were confined to a relatively small anatomical region, namely the subcallosal, dorsal medial area of the caudate-putamen. In contrast, striatal TH+ only neurons appeared in both the ventral and dorsal striatum with no evident bias in distribution. Lastly, morphologically, the AADC+ cells confined within this subcallosal region were of a comparatively and significantly smaller size and had a noticeably different morphology, said to be reminiscent of

“local-circuit neurons.” In contrast, the striatal TH+ neurons were reported as being larger and having prominent, extended varicose processes, which were said to be indicative of “projection neurons.”

While the issue as to whether striatal TH+ neurons were interneurons or projection neurons had remained unresolved for over two decades, the preliminary examination based on their morphology, as evidenced in Meredith et al. (1999), suggested they were projection cells. In a subsequent, very detailed neuroanatomical study, however, it was shown that striatal THINs are interneurons (Ibanez-Sandoval et al., 2010). Much of the initial observations made in the 1999 study by Meredith et al., however, are in agreement with many of the findings of the past work by our lab, including THINs possessing expansive axonal fields and varicose primary dendrites (Ibanez-Sandoval et al., 2010; Tepper et al., 2010) as well as THINs being neuroanatomically unconfined and evenly distributed throughout the striatum (Unal et al., 2011). Other groups have also reported similar morphology and distribution of striatal monoenzymatic TH+ neurons in the mouse (Nagatsu et al., 1997; Darmopil et al., 2008).

More revealingly, Meredith et al. (1999) reported at most 8-20 AADC+ neurons, whose somatic size and morphology were different from TH+ neurons but not different from a population of cells that were immunoreactive for DA and which neuroanatomically overlapped with AADC+ cells. These observed differences between striatal TH+ only neurons and those that were immunoreactive for DA or AADC, underscore that striatal TH+ neurons are a distinct population from AADC+ or DAergic neurons.

Moreover, although no systematic stereological analysis of the ratio of dopaminergic cells to striatal TH+ neurons have been performed, the fact that at most 20 cells were seen by Meredith et al., illustrates that the cells observed to be dopaminergic in the striatum can only represent a very small fraction of the striatal TH+ population. Striatal THINs number at least 4,500 cells per mouse hemisphere (Unal et al., 2013). This means less than 0.5 % of the total striatal TH+ population can be dopaminergic.

Lastly, based on reports of their size, morphology, and distribution, the far more numerous monoenzymatic striatal TH+ neurons seen by others (Nagatsu et al., 1997; Meredith et al., 1999; Darmopil et al., 2008) are almost certainly the same striatal THINs reported by our lab (Ibanez-Sandoval et al., 2010; Unal et al., 2011; Unal et al., 2013) and others (Luo et al., 2013). The controversy of whether THINs were projection neurons was ended with the work by Ibañez-Sandoval (2010), and this his current work brings resolution to whether striatal THINs are dopaminergic by showing there is no evidence to support THINs are. THINs neither contain dopamine or any of requisite enzymes for dopamine synthesis, nor release detectable amounts of dopamine, even during pharmacological manipulation to enhance release and detection.

Immunocytochemical evidence that THINs are non-dopaminergic

Immunocytochemistry was performed to determine whether striatal THIN interneurons are dopaminergic. These experiments were fundamentally different from previous studies in systemically examining whether TH colocalized DA, AADC, VMAT2, and the DAT. A BAC mouse transgenic line

that expresses the enhanced GFP reporter under control of the regulatory elements of TH was used. This transgenic line removed the need for double immunocytochemistry and allowed optimized immunocytochemical detection of each marker. Other studies have relied only on immunocytochemistry, in which inferences of colocalization were based on whether cells expressing different neurochemical marker overlapped or shared similar morphologies (Meredith et al., 1999; Porritt et al., 2000).

In addition, many of these studies used double-labeled in situ hybridization or immunofluorescence (Betarbet et al., 1997; Cossette et al., 2005), in which optimizing for a single let alone multiple neurochemical markers are difficult and often give false positive results (Facer et al., 1980; Burry, 2011). This is a likely explanation for the many widely varying reports of the totality of striatal TH+ neurons, even for a given species. For primates, for instance, reports ranged from as low as ~30 TH+ cells per 100 mm² 40 μ m transverse sections (Tande et al., 2006) to well over several 100,000s per striatal hemisphere (Palfi et al., 2002).

The EGFP-TH mouse line not only eliminated the need to optimize immunocytochemical procedures for two antibodies but also served as a standard for comparing colocalization of different neurochemical markers both within and across different anatomical regions, such as between the midbrain and striatum. Moreover, this BAC transgenic mouse gave a more accurate and sensitive reporting of TH+ cells than immunocytochemistry because of multiple copies of the BAC, which produces a high number of the EGFP reporter.

In addition, in all these studies a rigorous control was performed in the midbrain to demonstrate the efficacy of the immunocytochemical detection for

each marker. This allowed for intelligent comparisons and unambiguous conclusions to be made about the presence or absence of a given marker in the striatum. In none of the previous studies was such a careful comparative control employed.

Absence of colocalization of EGFP-TH with dopamine in THINs

To investigate whether striatal THIN interneurons are dopaminergic, fluorescent immunocytochemistry was performed on a 6-OHDA unilaterally lesioned EGFP-TH transgenic mouse line. A modified glutaraldehyde-based perfusion solution by McRae-Degueurce (1986) was used with a glutaraldehyde-conjugated antibody for dopamine (see methods sections). This method was found to successfully label and colocalize DA and EGFP-TH dopaminergic projection neurons of the midbrain, including both the VTA and SNc (Fig. 3). Numerous EGFP-TH somata, including their axonal and dendritic processes colocalized DA, further illustrating the efficacy and sensitivity of the antibody used (Fig. 4). There were some DA⁺ only cells that were not colocalizing EGFP-TH (Fig. 4, white arrows). These cells appeared indistinguishable from the size and morphology of typical large somata of mesencephalic DAergic neurons, strongly suggesting that the lack of colocalization was not owed to non-specific labeling. This leaves at least two alternative possibilities. One is that these cells are dopaminergic but not containing TH. While this might seem contradictory, there is strong evidence, including the work of this current study, supportive of a cooperativity between monoenzymatic TH⁺ only neurons and AADC⁺ neurons that do not express TH to manufacture dopamine (see below for further

discussion of this). Second, in addition to transcription-dependent mechanisms that primarily turn off transgenes (Calero-Nieto et al., 2010) , there are also epigenetic-mediated effects that down regulate gene transcription via methylation (Pikaart et al., 1998). Specifically for TH, there are so-called “CpG islands,” or high frequency repeats of cytosine and guanine held by phosphodiester bonds, which are located near the regulatory elements for TH (Aranyi et al., 2002). These regions can be methylated, which then leads to a down-regulation and even non-expression of TH (Aranyi et al., 2005) and could account for why there are some DA⁺ only cells. The fact that there is dopamine expression but no EGFP fluorescence in such cells would imply that these DA⁺ cells either manufacture dopamine directly via AADC enzymatic conversion of L-DOPA secured by neighboring TH⁺ cells that produce and release L-DOPA, as known to occur in the arcuate nucleus (Ugrumov, 2009), or as a possible alternative suggestion, sequester extracellular dopamine via the DAT transporter.

Regardless of the mechanisms dictating TH expression in the midbrain, it is known that the mesencephalon consists of a heterogeneous population expressing other neurotransmitters and markers besides dopamine, which do not necessarily colocalize with DA and play functionally diverse roles (Yamaguchi et al., 2007; Nair-Roberts et al., 2008; Matsumoto and Hikosaka, 2009; Tecuapetla et al., 2010). The non-TH expressing dopaminergic cells of the midbrain can be further reflection of this diverse heterogeneity of mesencephalic neurons.

Additionally, as previously mentioned, numerous reports have found an increase in the numbers of striatal TH⁺ neurons following depletion of nigrostriatal dopamine, a conditional state presumed to induced a DAergic

status in THINs (Tashiro et al., 1989a; Betarbet et al., 1997; Meredith et al., 1999; Porritt et al., 2000; Mao et al., 2001; Unal et al., 2013). This apparent increase, however, is due to an upregulation of TH in THINs and only a modest and transient increase (Unal et al., 2013). In EGFP-TH mice whose midbrains were unilaterally lesioned, the ipsilateral striatal hemisphere underwent an increase of EGFP-TH expression. In comparison, the control striatal hemisphere, contralateral to the side of the lesion, did not undergo an upregulation of TH. In this way, comparison between the striatal hemispheres, one with an intact and functional nigrostriatal pathway and one degenerated, could be made.

The control striatum of mice, which had DA immunofluorescent labeling of their midbrain DAergic neurons, revealed no colocalization of DA and TH in any of the striatal THINs inspected (Fig. 5A and Fig. 6A). A high-magnified fluorescent photomicrograph of a representative striatal THIN in the dorsal striatum is shown in Figure 5A. Although there is abundant immunofluorescent labeling of the nigrostriatal axons, there is no somatic expression or colocalization with dopamine. There were however numerous DA+ puncta surrounding the perisoma, revealing a nigrostriatal enervation of the THIN that further demonstrated the efficacy of detecting DA in the striatum (Fig. 5A, bottom row). Lastly, the overall distribution of EGFP+ THINs found on this control side was in agreement with previous reports performed with these same mice (Ibanez-Sandoval et al., 2010; Unal et al., 2011; Unal et al., 2013).

Compared to the control side, the contralateral striatal hemisphere whose nigrostriatal dopamine system was degenerated (Fig. 5B, top row) evidenced a slight increase of THINs (cf. Fig. 5A, top row). Despite this increase, there was no colocalization of DA with any of the EGFP-TH cells examined. A high-

magnified fluorescent photomicrograph of another representative THIN (Fig. 5B, bottom row) shows no colocalization of EGFP with DA. There are also far fewer DA⁺ puncta in the surrounding area, revealing the degeneration of the nigrostriatal pathway.

Additionally, as compared to the background immunofluorescent labeling for dopamine in the axons and terminals of the SNc seen in the contralateral control side (Fig. 5A), there was a marked decrease of immunofluorescent background for dopamine in the ipsilateral side (Fig. 5B), which testifies to an effective overall degeneration of the nigrostriatal DAergic pathway.

Furthermore, these same observations were also found consistent for the ventral striatum as well (Figure 6). Once again in neither the control side (Fig. 6A) nor the ipsilateral side where the depletion of nigrostriatal dopamine occurred, was there any evidence of any colocalization of EGFP with DA. As found in the dorsal striatum, there was a marked decrease in the background immunofluorescence for DA in the ipsilateral striatal hemisphere compared to the contralateral striatum, yet there was still no colocalization of EGFP with DA for any of the EGFP⁺ striatal neurons examined. Additionally, in terms of their size and morphologies, EGFP⁺ cells were different from AADC⁺ striatal cells reported (Mura et al., 1995; Meredith et al., 1999; Lopez-Real et al., 2003).

With regard to distribution, it was evident that THINs reside slightly more in the ventral versus the dorsal striatum, an observation previously reported and quantified by our lab (Unal et al., 2013). THINs however were found evenly distributed throughout the dorsal-ventral axis, an observation that also has been noted in past publications (Ibanez-Sandoval et al., 2010; Unal et al., 2011). As previously mentioned, however, there exists an interesting distribution

among THINs along the dorsal-ventral axis. Unal et al. (2011) showed that there is a distribution of THINs in terms of a patch-matrix compartmental organization. While there was no overall difference of THIN subtype distribution along the dorsal-ventral axis, THINs were found mostly in the matrix compartment in the dorsal striatum, whereas THINs were mostly confined to the patch in the ventral striatum.

Moreover, as detailed in the results section, these same experiments were done with unilaterally lesioned EGFP-TH mice that were injected with L-DOPA in an attempt to either induce or increase any conversion of L-DOPA into dopamine in THINs. It has been reported that such L-DOPA pre-treatment reveals the presence of dopamine in AADC+ striatal cells (Mura et al., 1995; Mura et al., 2000). However, at least one other study found that administration of L-DOPA decreased the number of striatal dopaminergic neurons (Huot et al., 2008). The results of this thesis showed that L-DOPA pretreatment had no effect in eliciting detection of dopamine in THINs or the apparent number of THINs.

Lastly, despite no evidence that any of the striatal THINs expressed dopamine, there were however a very few small, faintly DA+ immunofluorescent somata (~3-8 per 60 μ m thick section), whose morphology and size are indicative of the ones reported by Meredith et al., and which moreover were located in the same region as she observed, namely along the subcallosal region of the dorsal and medial striatum. None of these cells colocalized EGFP however and were highly confined neuroanatomically and moreover exceeded no more than 20 cells per entire mouse striatal hemisphere (typically found within 2-4 consecutive 60 μ m thick sections), thus making them a very small numbering population of cells that are less than 0.5% of the TH+

neurons and that are unquestionably distinct from the far more numerous, larger, and evenly distributed striatal THINs examined. The findings of this result are in agreement with the report by Meredith et al. (1999) of there being two distinct populations observed, one consisting of a far more numerous and evenly distributed TH+ only cell population, which were comparatively larger and possessed more prominent arbors, and another population consisting of AADC+ or DA+ cells, which were found similar if not identical to one other in both size and morphology. This later population had smaller somata compared to TH+ neurons and possessed one or at most two shorter dendrites and resided in the subcallosal area of the medial dorsal region. In contrast, the morphology of THINs examined typically had 2-3 prominent, long dendrites, which branched about 20 μ m from the soma (see bottom rows in Fig. 6A and B). It is evident that striatal THINs are a different cell population from striatal AADC+ or DAergic cells reported in the literature.

Absence of colocalization of EGFP-TH with AADC in THINs

Although there was no colocalization of DA with any of the striatal EGFP-TH interneurons, a similar set of experiments was also performed for AADC immunocytochemistry. EGFP-TH mice were again used. A positive control for the AADC antibody was performed on the midbrains and revealed abundant colocalization of EGFP with AADC immunofluorescence (Fig. 7), demonstrating the efficacy and specificity of the antibody.

Inspection of the striatum of the same brains that demonstrated colocalization of EGFP and AADC in the midbrain, revealed immunofluorescent

AADC labeling of the nigrostriatal fibers (middle panel of Figure 8A), which also amply colocalized with EGFP+ fibers, thus offering further testament to both the sensitivity and specificity of the AADC antibody used. Despite this antibody efficacy, however, none of the striatal THINs examined demonstrated presence of AADC (Fig. 8).

Moreover, there were a very few number of immunofluorescent AADC+ striatal cells that were encountered but which did not express EGFP (see Fig. 9). These cells were found chiefly in the subcallosal dorsal medial striatum and were of similar size, morphology, and number as the immunofluorescent DA+ cells encountered. Although no systematic stereological analysis of them was made, their somatic width were typically about 6-8 μm and like the DA+ cells encountered mostly confined to the subcallosal area of the dorsal medial striatum. These observations are all in keeping with previous reports of striatal AADC+ cells in rodents (Mura et al., 1995; Meredith et al., 1999; Lopez-Real et al., 2003).

Meredith et al. (1999) suggested that these striatal non-TH+ expressing AADC+ cells are most likely the same striatal non-TH expressing DA+ population of cells observed, since the two populations both have very similar if not identical size and morphology, and which are confined to the same neuroanatomical location. Moreover, it has been observed that unlike striatal TH+ neuron, where dopamine depletion of the nigrostriatal pathway leads to an increase in their numbers, there was no such increase in the numbers of striatal AADC+ cells following 6-OHDA induced denervation of the nigrostriatal system (Lopez-Real et al., 2003). This further implies that the striatal THINs are indeed a distinct population from the striatal DA+ / AADC+ cells observed, and moreover,

the differential responses of these populations to Parkinsonian-like states implies functionally distinct roles as well

Lastly, the existence of these non-TH⁺ cells further underscores again that having TH expression alone does not necessarily reflect a true dopaminergic phenotype by virtue of not having the full requisite complement of enzymes to synthesize dopamine. As for the functional role of these non-TH AADC⁺ cells, once again, as suggested and more elaborated below, they might subserve a cooperative interaction between distinct monoenzymatic populations, neither of which alone can complete the catecholamine production pathway, but working in union can.

Absence of colocalization of EGFP-TH with VMAT2 in THINs

To determine whether THINs possess the capacity to vesicularly load DA, immunocytochemistry was performed for vesicular monoamine transporter-2 (VMAT2). EGFP-TH mice were again used to test for colocalization of EGFP-TH with VMAT2. EGFP-TH mice were unilaterally lesioned with 6-OHDA in the midbrain. The intact midbrain revealed a high efficacy of colocalization of VMAT2 with EGFP+ midbrain neurons (Fig. 10). While there was widespread colocalization of VMAT2 with nigrostriatal fibers throughout the striatum (Fig. 11A), there was no colocalization of VMAT2 with any of the striatal EGFP+ examined in either striatum (Fig. 11A-B).

Absence of colocalization of EGFP-TH with DAT in THINs

Finally, immunocytochemistry was performed to determine whether the dopamine transporter (DAT) is expressed in striatal EGFP-TH cells. DAT is a traditional neurochemical marker of midbrain DAergic neurons (Ciliax et al., 1995). In the monkey at least, there have been double-labeled immunocytochemistry reports of striatal TH+ neurons colocalizing with the DAT (Betarbet et al., 1997; Tande et al., 2006). In the human, TH mRNA-labeled striatal cells were found colocalized with the DAT (Cossette et al., 2005).

Moreover, the dopamine transporter plays a primary role in the regulation of extrasynaptic dopamine spillover, where DA signaling is conveyed by receptors chiefly at extrasynaptic locations (Cragg and Rice, 2004). Although the lack of either DA or AADC colocalizing with striatal THINs show THINs have

no innate capacity to synthesize dopamine, the argument could be made that THINs could obtain dopamine via uptake and further help participate in the gating of extracellular dopamine.

As a positive control for the DAT antibody, the midbrains of EGFP-TH mice were inspected for DAT and showed perisomatic colocalization with EGFP-TH (Fig. 12, white arrows, bottom row). The antibody labeled both mesencephalic somata and their associated processes, thus demonstrating the effectiveness and specificity of the antibody.

In the striatum of the same mice where there was ample colocalization of EGFP with the DAT in the midbrain, a careful examination showed EGFP+ somata did not colocalize the DAT (Fig. 13).

Moreover, since it is well known that there are regional differences in both the evoked release of [DA] and the uptake of extracellular dopamine, which are profoundly altered in Parkinsonism (Cragg et al., 2000), the EGFP-TH mice under examination all had their midbrain unilaterally lesioned to further see if DAT expression could be induced in a Parkinsonian state. This possibility is suggested by the finding that there were observed striatal bipolar neurons in Parkinsonian humans that expressed the DAT (Porritt et al., 2000). In keeping with past observations, there was once again a slight increase in the number of striatal EGFP-TH neurons in the side of the lesioning (Fig. 13B) as compared to the control side of the striatum (Fig. 13A). Neither side however evidenced any colocalization of DAT and EGFP-TH. Hence, nigrostriatal degeneration of dopamine had no effect in inducing DAT expression.

While the initial report by Porritt et al. (2000) seems to contradict these findings, it is important to keep in mind that the immunocytochemistry

performed for the DAT was done in the tissue of post-mortem patients. There is therefore a possibility that cellular decay and the method of tissue preparation, which surely did not entail as readily a quick fixation as routinely done with rodents, could have lead to non-specific labeling. Alternatively, this finding could be reflective of a species difference between human and rodents.

Additionally, it was later reported in a follow up study that patients with advanced Parkinson's disease appeared to have lost what were termed "dopaminergic neurons" of the striatum (Porritt et al., 2006). It is interesting to note that it has been shown that the compound MPTP selectively kills mesencephalic neurons via the uptake of the reactive byproduct MPP⁺ through the DAT and that DAT knockout mice are resistant to MPTP treatment (Bezard et al., 1999). This then suggests that DAT expression in the neurons observed in the Porritt et al. (2006) study could have similarly made the newly expressed "dopaminergic cells" vulnerable to the progression of Parkinson's disease. However, unlike the early 2000 study done by Porritt et al., this later study only examined striatal cells that were immunoreactive for TH and not DAT, thus making interpretation between the two studies extremely difficult. Moreover, the two studies by Porritt et al., reported similar morphologies. A comparative examination of the photomicrographs between the reports however shows that aside from having two primary dendrites, the morphologies of the cells depicted in these reports bear little in common with one another, and moreover are different from the distinct morphology of striatal THINs. It is likely then that these cells observed in the Porritt et al. studies are of cell types other than the striatal THINs examined in this work and more likely to be the ones seen by others in the rodent (Meredith et al., 1999).

Lastly, the lack of the DAT in striatal EGFP-TH interneurons is yet another example of how TH expression alone does not impart the full repertoire of neurochemical markers conventionally used as a DAergic marker

Voltammetric Evidence that Striatal THINs are Non-Dopaminergic

Although the traditional neurochemical markers used to identify dopaminergic neurons of the midbrain were found immunocytochemically absent in any of the striatal EGFP-TH interneurons examined, it can be argued that all series of experiments for each respective marker failed due to antibody insensitivity. This possibility is highly improbable for several reasons. First, each antibody used for the neurochemical markers proved highly efficient in labeling the DAergic neurons of the mesencephalon, including not only their somata but also their dendritic and axonal processes. Moreover, in the striatum, the nigrostriatal fibers were similarly strongly labeled (e.g. Fig. 8A). Each protocol was also separately optimized. Thus, the likelihood of any one series of experiments failing, let alone all, is unlikely.

Nonetheless, while these experiments revealed no immunocytochemical evidence of striatal THINs being dopaminergic, *in vitro* fast-scan cyclic voltammetry (FSCV) was also performed to determine if during optogenetic activation of striatal THINs any detectable amounts of dopamine could be released.

It has been previously shown that striatal THINs are GABAergic interneurons that synaptically inhibit medium spiny projection neurons (SPNs) (Ibanez-Sandoval et al., 2010). Moreover, it has recently been shown that

midbrain DAergic neurons can inhibit SPNs via vesicular release of GABA, whose loading of GABA is claimed to be independent of the GABA transporter VGAT and instead achieved through the monoamine transporter VMAT2 (Tritsch et al., 2012). Such a presumed non-canonical loading mechanism would then enable DAergic neurons to co-release GABA with DA. Additionally, single-cell RT-PCR performed on striatal THINs revealed that THINs possess the monoamine transporter VMAT1 (Ibanez-Sandoval et al., 2010), therefore suggesting a possible means of loading dopamine into vesicles for synaptic release, which furthermore makes the prospect of THINs being dopaminergic to be taken seriously. By itself, then, the fact that striatal THINs are GABAergic does not exclude the possibility that THINs could also be dopaminergic.

Recently, a report claimed there was detectable amounts of dopamine coming from striatal neurons during local electrical stimulation following chronic L-DOPA treatment in mice whose nigrostriatal fibers were degenerated by 6-OHDA (Espadas et al., 2012). The claim that the source of release was local to the striatum was argued there was an effective destruction of the nigrostriatal pathway at the sites where the FSCV recordings were conducted. While it is possible that long-term L-DOPA treatment can alter striatal gene expression (Westin et al., 2001; El Atifi-Borel et al., 2009), it is more likely that the source of DA detection was from nigrostriatal fibers surviving an incomplete 6-OHDA lesion made in the striatum. This is suggested in their first figure, which shows fibers immunoreactive for TH but shows no nearby TH⁺ soma that would account for a local source of DA. Moreover, the arborization of a single nigrostriatal axon can subtend up to 5% of the striatal volume (Matsuda et al., 2009), thus making it more likely that the source of the detected dopamine was

from surviving nigrostriatal fibers that were electrically activated during local stimulation. The lack of selectively activating striatal TH⁺ neurons in this study and the use of local stimulation therefore does not allow for an unambiguous interpretation of the source of detected dopamine.

For the series of voltammetric experiments used in this thesis research, however, TH-Cre transgenic mice were employed in combination with optogenetics to selectively target the striatal THIN population. Additionally, as with the experiments for the immunocytochemical studies, these mice similarly had their midbrains unilaterally lesioned with 6-OHDA to have both a contralateral control side and an ipsilateral side that would be in a Parkinsonian state. It should be noted, moreover, that unlike the aforementioned experiments by Espadas et al., which were based on 6-OHDA lesions being made locally in the striatum, all the lesions done in this thesis work were made in the midbrain. The smaller volume of the midbrain compared to the striatum, and direct injection of 6-OHDA at the origin of the nigrostriatal projection thus make for a more widespread and effective destruction of this widely projecting system. Special attention was paid to the location and volume of the 6-OHDA injection in the midbrain. Immunocytochemical assessments of the efficacy of lesions were made to refine the effectiveness of the 6-OHDA lesions. Initially, this was done to prevent any possible retrograde transduction of the mesencephalic DAergic neurons via the nigrostriatal fibers during striatal injection of cre-dependent virus to express ChR2 in THINs, thus eliminating possible false positive voltammetric results. Coronal sections of the midbrain for all the animals used were saved and later processed for TH immunoreactivity and inspected for any EYFP⁺ somata. No retrograde labeling was seen, a further testament to the

effective destruction of the nigrostriatal pathway (see Fig. 23, panel A2). Moreover, no local *electrically* evoked dopamine was observed in the ipsilateral striatal side of where the 6-OHDA lesions were made in the midbrains, further demonstrating an effective destruction of the nigrostriatal pathway.

Bilateral injections of both sides of the striatum with AAV-ChR2-EYFP lead to widespread transduction of the striatal THIN population (see Fig. 18). There was no apparent difference in the effectiveness of transduction for either side of the striatum relative to the side where the lesion in the midbrain was made. As detailed in the results section, the transduced EYFP⁺ THINs that were examined in TH-Cre mice possessed no differences in either their morphology or electrophysiology as compared to the EGFP⁺ THINs studied in EGFP-TH mice. Moreover, every EYFP⁺ THIN that was recorded was readily optogenetically activated, strongly demonstrating that the population as a whole was synchronously active during light stimulation.

As a positive control for the subsequent FSCV experiments conducted in the striatum, the midbrains of TH-Cre mice were injected with AAV-ChR2-EYFP, which transduced the nigrostriatal fibers (Fig. 18). FSCV recordings made in the striatum during optogenetic activation of the nigrostriatal axons demonstrated that dopamine was reliably detected and that the optogenetic approach was effective in eliciting dopamine release from DAergic neurons.

Optogenetic activation of the striatal THIN interneurons however elicited no detectable release of dopamine in either side of the striatum. The fact that no dopamine release was detected from the striata that had their nigrostriatal pathway depleted (see Fig. 23, A2 and Fig. 24B) is especially revealing that THINs are not dopaminergic, as depletion of striatal dopamine has been said to

convert TH⁺ neurons into DAergic neurons (Betarbet et al., 1997; Jollivet et al., 2004; Huot and Parent, 2007). An even more compelling conclusion that THINs do not release dopamine is that neither L-DOPA pretreatment, which increases DA production, nor use of pharmacological reagents, which enhance release and detection of dopamine, had any effect in detecting evoked dopamine release. Specifically bath applications of the D2 autoreceptor blocker raclopride and the dopamine reuptake blocker nomifensine had no effect in detecting released dopamine from THINs during their optogenetic activation. These reagents however were shown to have significantly increased the release of dopamine from the nigrostriatal pathway during local electrical stimulation of the striatum (see Fig 24. and Fig. 25).

Moreover, careful characterization of the detection sensitivity of the carbon fiber electrodes (CFE) used for these FSCV experiments were made, where the detection sensitivity for a given CFE was typically in the tens of nM range (see Fig. 17 and Fig. 25). Calibrations were made before and after a round of experiments and electrodes that were noisy were discarded. So as to minimize CFE surface obstruction from tissue during multiple insertions, no electrode was used for more than at most three times for recording at different sites. In addition, all CFEs were tested within the striatum of the control side during local electrical stimulation to verify that all the CFEs used during optogenetic activation of striatal THINs were functional, thus eliminating any false negative finding. This procedure was done both prior and after FSCV recordings done in the lesioned side of the striatum. These rigorous controls and precautions and high detection sensitivity are further convincing of there being no release of dopamine from striatal THINs.

Lastly, it should be further underscored that this optogenetic based strategy allowed for the synchronous activation of the striatal THINs during simultaneous FSCV recording (Fig. 21), which would further have maximized the concentration of any evoked dopamine release. This synchronous activation in combination with both L-DOPA pretreatment and the use of neuropharmacology to enhance dopamine detection make it extremely unlikely that any amount of dopamine released from THINs would have gone undetected. Therefore, insofar as physiological relevant amounts of dopamine are concerned, especially during behavior, *in vivo* voltammetry experiments show that naturally released dopamine are usually in the tens to hundreds of nM range (Robinson et al., 2002; Roitman et al., 2004; Beyene et al., 2010). Compared to the phasic firing of DAergic neurons, known to release as much as 1 μ M of dopamine, so-called “pacemaker” DAergic neurons tonically fire to release 5-20 nM of dopamine (Wanat et al., 2009). This low level of tonic firing release of dopamine being just under the detection threshold of the voltammetric setup used for these experiments might suggest the possibility that striatal THINs could normally be releasing very low levels of dopamine, as Type I and Type II THINs are found to be both spontaneously active. During optogenetic activation, however, a sufficiently long pulse of light was used to typically evoke 2 spikes from THINs and again synchronously as a population. For the transduced DAergic neurons of the midbrain, this duration of light stimulation typically produced around a 1 μ M release of dopamine (see Fig. 22E). However, during simultaneous FSCV, an optical train stimulation of striatal THINs using 10 blue light pulses of 5 ms duration with an interstimulus interval of 25 ms (Fig. 21B) did not produce any detectable amount of DA. Additionally, in several

experiments ($n = 3$; not shown) an optical stimulus of 5 pulses of 50 ms at 10 Hz was applied and still elicited no dopamine from either side of the striatum with respect to where the lesion in the midbrain was made. Reports by others using lower stimulation frequencies to mimic tonic firing during *in vivo* FSCV have shown evoked release of at least 40 nM (Howard et al., 2011), well above the noise level of the CFEs used for the voltammetric recordings during the optogenetic activation of THINs. Assuming there was any evoked dopamine released during optogenetic activation of striatal THINs that could have escaped detection by being below the sensitivity range of the CFEs used, it would also mean that such released concentrations would be below the ranges for behavioral importance, especially for any compensatory roles during Parkinson's disease, where phasic dopamine spillover of much higher concentrations would be required.

Electrophysiological Properties of THINs

In addition to conducting optogenetic-based voltammetry experiments, a series of optogenetic-based electrophysiology experiments were also conducted. This was to extend the study previously done by Ibañez-Sandoval et al. (2010) and compare the unitary versus population IPSP responses of SPNs from striatal THINs. For these experiments, TH-cre mice were again used, and bilateral intracerebral injections of AAV-ChR2-EYFP were made in the striatum. As observed for the voltammetric series of experiments, this led to widespread transduction of striatal THINs. Unlike EGFP-TH mice, where there is a background of nigrostriatal fibers, this optogenetic approach allowed for a

cleaner background, where the high level of EYFP+ expression in THINs permitted the striatal THIN network to be more readily seen and appreciated. THINs exhibit extraordinarily branched axonal and dendritic arbors, which extend appreciably far from their parent somata to overlap with the numerous arbors of other THINs (see Fig. 18 B-C). This visualization of a rich network of processes covering large areas of the striatum by itself suggests THINs have a widespread influence over the striatal microcircuitry. To further examine this, SPNs were patched in whole-cell while THINs were optogenetically activated. Lastly, this was done in unilaterally lesioned TH-Cre mice, where patch recordings were performed in both sides of the striatum, including the ipsilateral side to the lesion. This was done so as to demonstrate that no possible GABAergic contribution from the midbrain was made (Tritsch et al., 2012).

THINs control spike-timing and inhibit SPNs

It was previously shown in a limited but revealing number of paired recordings that THINs exerted powerful inhibition on SPNs (Ibanez-Sandoval et al., 2010). Optogenetic activation of THINs showed that SPNs were readily inhibited (Fig. 26) and that moreover, this inhibition was indeed GABA_A-mediated (see Fig. 27). Evoked IPSPs in SPNs during synchronous firing of THINs were more than sufficient to either delay spike arrival or ablate firing altogether (Fig. 26, red traces). Moreover, every SPN recorded was inhibited by THIN activation, revealing two findings. One, THINs exert a widespread inhibition onto SPNs throughout the striatum. Two, by fact that numerous SPNs were recorded during THIN activation, both D1 and D2 class dopamine receptor

expressing SPNs must be innervated and synaptically inhibited by THINs. While this study could not discern any subtype specificity, connection probabilities, or bias of THIN innervation for either the direct or indirect pathway system, it showed that THINs are positioned to exert widespread and rapid inhibitory influence on striatal output. The ability of THINs to exert this widespread inhibition on SPNs and affect spike timing therefore has important implications for spike-timing dependent plasticity (STDP).

Moreover, based on comparisons between unitary versus population IPSPs of SPNs by THINs, it was determined that the mean amplitude of the synaptic response to optogenetic stimulation was only about 3 times greater than the amplitude of the unitary response seen in paired recordings (see Fig.28). This would suggest that there is a sparse but strong inhibitory convergence of THINs onto SPNs, ranging from a minimum of two to as many as 5 THINs innervating each SPN. The fact that dopamine and acetylcholine have been found to powerfully excite THINs and even cause them to fire (Ibañez-Sandoval, unpublished work now in revision), moreover suggests that these cells can be synchronously activated by the widely projecting nigrostriatal pathway and cholinergic interneuron network. Intriguingly, in a recent publication, it has been shown that thalamic activation can trigger a synchronous activation of the striatal cholinergic interneurons, which in turn elicit an acetylcholine-evoked release of dopamine from nigrostriatal terminals (Threlfell et al., 2012). This same synchronous activation of cholinergic interneurons would then serve as a possible mechanism to synchronize the coordinated activity of THINs, in which their diverse electrophysiological subtypes could in turn differentially affect the spike timing of SPNs.

Neuromodulation of THINs

In addition to their subtype specific electrophysiology, striatal THINs also exhibited sustained plateau potentials and subthreshold membrane oscillations that were evident during depolarization (Fig. 29). Both of these separate features were found to be modulated by dopamine, a widely projecting neuromodulator that serves to sculpt both the sub- and suprathreshold activities of both striatal interneurons and projection neurons (Surmeier and Kitai, 1994; Tepper and Bolam, 2004; Surmeier et al., 2010). In addition, acetylcholine has been found to powerfully modulate THINs, evoking both burst firing and prolonged plateau potentials (Ibañez-Sandoval et al., in revision). Thus, striatal THINs, like other interneurons, are also modulated by dopamine and acetylcholine, which broadens their electrophysiological properties beyond those previously reported (Ibanez-Sandoval et al., 2010)

As previously mentioned, a separate study to investigate the modulatory role of DA and ACh on the PPs and SMOs of THINs was undertaken (Ibañez-Sandoval, Xenias et al., in revision). Three major findings were found. One, was that Type I and Type II THINs that evidenced intrinsic plateau potentials evoked from depolarizing pulses are facilitated by dopamine activation of the D1/D5-like dopamine receptor. Moreover, in Type I and Type II THINs that did not evidence intrinsic plateau potentials, dopamine instated their appearance, which again was effected via D1/D5-like dopamine receptor activation. In addition, Type IV THINs, which under normal condition never display a plateau potential, do so in the presence of dopamine, where it was shown that the expression of the plateau potential was also mediated via D1/D5-like dopamine receptor

activation. In each case where a plateau potential was evident, it was determined that I_{CAN} was the conductance responsible for the plateau potential (PP) and activated via an L-type Ca^{2+} -channel.

Second, THINs also exhibited subthreshold membrane oscillations (SMOs) that evidenced a broad spectrum of frequencies with varying powers. SMOs were systemically evoked by a depolarizing current, which enabled their analysis. It was found that dopamine significantly increased the power of the beta frequency range and shown to be mediated through D1/D5-like receptor activation.

Lastly, this same separate study by Ibañez-Sandoval (submitted and in revision) found that all THINs examined were excited by a puff application of carbachol, an acetylcholine agonist, which depolarized THINs with varying response profiles that were subtype dependent and which was mediated through Type 3 nicotinic receptor activation, which were moreover shown to be localized to THINs by use of TTX simultaneously present during carbachol puff applications.

DA modulation of plateau potentials

It was previously found that GABAergic neurons of the substantia nigra exhibit a plateau potential mediated by a calcium-activated non-specific cation conductance. Previous studies of other PPs showed the underlying conductance responsible for the PP was an I_{CAN} conductance (Lee and Tepper, 2007). This then suggested that the underlying ionic mechanism of the PP of THINs was similarly I_{CAN} .

It was found that substitution of sodium for choline chloride markedly decreased the duration of the PP (Ibañez-Sandoval, Xenias et al., in revision). Additionally, the substitution of calcium for sucrose or the use of the L-type Ca^{2+} channel blocker nimodipine completely removed the remaining PP. Moreover, flufenamic acid was found to completely abolish the PP, demonstrating that I_{CAN} is the charge carrier responsible for the PP. Together this data revealed that the underlying mechanism of the PP is a calcium-activated I_{CAN} cation conductance. The fact that this conductance is activated by calcium and dependent on sodium most identifies the I_{CAN} conductance as most likely mediated by the transient receptor potential cation channel melastatin (TRPM). More specifically, it is likely TRPM2, which is found chiefly in the brain, and activated by calcium, and nonselective to both calcium and sodium monovalent cations, and more revealingly inhibited by flufenamic acid (Fleig and Penner, 2004; Hill et al., 2004; Lee and Tepper, 2007; Lee et al., 2013).

In addition, THINs that do not express intrinsic PPs, including the Type IV THIN, which normally never evidence PPs, could be made to do so by blockade of a TEA-sensitive potassium channel conductance that otherwise masks the PP (Ibañez-Sandoval, Xenias et al., in revision). This finding is keeping with previous findings of the I_{CAN} expressed in GABAergic neurons of the substantia nigra that similarly have a persistently active potassium conductance that prevents expression of a PP (Lee and Tepper, 2007).

Moreover, dopamine greatly extends the duration of the intrinsic PPs, where the effect was observed after a bath application of the selective D1/D5-like dopamine receptor agonist SKF38393 (Ibañez-Sandoval, Xenias et al., in revision). Interestingly, a bath application of dopamine was also found to not only increase

the PP but also instate its expression when a THIN did not otherwise evidence a PP (see Fig. 31). These effects were abolished with the selective D1/D5-like dopamine receptor antagonist SCH-23390. It is worth noting that it has been reported that in EGFP-TH mice whose midbrains were unilaterally lesioned, the PPs of THINs had markedly reduced durations and a lower frequency of occurrences (Unal et al., 2013). This, then, reveals that dopamine can powerfully modulate THINs in not only prolonging PPs but also evoking them. Moreover, the underlying mechanism of the evoked PPs were found to be identical as with endogenously expressed PPs, namely those initiated by L-type calcium channel activation, where an influx of Ca^{2+} then activated an I_{CAN} conductance, identified by blockade with flufenamic acid (Ibañez-Sandoval, Xenias et al., in revision).

The likely site of initiating these modulatory effects is the L-type channel, which has been shown readily modulated by dopamine in a wide variety of neurons of the basal ganglia. For example, it has been reported that D1 receptor activation on a subset of striatal neurons can enhance L-type calcium currents via a cyclic AMP-dependent protein kinase A (PKA) pathway (Surmeier et al., 1995). Similar findings have been also seen in SPNs, where D1 activation can enhance L-type conductance sufficiently well to discharge SPNs (Hernandez-Lopez et al., 1997). Still more, the D5 but not the D1 receptor has been shown responsible for modulating L-type calcium conductance strong enough to lead to burst-firing of the neurons in the STN (Baufreton et al., 2003). In addition, dopamine has been found to similarly excite through D5 dopamine receptor activation both FS interneurons (Bracci et al., 2002) as well as PLTS interneurons (Centonze et al., 2002).

Interestingly, there is a differential expression of D1 and D5 dopamine receptors that is reflected in their differential levels between the SPNs and striatal interneurons. The D1 dopamine receptor, for example, is predominantly expressed in SPNs, whereas the D5 dopamine receptor is found expressed in the striatal interneurons and at particularly high levels in FS, PLTS, and cholinergic interneurons (Rivera et al., 2002). This differential expression of dopamine receptor subtype between the projection neurons and interneurons might perhaps reflect some organizational logic for the processing of excitatory input on SPNs. For instance, the interneurons play a major role in modifying both corticostriatal and thalamostriatal synaptic inputs onto SPNs via feed-forward inhibition (Koos and Tepper, 1999; Tepper and Bolam, 2004; Tepper et al., 2004; Tepper, 2006; Tepper et al., 2010). The main excitatory drive of the SPNs are massively convergent cortical innervation (Kress et al., 2013). The interneurons however are typically first activated before the SPNs and exhibit cell-type specific differences in their intrinsic spike-timing-dependent plasticity (STDP) that are dependent upon the temporal ordering and intervals between pre- and postsynaptic firing (Fino et al., 2008). Moreover, SPNs exhibit bidirectional plasticity that is also spike-timing dependent and exhibit both long-term depression (LTD) and long-term potentiation (LTP), which moreover are D1/D5 dopamine receptor dependent (Pawlak and Kerr, 2008).

In addition, with the exception of the FS interneurons, the input resistance of the SPNs is substantially lower compared to striatal interneurons (Kawaguchi, 1993), thus requiring SPNs to receive a higher convergent excitatory drive for them to reach spike threshold. The higher expression of the D5 dopamine receptor in FS interneurons compared to SPNs however positions FS

interneurons to be more readily activated during the presence of dopamine and brings them to threshold much sooner than SPNs. In addition, the D5 dopamine receptor has a higher affinity for dopamine compared to the D1 receptor (Pivonello et al., 2007; Beaulieu and Gainetdinov, 2011), which again is found more expressed in SPNs. This then endows the striatal interneuron population as a whole to be particularly sensitive to dopamine modulation. Evidence for dopamine playing this important modulatory role in the striatum is widespread (Tecuapetla et al., 2007; Surmeier et al., 2010; Surmeier et al., 2011), particularly in its involvement for the processing of reward-based information (Schultz, 2007, 2010a), and found playing similar roles for reward-related activity in other brain areas that have been shown to be dopamine D1/D5 receptor dependent (Hansen and Manahan-Vaughan, 2014).

Lastly, it might be that the higher expression levels of the D5 dopamine receptors in the FS, PLTS, and cholinergic interneurons are a specialized feature of striatal interneurons, which moreover striatal THINs could also possess. THINs, being powerfully modulated and frequently brought to threshold by dopamine, would appear to most likely also have a higher expression of the D5 receptor, which having a higher affinity for dopamine could be why THINs are so readily excited by dopamine, by again initiating L-type calcium channel activation (Surmeier et al., 1995).

DA modulation of subthreshold membrane oscillations

In addition to the plateau potentials, THINs also exhibited subthreshold membrane oscillations (SMOs), which have been observed in other striatal

interneurons (Bracci et al., 2002). It was found that either DA or the selective D1/D5 agonist SKF38393 powerfully modulated SMOs by significantly increasing the power in the beta frequency spectrum (see Fig. 31). There was a notable difference between the effects of dopamine and SKF38393 however. Whereas the effect of dopamine was transient (Fig. 31A), SKF38393 elicited a more prolonged enhancement of the power in the beta spectrum band (Fig. 31B). This is most likely reflected in the differences between the dissociation constants of the two ligand, where the K_d of dopamine for the high-affinity state for D1R is 0.6 nM (Seeman, 1987) and the K_d of SKF38393 for D1R is 9.9 nM (Dubois et al., 1986), thus reflecting a ten-fold difference. Others have reported these differences as well (Komiskey et al., 1978; Gredal and Nielsen, 1987). Unfortunately, there is currently no reagent to distinguish between the dopamine D1 and D5 receptor types (Pivonello et al., 2007), however the higher affinity of dopamine compared to SKF38393 for the D1 dopamine receptor suggests that the transient effects seen for dopamine compared to SKF38393 were due to dopamine more readily desensitizing the dopamine receptors, where D1R is known to be variably desensitize in an agonist-dependent manner (Ng et al., 1994). Moreover, while the mechanism by which dopamine modulates this change in the power of the SMOs remains to be clarified, it is however known that voltage-gated potassium (Kv) channels effect a decrease in axonal potassium current that are mediated by an increased cyclic AMP-dependent protein kinase A (cAMP-PKC) pathway (Yang et al., 2013), which in theory could effect the increase in the oscillatory power seen. Moreover, it appears a sodium conductance also contributes to the SMOs, as bath applications of TTX greatly reduced but did not completely eliminate the oscillations (Fig. 32 & Fig. 33). If Kv channels are involved, an

interplay between voltage-gated sodium and potassium conductances could underlay the SMOs observed.

Additionally, it is interesting to note that striatal beta power has been reported to increase following an instructive cue during an operant behavioral task and it has been suggested that this increase in beta oscillatory power serves to stabilize the striatal network and reduce interference from alternative actions (Leventhal et al., 2012). Such cues are also known to elicit transient phasic dopamine release, which encode reward prediction and incentive salience (Schultz, 1998). The dopamine-induced increase in the power of the beta band in THINs then suggests that these interneurons could be involved in the overall increase of power of beta oscillations in the striatum following cue presentation.

Lastly, one way in which THINs could contribute to this increase of beta frequency power in the basal ganglia is through their GABAergic synapses onto SPNs. While the means by which synchronization of oscillations in the neostriatum occurs are not fully understood, striatal neuron entrainment (Berke et al., 2004) and neuronal subtype specific modulation by oscillatory drive is known to occur (Sharott et al., 2009). Moreover, GABAergic interneurons play a pivotal role in both synchronizing and rhythmically entraining the coordinated activity of neural assemblies (Buzsaki, 2010; Egorov and Draguhn, 2013). In the striatum, for example, parvalbumin (PV)-expressing fast-spiking (FS) interneurons are known to intrinsically resonate in the gamma frequency range (Sciamanna and Wilson, 2011) and fire in phase with striatal local field potentials (LFPs) and oscillate in the gamma frequency range. This coordinated phase-locked firing, in turn, contributes to the entrainment of a subset of SPNs through inhibitory sculpting or selective modification of excitatory input (Popescu et al.,

2009). By analogy THINs might selectively coordinate their subthreshold membrane oscillatory activity by resonant entrainment to beta frequency oscillatory synaptic inputs onto THINs and in turn transmit these rhythmic patterns through their GABAergic synaptic inputs onto SPNs, thereby propagating beta frequency oscillations throughout the entire cortico-basal ganglia circuit.

ACh modulation of THINs

Like GABA, the effects of acetylcholine are mediated by both metabotropic and ionotropic receptors, which are diversely expressed in both a cell-type and subcellular manner (Bolam et al., 1988; Tepper and Bolam, 2004). Unlike the nicotinic receptors, muscarinic receptors are found postsynaptically expressed both on SPNs and striatal interneurons where they serve to modulate output excitability (Figueroa et al., 2002; Perez-Rosello et al., 2005; Shen et al., 2005; Shen et al., 2007). Their expression is also found on both GABAergic (Koos and Tepper, 2002) and glutamatergic terminals (Pakhotin and Bracci, 2007), where ACh exerts strong presynaptic inhibition (Zhou et al., 2003).

In contrast, the nicotinic receptors are chiefly limited to the striatal interneurons (Goldberg et al., 2012) where they are known to elicit excitatory effects on GABAergic interneuron firing (Koos and Tepper, 2002; English et al., 2012). In addition, they are also found directly on dopaminergic terminals (Marshall et al., 1997). Recently, it has been found that synchronous activation of cholinergic interneurons leads to the evoked release of dopamine, which is independent of DAergic neuronal discharge and most likely mediated by direct

activation of nAChRs that are located at the dopaminergic terminals (Cachope et al., 2012; Threlfell et al., 2012). Thus, acetylcholine serves to activate not only the striatal interneurons but also effect the release of yet another widely projecting neurotransmitter, dopamine, which itself has diverse effects on the striatal microcircuitry.

In EGFP-TH mice, striatal THINS were recorded in whole-cell during current clamp mode, where each THIN subtype was electrophysiologically identified and then a puff application of the acetylcholine agonist carbachol was made while each THIN was recorded at its resting membrane potential (Ibañez-Sandoval, Xenias et al., in revision). Type I, II, and IV all respond to carbachol, with Type I and Type IV THINs responding most powerfully, exhibiting strong bursts of firing, followed by prolonged plateau potentials that were, especially for Type IV, accompanied by action potential (AP) firing. Type II THINs, in contrast, only respond with modest EPSPs, typically being no more than 5 mV in amplitude (Ibañez-Sandoval, Xenias et al., in revision). Thus, THINs are strongly modulated by acetylcholine, in addition to DA, and exhibit subtype specific responses to the modulatory effects of ACh.

Additionally, the elicited depolarizations in response to puff applications of carbachol are unaffected by either MLA or DH β E but are eliminated by a bath application of the selective Type 3 nicotinic receptor antagonist mecamylamine, where moreover, a bath application of TTX during puff application of carbachol further demonstrated that the type 3 nAChRs are localized to THINs (Ibañez-Sandoval, Xenias et al., in revision). While the nicotinic receptor profile of this result differs from that more customarily seen with striatal GABAergic FS (Koos and Tepper, 2002) and NPY-NGF interneurons (English et al., 2012), it has been

similarly confirmed recently by another group (Luo et al., 2013) who show the same antagonist sensitivities for striatal Type I THINs and with cytisine, a selective $\alpha 3\beta 4$ agonist nicotinic agonist, which identifies the nicotinic receptor as again being Type 3.

Lastly, the fact that THINs powerfully exert GABAergic inhibition on SPNs and in a subtype specific manner further means that there is a more complex inhibitory striatal network through which *both dopamine and acetylcholine* can mediate their modulation, both directly on THINs and indirectly on SPNs through the elicited firing of THINs that synaptically inhibit SPNs.

But why TH? : The Monoenzymatic Cooperativity Hypothesis

Both the voltammetric and immunocytochemical results of this research showed that the striatal THINs are not dopaminergic. They do not have the intrinsic ability to express much less release DA. THINs were shown to not express DA, AADC, or the DAT and even with the use of pharmacology to enhance detection of evoked DA release, THINs evidenced no such capacity. It might seem puzzling then as to why THINs express the TH enzyme, which has conventionally been associated with cells having a dopaminergic status. As has been the case with other neurochemical markers, the inability to fully understand their function does not prevent their expression to be useful in their classification. For example, only recently has it become more fully understood what the functional role of parvalbumin is in striatal PV+ GABAergic FS interneurons (Ordaz et al., 2013). Similarly, the expression of TH can be thought of as a classifier of another GABAergic interneuron cell-type, whose unique neurochemical

composition also reflects unique electrophysiological profiles from that of other GABAergic interneurons.

While the exact role of TH in THINs still remains unclear, the work of this research showed that THINs are monoenzymatic TH⁺ only expressing GABAergic interneurons. Moreover, during the course of this work, it was discovered that there were other striatal non-TH monoenzymatic neurons as well, namely AADC⁺ neurons (see Fig. 9), which have also been reported by others (Mura et al., 1995; Meredith et al., 1999; Mura et al., 2000). The striatum, however, is not the only brain region where such examples of monoenzymatic TH⁺ or AADC⁺ neurons reside, in which there are many examples throughout the central nervous system, including the arcuate nucleus of the hypothalamus (Panayotacopoulou et al., 1994), the olfactory bulbs (Weihe et al., 2006), the cerebellum (Sakai et al., 1995), and the habenula (Weihe et al., 2006), to name only a few. Additionally, it has been shown that in addition to the true dopaminergic TH⁺ neurons that express AADC and VMAT2, there are also two other unique TH⁺ populations, respectively termed “nonexocytotic neurons” and “DOPAergic” neurons (Weihe et al., 2006).

The “nonexocytotic” TH⁺ neurons coexpress AADC but not VMAT2, giving them the capacity to synthesize dopamine but not the ability to vesicularly release DA. These neurons have been found in the striatum, but again are highly confined to the subcallosal dorsal medial area (Meredith et al., 1999) and are of a somatic size and morphology that are distinct from those of the THINs. Such examples of TH⁺ neurons colocalizing AADC

have also been observed by others and termed “bienzymatic neurons” (Ershov et al., 2002).

In contrast, the “DOPAergic” neurons are TH⁺ but have neither AADC nor VMAT2. These neurons do not possess the capacity to manufacture dopamine or the ability to vesicularly load and release any DA that they might be otherwise transported into them. However they still retain the ability to synthesize L-DOPA from the amino acid L-Tyrosine. L-DOPA, in turn can be readily transported across the cell membrane to and from the intercellular space through amino acid transporters (Kageyama et al., 2000; Quinones et al., 2004; Soares-da-Silva and Serrao, 2004).

Additionally, it has been reported that monoenzymatic TH⁺ or DOPAergic neurons do not coexpress VMAT2, and it has been proposed that the lack of VMAT2 expression is owed to a regulatory control dictated by a lack of bienzymatic expression (Weihe et al., 2006). This suggests that these two cell populations are mutually partitioned with tight regulatory control.

It has also been proposed that there might be a cooperative interaction between the monoenzymatic DOPAergic neurons and both the monoenzymatic AADC cells and bienzymatic nonexocytotic neurons, in which a monoenzymatic TH⁺ neuron can release L-DOPA to the intercellular space, where L-DOPA is then taken up by either monoenzymatic AADC⁺ cells or bienzymatic TH⁺/AADC⁺ neurons that would continue the catecholamine production pathway and synthesize dopamine (Ugrumov et al., 2002; Ugrumov et al., 2004; Ugrumov, 2009). In competitive inhibition studies of L-DOPA and the amino acid transporter with L-tyrosine, it was shown that suspended cells from the arcuate nucleus

of rat fetuses that contained TH⁺/AADC⁻ and TH⁻/AADC⁺ monoenzymatic cells but not DAergic cells, resulted in decreases of detected dopamine, as measured by high performance liquid chromatography (Ugrumov et al., 2004). In this same study, it was shown that the identical competitive inhibition procedure done in a cell suspension of the substantia nigra from the same fetuses, which contained genuine DAergic cells, lead to increases in dopamine. This supported the hypothesis that dopamine production among the monoenzymatic cells of the arcuate nucleus is done by transport of L-DOPA from TH⁺ only cells to AADC⁺ only cells that then synthesize DA, in which the decrease of dopamine production in the competitive inhibition study was due to L-tyrosine competitively inhibiting L-DOPA entry into AADC⁺ monoenzymatic cells, where moreover any L-tyrosine entry into these cells would have been unable to have been converted to DA because of the lack of TH. In contrast, for the cell suspension from the nigra, which were bienzymatic for TH and AADC, increases of L-tyrosine led to a concomitant increase in DA production.

It still remains unclear however how DA would then be released from the AADC monoenzymatic neurons. The synthesis of L-DOPA by monoenzymatic TH cells, however, would lead to an increase in DA production in bienzymatic exocytotic DAergic cells, being able to not only uptake L-DOPA but convert it directly to DA for synaptic release. In addition, it has been further suggested that L-DOPA may be subserving three other possible functions, including an intracellular signal to regulate metabolism, an ontogenetic regulator of neural differentiation, and an

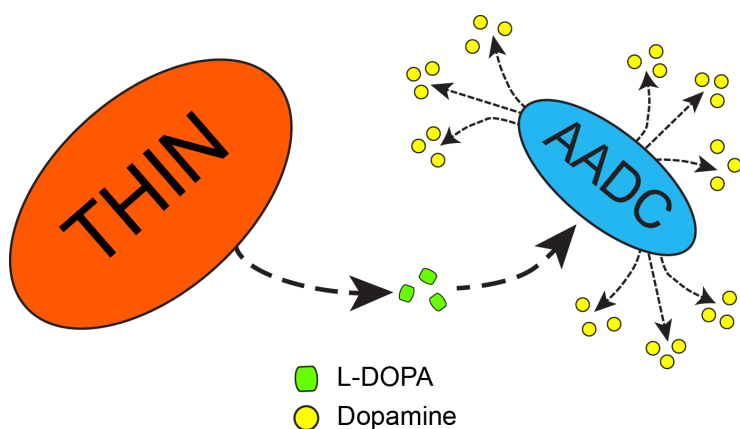


Figure 34. Monoenzymatic Cooperativity. Striatal THINs, having TH but not AADC can synthesize L-DOPA, which is then transported out into the intracellular space via the amino acid transporter (AAT). L-DOPA in turn is taken up by AATs located on the membrane of monoenzymatic AADC+ containing cells or nigrostriatal terminals, which then use the imported L-DOPA to synthesize DA.

intercellular
modulator
controlling both
AADC activity and
DA output from
DAergic cells
(Ugrumov, 2009).

Finally, the
findings of THINs
neither expressing
nor releasing DA,

strongly supports that THINs are monoenzymatic TH⁺ only cells. Similar to the TH⁺ neurons of the hypothalamus that do not express DA, even after L-DOPA treatment (Zoli et al., 1993), THINs do not express AADC. Moreover, in light of the fact that the number of THINs increase during degeneration of the nigrostriatal dopamine system (Unal et al., 2013), which is not owed to neurogenesis (Tande et al., 2006), reveals that this increase is due to an upregulation of TH. Commensurate with this upregulation of TH must be an accompanying increase in L-DOPA, which can then be transported to the intercellular space through the aforementioned amino acid transporters. Perhaps, then, while not being DAergic themselves, THINs could nonetheless be participating in an indirect compensatory manner for the loss of nigrostriatal dopamine by supplying monoenzymatic AADC cells and surviving nigrostriatal terminals with L-DOPA for increased dopamine production in Parkinsonian states (Fig. 34). Most of the striatal AADC is

found in nigrostriatal terminals (Koller and Rueda, 1998), which suggests any monoenzymatic cooperativity is most likely taking place between THINs and the terminals of the nigrostriatal pathway. In normal conditions, THINs might be serving to help regulate the basal level of extracellular dopamine by maintaining a steady supply of L-DOPA to the extracellular space to be converted into DA by AADC containing cells or the nigrostriatal terminals. Indeed, the large arbors that THINs possess would make them ideal for this possibility, as they could supply L-DOPA over relatively large regions.

Functional Significance and Concluding Remarks

The striatum is involved in learning (Graybiel et al., 1994; Dezfouli and Balleine, 2012) and processing salient cues that predict reward (Schultz, 1998, 1999). Synaptic plasticity underlies most forms of learning and is dependent upon both non-Hebbian and Hebbian forms to effect either long-term potentiation (LTP) or long-term depression (LTD) and in a bidirectional, synapse-specific manner (Abbott and Nelson, 2000; Fino et al., 2005; Piochon et al., 2012). Striatal interneurons are involved in these processes (Apicella, 2002; Kimura et al., 2003; Yamada et al., 2004; Fino and Venance, 2011), which are affected by spike-timing-dependent plasticity (STDP) (Fino et al., 2008; Fino and Venance, 2011) and the organized timing of pre- and postsynaptic firing (Bi and Rubin, 2005; Florian, 2007; Fiorillo et al., 2008) that effect bidirectional changes between LTP and LTD (Fino et al., 2005; Fino et al., 2008; Shen et al., 2008).

In addition, striatal interneurons exhibit cell-specific STDP and are intimately involved in modifying the integration of corticostriatal inputs onto SPNs (Fino et al., 2008) and play a permissive role in determining striatal output,

which is achieved in a feed-forward fashion by a coordinate interplay of LTP and LTD effected by the diverse striatal interneurons that synapse onto a projection neuron (Centonze et al., 1999). The temporal relationships between the presynaptic firing of corticostriatal projection cells and their postsynaptic striatal targets is a key determinant of the particular form of STDP an interneuron will display, namely LTP or LTD (Spencer and Murphy, 2000; Sjostrom and Nelson, 2002; Bi and Rubin, 2005; Dan and Poo, 2006; Caporale and Dan, 2008; Hopf et al., 2010). These temporal relationships are in part determined by corticostriatal excitatory input, which evokes differential activation times among the different interneurons in a cell-specific manner that is dependent upon intrinsic postsynaptic latencies and rise times (Fino et al., 2008). For instance, in response to cortical input, both NOS-expressing PLTS and FS GABAergic interneurons are activated before cholinergic interneurons, and all three types of interneurons are activated before SPNs, where LTP and LTD of the GABAergic interneurons are evoked, respectively, by a pre-post and post-pre STDP activation sequence (Fino et al., 2005; Fino et al., 2008; Fino et al., 2009; Fino et al., 2010; Fino and Venance, 2011). Moreover, each cell type of the heterogeneous striatal interneuron population exhibits distinct synapse specificities with SPNs, which in turn orchestrate together to determine the degree of inhibitory influence on striatal output (Fino et al., 2008). Fast-spiking interneurons, for example, exert powerfully feed-forward inhibition onto SPNs (Koos and Tepper, 1999, 2002) by making numerous postsynaptic contacts preferentially with the somata of SPNs (Kita et al., 1990; Bennett and Bolam, 1994). FS cells are then positioned to efficiently veto or delay excitatory input onto SPNs (Kita, 1996; Plenz and Kitai, 1998; Koos and Tepper, 1999). In contrast, NOS-expressing interneurons make a

comparatively smaller number of synapses that are chiefly located on the necks of spines of the projection neurons (Kawaguchi, 1993; Kubota and Kawaguchi, 2000). While the fewer number of synapses made by NOS GABAergic interneurons onto SPNs cells does translate into a lower inhibition level compared to FS (Gittis et al., 2010), it does not however affect their ability to likewise efficiently inhibit projection neuron activity in either delaying the arrival of an action potential or preventing it altogether (Koos and Tepper, 1999; Tepper and Bolam, 2004). Still more, there are also secondary modulatory effects that are concomitant with NOS-expressing cells that release NO, which exerts an excitatory role on SPNs (Sardo et al., 2002; West and Grace, 2004). Together, all these factors serve to affect striatal output, where in part the net plasticity of the inhibitory network on a SPN will then determine the modified output of the SPN (Centonze et al., 1999; Fino and Venance, 2011).

In addition, there are also the cholinergic interneurons (CINs), which although not GABAergic can effect inhibition via M4 muscarinic receptors, which modulate voltage-gated channels (Zhou et al., 2002). Their arbors are widely projecting, forming up to a 1 mm wide dendritic field and receive both cortical and thalamic innervation (Tepper and Bolam, 2004). More importantly they are well integrated into the striatal microcircuitry, both receiving inhibitory inhibition through recurrent inhibitory networks (Sullivan et al., 2008) and innervating other interneurons (Koos and Tepper, 2002) as well as the SPNs (Ding et al., 2010). In general, the responses of cholinergic interneurons are more complex, effecting differential inhibitory as well as excitatory roles (McCool et al., 2008) and are implemented with reward-based behaviors (Aosaki et al., 1994b; Apicella, 2002; Tepper and Bolam, 2004; Yamada et al., 2004). In addition

to acetylcholine released by CINs, there is also dopamine, another widely projecting neuromodulator that is released by the nigrostriatal terminals and plays a significant role in sculpting the activity of both the striatal interneurons and the SPNs (Fiorillo et al., 2008; Shen et al., 2008; Flores-Barrera et al., 2011; Hong and Hikosaka, 2011; Freeze et al., 2013). Both acetylcholine and dopamine, moreover, are in intimate overlap with one another (Centonze et al., 2003; Tepper and Bolam, 2004; Aosaki et al., 2010) and both are intricately involved in the information processing of reward-based events and salient cues (Schultz, 1998, 1999; Apicella, 2002; Kimura et al., 2003; Schultz, 2007; Beyene et al., 2010; Goldberg and Reynolds, 2011; Threlfell and Cragg, 2011; Baik, 2013).

This interneuron-level network, then, is highly dependent upon the overall *dynamical state* of the system. The timing of the respective activities of each component member in terms of the temporal dynamics between pre- and postsynaptic cells and level of modulation lead to readily observed network states encoded by large ensembles of neurons whose activities are highly correlated with one another (Carrillo-Reid et al., 2008; Carrillo-Reid et al., 2009). It is now understood that feedforward inhibition by the GABAergic interneurons modify corticostriatal input and determine the spike timing of the activity of SPNs, and that the ACh released by CINs, as well as nigrostriatal dopamine, play mostly a modulatory role, the two neuromodulators released and temporally overlapping with one another during reward-based behaviors (Schultz, 1998, 1999; Roitman et al., 2004; Hikosaka et al., 2006; Calabresi et al., 2007; Schultz, 2007; Hikosaka et al., 2008; Matsumoto and Hikosaka, 2009; Beyene et al., 2010; Schultz, 2010a).

THINs, receiving both dopaminergic and cholinergic input, are capable of being affected by both neuromodulators to participate with the rest of the GABAergic interneuronal networks to modify corticostriatal information. Their ability to be modulated by both DA and ACh, moreover, suggests they are involved in the processing of the saliency of cues and reward prediction. It is thought that the DAergic neurons of the midbrain predict reward and encode the discrepancy between reward expectation and outcome (Schultz, 1998, 1999). Salient cues that signal reward are followed by a so-called “pause” in the tonically firing of CINs, which is sometimes preceded by an increase in their firing but more frequently followed by a short rebound burst-like increase in firing (Aosaki et al., 1994a; Aosaki et al., 1994b; Aosaki et al., 1995; Apicella, 2002; Aosaki et al., 2010). The pauses of CINs prove to be very stereotyped in duration, typically lasting a few 100 ms in length, and determined by two hyperpolarization-activated currents, which are regeneratively amplified by a Kir current and whose cessation is triggered by a time-dependent nonspecific cation current mediated by the hyperpolarization-activated cyclic nucleotide-gated (HCN) channel (Wilson, 2005).

Moreover, associated with a salient cue is also a burst in midbrain DAergic neurons, which effects a reciprocal relationship between the release of dopamine and acetylcholine (Aosaki et al., 2010) and where concomitant with the pause is an accompanying burst of midbrain DAergic neurons. The mechanisms underlying this relationship remains still not fully known, however recently it has been shown that the DAergic midbrain neurons themselves via dopamine release can evoke the pause seen in CINs (Chuhma et al., 2014).

During the pause there might be regional differences of ongoing striatal activity dictated in a regional manner. For example English et al (2011) found no apparent changes in firing rate of SPNs recorded in the dorsal striatum, whereas it has been reported that photoinhibition of the CINs increases the firing of the SPNs in the ventral striatum (Witten et al., 2010). However, after the rebound firing of the CINs, there is a powerful feedforward disynaptic GABA_A-mediate inhibition of SPNs effected by GABAergic NPY-NGF interneurons (Ibanez-Sandoval et al., 2011). This inhibition is initiated by activation of Type 2 nAChRs on the NPY-NGF interneurons (English et al., 2012) and effects a particularly long lasting, slowly inactivating IPSC (Ibanez-Sandoval et al., 2011).

It has also been shown that in addition to dopamine controlling CIN activity, synchronous release of ACh in turn can evoke dopamine release (Cachope et al., 2012; Threlfell et al., 2012). This then suggests a context of functional integration of THINs with the rest of the striatal microcircuit, in which upon presentation of a salient cue, midbrain DAergic neurons would fire and trigger release of DA that in turn would activate both THINs and the NPY-NGF interneurons as well. This phasic release of dopamine would be coincident with a synchronous pause of CINs, where followed a few hundred ms later, a synchronous release of acetylcholine would occur during rebound firing of the CINs. This in turn would result in an ACh-evoked release of dopamine from nAChR activation of the nigrostriatal terminals as well as an ACh-induced activation of THINs.

In addition to both the THINs and NPY-NGF interneurons firing after the rebound of the CINs, the THINs would have the additional ability to fire earlier during the nigrostriatal reward prediction signal, thus involving them in the

learning process. It is worth noting that dopamine is required for corticostriatal STDP (Pawlak and Kerr, 2008) and that informational saliency that leads to learning in the hippocampus is dopamine D1/D5 receptor mediated (Hansen and Manahan-Vaughan, 2014).

During firing, an AP can back-propagate into the higher order dendrites of a neuron, thus affecting dendritic calcium levels, where the particular form of plasticity it will take is dependent on whether the arrival of a presynaptic corticostriatal input preceded or followed the back-propagating AP (Pawlak and Kerr, 2008). One way, then, that THINs might be involved in reward learning is through their L-type calcium channels being modulated by dopamine, in which D1R activation is known to enhance L-Type currents (Surmeier et al., 1995) that in turn would enhance calcium levels and might subserve the strengthening of plasticity during release of dopamine.

Lastly, while the THINs themselves are not DAergic, they are highly responsive to dopamine and most likely involved in the reward prediction circuitry of the striatum. The view of them being “dopaminergic” has taken focus away from their important electrophysiological properties and effecting of SPN activity. They are to be no less considered than any of the other GABAergic interneurons in terms of wanting to understand the striatal microcircuitry and how individual interneurons are activated to produce the ensemble responses known occurring during striatal information processing. The fact that more than one neuron is involved with different informational processes then begs the question of how an interneuron can subserve different functional roles. THINs offer an illustrative example of how this might be done through the use of neuromodulators that would serve to both coordinate and pattern their activity

as an ensemble.

The nigrostriatal

reward

prediction signal

would, along

with the

consequent

synchronous

release of ACh,

trigger a

patterned

“doublet” firing

(Fig. 35),

whereas for the

NPY-NGF cells,

the same

eliciting firing of

midbrain

DAergic firing

would evoke only a “singlet” firing. Moreover, the ensemble firing of THINs and NPY-NGF interneurons would be patterned in sequence with THINs firing first, followed by a few hundred milliseconds later with both THINs and NPY-NGF interneurons firing. In addition, DA could help coordinate the subthreshold membrane oscillations of an ensemble of THINs through a resonant entrainment to beta frequency oscillatory synaptic inputs onto THINs, which in

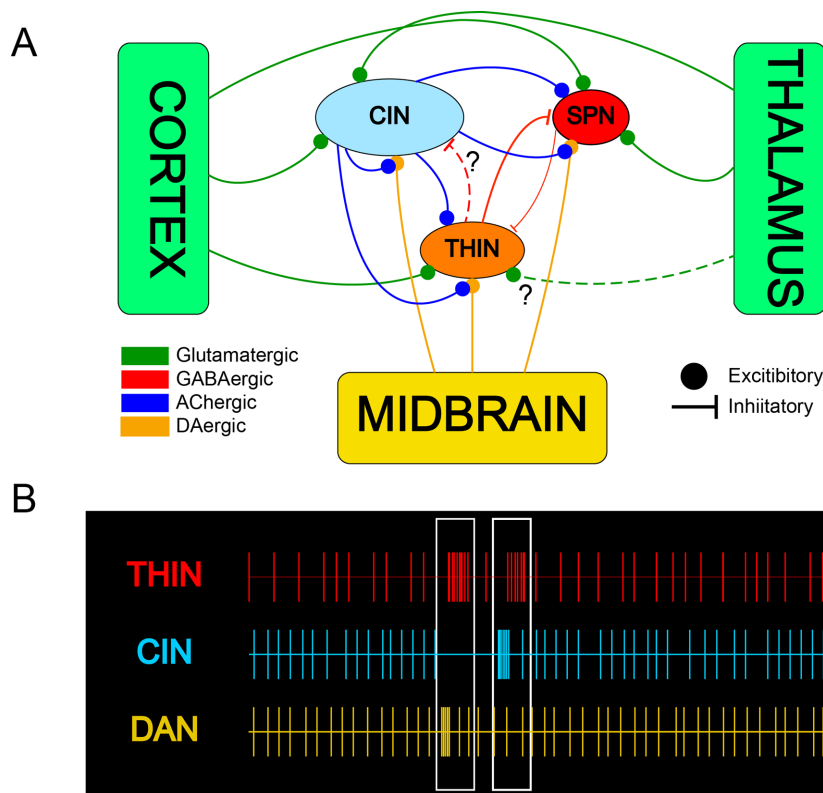


Figure 35. Proposed coordinated neuromodulation of THINs. A. Schematic wire diagram of a striatal microcircuitry between a THIN, CIN, and SPN. CINs innervate THINs and SPNs, as well as DAergic nigrostriatal terminals, which innervate SPNs and the other cell types. B. Illustration of a temporal raster plot of a THIN, CIN, and SPN. During a burst of midbrain DAergic neurons encoding the reward prediction error, THINs will first burst while CINs are paused in unison for a stereotyped duration, where upon their rebound, synchronously release ACh, which induces a synchronous release of DA from nigrostriatal terminals. During this synchronous release of ACh, followed immediately by DA, THINs are induced to burst a second time, with ACh and DA most likely synergistically enhancing the second burst of THINs. Thus this coordinated neuromodulation of THINs leads to a “doublet” firing of THINs.

turn would broadcast this rhythmic pattern throughout the basal ganglia through their GABAergic synaptic inputs onto SPNs and other interneurons. In the absence of dopamine, individual THINs would then be free to carry out other informational processes. With such a viewpoint, how individual cell types can be elicited wholesale for a given neural computation and coordinated with other cell types to process one type of information over another becomes clearer when seen as patterned groupings of sequences and offers a way of looking at how the small scale microcircuits studied in vitro give rise to the large-scale orchestration of networks that lead to learning and behavior.

REFERENCES

- Abbott LF, Nelson SB (2000) Synaptic plasticity: taming the beast. *Nat Neurosci* 3 Suppl:1178-1183.
- Adams JC (1981) Heavy metal intensification of DAB-based HRP reaction product. *J Histochem Cytochem* 29:775.
- Airan RD, Thompson KR, Fenno LE, Bernstein H, Deisseroth K (2009) Temporally precise in vivo control of intracellular signalling. *Nature* 458:1025-1029.
- Alexander GE, Crutcher MD, DeLong MR (1990) Basal ganglia-thalamocortical circuits: parallel substrates for motor, oculomotor, "prefrontal" and "limbic" functions. *Prog Brain Res* 85:119-146.
- Aoki C, Pickel VM (1989) Neuropeptide Y in the cerebral cortex and the caudate-putamen nuclei: ultrastructural basis for interactions with GABAergic and non-GABAergic neurons. *J Neurosci* 9:4333-4354.
- Aosaki T, Graybiel AM, Kimura M (1994a) Effect of the nigrostriatal dopamine system on acquired neural responses in the striatum of behaving monkeys. *Science* 265:412-415.
- Aosaki T, Kimura M, Graybiel AM (1995) Temporal and spatial characteristics of tonically active neurons of the primate's striatum. *J Neurophysiol* 73:1234-1252.
- Aosaki T, Miura M, Suzuki T, Nishimura K, Masuda M (2010) Acetylcholine-dopamine balance hypothesis in the striatum: an update. *Geriatr Gerontol Int* 10 Suppl 1:S148-157.
- Aosaki T, Tsubokawa H, Ishida A, Watanabe K, Graybiel AM, Kimura M (1994b) Responses of tonically active neurons in the primate's striatum undergo systematic changes during behavioral sensorimotor conditioning. *J Neurosci* 14:3969-3984.
- Apicella P (2002) Tonically active neurons in the primate striatum and their role in the processing of information about motivationally relevant events. *Eur J Neurosci* 16:2017-2026.
- Aranyi T, Kerjean A, Toth S, Mallet J, Meloni R, Paldi A (2002) Paradoxical methylation of the tyrosine hydroxylase gene in mouse preimplantation embryos. *Genomics* 80:558-563.
- Aranyi T, Faucheux BA, Khalfallah O, Vodjdani G, Biguet NF, Mallet J, Meloni R (2005) The tissue-specific methylation of the human tyrosine hydroxylase gene reveals new regulatory elements in the first exon. *J Neurochem* 94:129-139.
- Aslan A, Bauml KH (2012) Adaptive memory: young children show enhanced retention of fitness-related information. *Cognition* 122:118-122.
- Baik JH (2013) Dopamine signaling in reward-related behaviors. *Front Neural Circuits* 7:152.
- Bateup HS, Santini E, Shen W, Birnbaum S, Valjent E, Surmeier DJ, Fisone G, Nestler EJ, Greengard P (2010) Distinct subclasses of medium spiny neurons differentially regulate striatal motor behaviors. *Proc Natl Acad Sci U S A* 107:14845-14850.
- Baufreton J, Garret M, Rivera A, de la Calle A, Gonon F, Dufy B, Bioulac B, Taupignon A (2003) D5 (not D1) dopamine receptors potentiate burst-

- firing in neurons of the subthalamic nucleus by modulating an L-type calcium conductance. *J Neurosci* 23:816-825.
- Beaulieu JM, Gainetdinov RR (2011) The physiology, signaling, and pharmacology of dopamine receptors. *Pharmacol Rev* 63:182-217.
- Bennett BD, Bolam JP (1993) Characterization of calretinin-immunoreactive structures in the striatum of the rat. *Brain Res* 609:137-148.
- Bennett BD, Bolam JP (1994) Synaptic input and output of parvalbumin-immunoreactive neurons in the neostriatum of the rat. *Neuroscience* 62:707-719.
- Bennett BD, Wilson CJ (1999) Spontaneous activity of neostriatal cholinergic interneurons in vitro. *J Neurosci* 19:5586-5596.
- Bennett BD, Callaway JC, Wilson CJ (2000) Intrinsic membrane properties underlying spontaneous tonic firing in neostriatal cholinergic interneurons. *J Neurosci* 20:8493-8503.
- Berke JD, Breck JT, Eichenbaum H (2009) Striatal versus hippocampal representations during win-stay maze performance. *J Neurophysiol* 101:1575-1587.
- Berke JD, Okatan M, Skurski J, Eichenbaum HB (2004) Oscillatory entrainment of striatal neurons in freely moving rats. *Neuron* 43:883-896.
- Betarbet R, Turner R, Chockkan V, DeLong MR, Allers KA, Walters J, Levey AI, Greenamyre JT (1997) Dopaminergic neurons intrinsic to the primate striatum. *J Neurosci* 17:6761-6768.
- Beyene M, Carelli RM, Wightman RM (2010) Cue-evoked dopamine release in the nucleus accumbens shell tracks reinforcer magnitude during intracranial self-stimulation. *Neuroscience* 169:1682-1688.
- Bezard E, Gross CE (1998) Compensatory mechanisms in experimental and human parkinsonism: towards a dynamic approach. *Prog Neurobiol* 55:93-116.
- Bezard E, Gross CE, Fournier MC, Dovero S, Bloch B, Jaber M (1999) Absence of MPTP-induced neuronal death in mice lacking the dopamine transporter. *Exp Neurol* 155:268-273.
- Bi GQ, Rubin J (2005) Timing in synaptic plasticity: from detection to integration. *Trends Neurosci* 28:222-228.
- Bibbig A, Faulkner HJ, Whittington MA, Traub RD (2001) Self-organized synaptic plasticity contributes to the shaping of gamma and beta oscillations in vitro. *J Neurosci* 21:9053-9067.
- Bockamp E, Sprengel R, Eshkind L, Lehmann T, Braun JM, Emmrich F, Hengstler JG (2008) Conditional transgenic mouse models: from the basics to genome-wide sets of knockouts and current studies of tissue regeneration. *Regen Med* 3:217-235.
- Bolam JP, Bennett BD (1995) Microcircuitry of the neostriatum. In: *Neuroscience Intelligence Unit, Molecular and Cellular Mechanisms of Neostriatal Function* (Surmeier DJ, Ariano MA, eds), pp 1-20. Austin: R.G. Landes.
- Bolam JP, Izzo PN, Graybiel AM (1988) Cellular substrate of the histochemically defined striosome/matrix system of the caudate nucleus: a combined Golgi and immunocytochemical study in cat and ferret. *Neuroscience* 24:853-875.
- Bolam JP, Clarke DJ, Smith AD, Somogyi P (1983) A type of aspiny neuron in the rat neostriatum accumulates [3H]gamma-aminobutyric acid: combination

- of Golgi-staining, autoradiography, and electron microscopy. *J Comp Neurol* 213:121-134.
- Bolam JP, Hanley JJ, Booth PA, Bevan MD (2000) Synaptic organisation of the basal ganglia. *J Anat* 196 (Pt 4):527-542.
- Bracci E, Centonze D, Bernardi G, Calabresi P (2002) Dopamine excites fast-spiking interneurons in the striatum. *J Neurophysiol* 87:2190-2194.
- Burry RW (2011) Controls for immunocytochemistry: an update. *J Histochem Cytochem* 59:6-12.
- Buzsaki G (2010) Neural syntax: cell assemblies, synapsembles, and readers. *Neuron* 68:362-385.
- Cachope R, Mateo Y, Mathur BN, Irving J, Wang HL, Morales M, Lovinger DM, Cheer JF (2012) Selective activation of cholinergic interneurons enhances accumbal phasic dopamine release: setting the tone for reward processing. *Cell Rep* 2:33-41.
- Calabresi P, Picconi B, Tozzi A, Di Filippo M (2007) Dopamine-mediated regulation of corticostriatal synaptic plasticity. *Trends Neurosci* 30:211-219.
- Calabresi P, Centonze D, Gubellini P, Pisani A, Bernardi G (2000) Acetylcholine-mediated modulation of striatal function. *Trends Neurosci* 23:120-126.
- Calero-Nieto FJ, Bert AG, Cockerill PN (2010) Transcription-dependent silencing of inducible convergent transgenes in transgenic mice. *Epigenetics Chromatin* 3:3.
- Caporale N, Dan Y (2008) Spike timing-dependent plasticity: a Hebbian learning rule. *Annu Rev Neurosci* 31:25-46.
- Carrillo-Reid L, Tecuapetla F, Ibanez-Sandoval O, Hernandez-Cruz A, Galarraga E, Vargas J (2009) Activation of the cholinergic system endows compositional properties to striatal cell assemblies. *J Neurophysiol* 101:737-749.
- Carrillo-Reid L, Tecuapetla F, Tapia D, Hernandez-Cruz A, Galarraga E, Drucker-Colin R, Vargas J (2008) Encoding network states by striatal cell assemblies. *J Neurophysiol* 99:1435-1450.
- Centonze D, Gubellini P, Bernardi G, Calabresi P (1999) Permissive role of interneurons in corticostriatal synaptic plasticity. *Brain Res Brain Res Rev* 31:1-5.
- Centonze D, Gubellini P, Pisani A, Bernardi G, Calabresi P (2003) Dopamine, acetylcholine and nitric oxide systems interact to induce corticostriatal synaptic plasticity. *Rev Neurosci* 14:207-216.
- Centonze D, Bracci E, Pisani A, Gubellini P, Bernardi G, Calabresi P (2002) Activation of dopamine D1-like receptors excites LTS interneurons of the striatum. *Eur J Neurosci* 15:2049-2052.
- Cerri RD, F. FD (1983) Predation and risk in foraging minnows: balancing conflicting demands. *Amer Nat* 121:552-561.
- Chang HT, Wilson CJ, Kitai ST (1982) A Golgi study of rat neostriatal neurons: light microscopic analysis. *J Comp Neurol* 208:107-126.
- Chen X, Xu L, Radcliffe P, Sun B, Tank AW (2008) Activation of tyrosine hydroxylase mRNA translation by cAMP in midbrain dopaminergic neurons. *Mol Pharmacol* 73:1816-1828.

- Chesselet MF, Graybiel AM (1986) Striatal neurons expressing somatostatin-like immunoreactivity: evidence for a peptidergic interneuronal system in the cat. *Neuroscience* 17:547-571.
- Chuhma N, Tanaka KF, Hen R, Rayport S (2011) Functional connectome of the striatal medium spiny neuron. *J Neurosci* 31:1183-1192.
- Chuhma N, Mingote S, Moore H, Rayport S (2014) Dopamine Neurons Control Striatal Cholinergic Neurons via Regionally Heterogeneous Dopamine and Glutamate Signaling. *Neuron* 81:901-912.
- Ciliax BJ, Heilman C, Demchyshyn LL, Pristupa ZB, Ince E, Hersch SM, Niznik HB, Levey AI (1995) The dopamine transporter: immunochemical characterization and localization in brain. *J Neurosci* 15:1714-1723.
- Cossette M, Levesque D, Parent A (2005) Neurochemical characterization of dopaminergic neurons in human striatum. *Parkinsonism Relat Disord* 11:277-286.
- Cragg SJ, Rice ME (2004) DAncing past the DAT at a DA synapse. *Trends Neurosci* 27:270-277.
- Cragg SJ, Hille CJ, Greenfield SA (2000) Dopamine release and uptake dynamics within nonhuman primate striatum in vitro. *J Neurosci* 20:8209-8217.
- Cui G, Jun SB, Jin X, Pham MD, Vogel SS, Lovinger DM, Costa RM (2013) Concurrent activation of striatal direct and indirect pathways during action initiation. *Nature* 494:238-242.
- Dan Y, Poo MM (2006) Spike timing-dependent plasticity: from synapse to perception. *Physiol Rev* 86:1033-1048.
- Darmopil S, Muneton-Gomez VC, de Ceballos ML, Bernson M, Moratalla R (2008) Tyrosine hydroxylase cells appearing in the mouse striatum after dopamine denervation are likely to be projection neurones regulated by L-DOPA. *Eur J Neurosci* 27:580-592.
- Darwin C (1859) *On the origin of species*. London: John Murray.
- De Carlos JA, Borrell J (2007) A historical reflection of the contributions of Cajal and Golgi to the foundations of neuroscience. *Brain Res Rev* 55:8-16.
- DeCoteau WE, Thorn C, Gibson DJ, Courtemanche R, Mitra P, Kubota Y, Graybiel AM (2007) Learning-related coordination of striatal and hippocampal theta rhythms during acquisition of a procedural maze task. *Proc Natl Acad Sci U S A* 104:5644-5649.
- Deisseroth K (2011) Optogenetics. *Nat Methods* 8:26-29.
- Deisseroth K, Feng G, Majewska AK, Miesenbock G, Ting A, Schnitzer MJ (2006) Next-generation optical technologies for illuminating genetically targeted brain circuits. *J Neurosci* 26:10380-10386.
- Deister CA, Chan CS, Surmeier DJ, Wilson CJ (2009) Calcium-activated SK channels influence voltage-gated ion channels to determine the precision of firing in globus pallidus neurons. *J Neurosci* 29:8452-8461.
- Dezfouli A, Balleine BW (2012) Habits, action sequences and reinforcement learning. *Eur J Neurosci* 35:1036-1051.
- Dezfouli A, Balleine BW (2013) Actions, action sequences and habits: evidence that goal-directed and habitual action control are hierarchically organized. *PLoS Comput Biol* 9:e1003364.
- Ding JB, Guzman JN, Peterson JD, Goldberg JA, Surmeier DJ (2010) Thalamic gating of corticostriatal signaling by cholinergic interneurons. *Neuron* 67:294-307.

- Dubach M, Schmidt R, Kunkel D, Bowden DM, Martin R, German DC (1987) Primate neostriatal neurons containing tyrosine hydroxylase: immunohistochemical evidence. *Neurosci Lett* 75:205-210.
- Dubois A, Savasta M, Curet O, Scatton B (1986) Autoradiographic distribution of the D1 agonist [3H]SKF 38393, in the rat brain and spinal cord. Comparison with the distribution of D2 dopamine receptors. *Neuroscience* 19:125-137.
- Earl CD, Sautter J, Xie J, Kruk ZL, Kupsch A, Oertel WH (1998) Pharmacological characterisation of dopamine overflow in the striatum of the normal and MPTP-treated common marmoset, studied in vivo using fast cyclic voltammetry, nomifensine and sulpiride. *J Neurosci Methods* 85:201-209.
- Egorov AV, Draguhn A (2013) Development of coherent neuronal activity patterns in mammalian cortical networks: common principles and local heterogeneity. *Mech Dev* 130:412-423.
- Ehrnhoefer DE, Butland SL, Pouladi MA, Hayden MR (2009) Mouse models of Huntington disease: variations on a theme. *Dis Model Mech* 2:123-129.
- El Atifi-Borel M, Buggia-Prevot V, Platet N, Benabid AL, Berger F, Sgambato-Faure V (2009) De novo and long-term l-Dopa induce both common and distinct striatal gene profiles in the hemiparkinsonian rat. *Neurobiol Dis* 34:340-350.
- English DF, Ibanez-Sandoval O, Stark E, Tecuapetla F, Buzsaki G, Deisseroth K, Tepper JM, Koos T (2012) GABAergic circuits mediate the reinforcement-related signals of striatal cholinergic interneurons. *Nat Neurosci* 15:123-130.
- Ericsson J, Stephenson-Jones M, Kardamakis A, Robertson B, Silberberg G, Grillner S (2013a) Evolutionarily conserved differences in pallial and thalamic short-term synaptic plasticity in striatum. *J Physiol* 591:859-874.
- Ericsson J, Stephenson-Jones M, Perez-Fernandez J, Robertson B, Silberberg G, Grillner S (2013b) Dopamine differentially modulates the excitability of striatal neurons of the direct and indirect pathways in lamprey. *J Neurosci* 33:8045-8054.
- Ershov PV, Ugrumov MV, Calas A, Krieger M, Thibault J (2002) Differentiation of tyrosine hydroxylase-synthesizing and/or aromatic L-amino acid decarboxylase-synthesizing neurons in the rat mediobasal hypothalamus: quantitative double-immunofluorescence study. *J Comp Neurol* 446:114-122.
- Ershov PV, Ugrumov MV, Calas A, Krieger M, Thibault J (2005) Degeneration of dopaminergic neurons triggers an expression of individual enzymes of dopamine synthesis in non-dopaminergic neurons of the arcuate nucleus in adult rats. *J Chem Neuroanat* 30:27-33.
- Espadas I, Darmopil S, Vergano-Vera E, Ortiz O, Oliva I, Vicario-Abejon C, Martin ED, Moratalla R (2012) L-DOPA-induced increase in TH-immunoreactive striatal neurons in parkinsonian mice: insights into regulation and function. *Neurobiol Dis* 48:271-281.
- Facer P, Bishop AE, Polak JM (1980) Immunocytochemistry: its applications and drawbacks for the study of gut neuroendocrinology. *Invest Cell Pathol* 3:13-19.
- Fenno L, Yizhar O, Deisseroth K (2011) The development and application of optogenetics. *Annu Rev Neurosci* 34:389-412.

- Figueroa A, Galarraga E, Bargas J (2002) Muscarinic receptors involved in the subthreshold cholinergic actions of neostriatal spiny neurons. *Synapse* 46:215-223.
- Fino E, Venance L (2011) Spike-timing dependent plasticity in striatal interneurons. *Neuropharmacology* 60:780-788.
- Fino E, Glowinski J, Venance L (2005) Bidirectional activity-dependent plasticity at corticostriatal synapses. *J Neurosci* 25:11279-11287.
- Fino E, Deniau JM, Venance L (2008) Cell-specific spike-timing-dependent plasticity in GABAergic and cholinergic interneurons in corticostriatal rat brain slices. *J Physiol* 586:265-282.
- Fino E, Paille V, Deniau JM, Venance L (2009) Asymmetric spike-timing dependent plasticity of striatal nitric oxide-synthase interneurons. *Neuroscience* 160:744-754.
- Fino E, Paille V, Cui Y, Morera-Herreras T, Deniau JM, Venance L (2010) Distinct coincidence detectors govern the corticostriatal spike timing-dependent plasticity. *J Physiol* 588:3045-3062.
- Fiorillo CD, Newsome WT, Schultz W (2008) The temporal precision of reward prediction in dopamine neurons. *Nat Neurosci*.
- Fleig A, Penner R (2004) The TRPM ion channel subfamily: molecular, biophysical and functional features. *Trends Pharmacol Sci* 25:633-639.
- Flores-Barrera E, Vizcarra-Chacon BJ, Bargas J, Tapia D, Galarraga E (2011) Dopaminergic modulation of corticostriatal responses in medium spiny projection neurons from direct and indirect pathways. *Front Syst Neurosci* 5:15.
- Florian RV (2007) Reinforcement learning through modulation of spike-timing-dependent synaptic plasticity. *Neural Comput* 19:1468-1502.
- Freeze BS, Kravitz AV, Hammack N, Berke JD, Kreitzer AC (2013) Control of basal ganglia output by direct and indirect pathway projection neurons. *J Neurosci* 33:18531-18539.
- Gerfen C. R. WCJ, ed (1996) *The basal ganglia*, 12 Edition. Amsterdam: Elsevier Science.
- Gerfen CR (1992) The neostriatal mosaic: multiple levels of compartmental organization. *Trends Neurosci* 15:133-139.
- Gerfen CR, Surmeier DJ (2011) Modulation of striatal projection systems by dopamine. *Annu Rev Neurosci* 34:441-466.
- Gerfen CR, Baimbridge KG, Miller JJ (1985) The neostriatal mosaic: compartmental distribution of calcium-binding protein and parvalbumin in the basal ganglia of the rat and monkey. *Proc Natl Acad Sci U S A* 82:8780-8784.
- Gerfen CR, Engber TM, Mahan LC, Susel Z, Chase TN, Monsma FJ, Jr., Sibley DR (1990) D1 and D2 dopamine receptor-regulated gene expression of striatonigral and striatopallidal neurons. *Science* 250:1429-1432.
- Gittis AH, Kreitzer AC (2012) Striatal microcircuitry and movement disorders. *Trends Neurosci* 35:557-564.
- Gittis AH, Nelson AB, Thwin MT, Palop JJ, Kreitzer AC (2010) Distinct roles of GABAergic interneurons in the regulation of striatal output pathways. *J Neurosci* 30:2223-2234.
- Goldberg JA, Reynolds JN (2011) Spontaneous firing and evoked pauses in the tonically active cholinergic interneurons of the striatum. *Neuroscience*.

- Goldberg JA, Ding JB, Surmeier DJ (2012) Muscarinic modulation of striatal function and circuitry. In: *Handb Exp. Pharmacol.*, pp 223-241.
- Gong S, Doughty M, Harbaugh CR, Cummins A, Hatten ME, Heintz N, Gerfen CR (2007) Targeting Cre recombinase to specific neuron populations with bacterial artificial chromosome constructs. *J Neurosci* 27:9817-9823.
- Gradinaru V, Mogri M, Thompson KR, Henderson JM, Deisseroth K (2009) Optical deconstruction of parkinsonian neural circuitry. *Science* 324:354-359.
- Gradinaru V, Thompson KR, Zhang F, Mogri M, Kay K, Schneider MB, Deisseroth K (2007) Targeting and readout strategies for fast optical neural control in vitro and in vivo. *J Neurosci* 27:14231-14238.
- Gradinaru V, Zhang F, Ramakrishnan C, Mattis J, Prakash R, Diester I, Goshen I, Thompson KR, Deisseroth K (2010) Molecular and cellular approaches for diversifying and extending optogenetics. *Cell* 141:154-165.
- Graveland GA, DiFiglia M (1985) The frequency and distribution of medium-sized neurons with indented nuclei in the primate and rodent neostriatum. *Brain Res* 327:307-311.
- Graybiel AM, Hirsch EC, Agid YA (1987) Differences in tyrosine hydroxylase-like immunoreactivity characterize the mesostriatal innervation of striosomes and extrastriosomal matrix at maturity. *Proc Natl Acad Sci U S A* 84:303-307.
- Graybiel AM, Aosaki T, Flaherty AW, Kimura M (1994) The basal ganglia and adaptive motor control. *Science* 265:1826-1831.
- Graybiel AM, Pickel VM, Joh TH, Reis DJ, Ragsdale CW, Jr. (1981) Direct demonstration of a correspondence between the dopamine islands and acetylcholinesterase patches in the developing striatum. *Proc Natl Acad Sci U S A* 78:5871-5875.
- Gredal O, Nielsen M (1987) Binding of [3H]SKF 38393 to dopamine D-1 receptors in rat striatum in vitro; estimation of receptor molecular size by radiation inactivation. *J Neurochem* 48:370-375.
- Grillner S, Robertson B, Stephenson-Jones M (2013) The evolutionary origin of the vertebrate basal ganglia and its role in action selection. *J Physiol* 591:5425-5431.
- Grillner S, Wallen P, Saitoh K, Kozlov A, Robertson B (2008) Neural bases of goal-directed locomotion in vertebrates--an overview. *Brain Res Rev* 57:2-12.
- Groenewegen HJ (2003) The basal ganglia and motor control. *Neural Plast* 10:107-120.
- Grofova I (1979) Types of striatonigral neurons labeled by retrograde transport of horseradish peroxidase. *Appl Neurophysiol* 42:25-28.
- Hammond C, Bergman H, Brown P (2007) Pathological synchronization in Parkinson's disease: networks, models and treatments. *Trends Neurosci* 30:357-364.
- Han X (2012) Optogenetics in the nonhuman primate. *Prog Brain Res* 196:215-233.
- Hansen N, Manahan-Vaughan D (2014) Dopamine D1/D5 Receptors Mediate Informational Saliency that Promotes Persistent Hippocampal Long-Term Plasticity. *Cereb Cortex* 24:845-858.

- Hawes SL, Gillani F, Evans RC, Benkert EA, Blackwell KT (2013) Sensitivity to theta-burst timing permits LTP in dorsal striatal adult brain slice. *J Neurophysiol* 110:2027-2036.
- Hernandez-Lopez S,argas J, Surmeier DJ, Reyes A, Galarraga E (1997) D1 receptor activation enhances evoked discharge in neostriatal medium spiny neurons by modulating an L-type Ca^{2+} conductance. *J Neurosci* 17:3334-3342.
- Hikosaka O, Nakamura K, Nakahara H (2006) Basal ganglia orient eyes to reward. *J Neurophysiol* 95:567-584.
- Hikosaka O, Bromberg-Martin E, Hong S, Matsumoto M (2008) New insights on the subcortical representation of reward. *Curr Opin Neurobiol* 18:203-208.
- Hill K, Benham CD, McNulty S, Randall AD (2004) Flufenamic acid is a pH-dependent antagonist of TRPM2 channels. *Neuropharmacology* 47:450-460.
- Hollerman JR, Tremblay L, Schultz W (2000) Involvement of basal ganglia and orbitofrontal cortex in goal-directed behavior. *Prog Brain Res* 126:193-215.
- Holt DJ, Graybiel AM, Saper CB (1997) Neurochemical architecture of the human striatum. *J Comp Neurol* 384:1-25.
- Hong S, Hikosaka O (2011) Dopamine-mediated learning and switching in cortico-striatal circuit explain behavioral changes in reinforcement learning. *Front Behav Neurosci* 5:15.
- Hopf FW, Seif T, Mohamedi ML, Chen BT, Bonci A (2010) The small-conductance calcium-activated potassium channel is a key modulator of firing and long-term depression in the dorsal striatum. *Eur J Neurosci* 31:1946-1959.
- Howard CD, Keefe KA, Garriss PA, Daberkow DP (2011) Methamphetamine neurotoxicity decreases phasic, but not tonic, dopaminergic signaling in the rat striatum. *J Neurochem* 118:668-676.
- Huot P, Parent A (2007) Dopaminergic neurons intrinsic to the striatum. *J Neurochem* 101:1441-1447.
- Huot P, Levesque M, Parent A (2007) The fate of striatal dopaminergic neurons in Parkinson's disease and Huntington's chorea. *Brain* 130:222-232.
- Huot P, Levesque M, Morissette M, Calon F, Dridi M, Di Paolo T, Parent A (2008) L-Dopa treatment abolishes the numerical increase in striatal dopaminergic neurons in parkinsonian monkeys. *J Chem Neuroanat* 35:77-84.
- Ibanez-Sandoval O, Tecuapetla F, Unal B, Shah F, Koos T, Tepper JM (2010) Electrophysiological and morphological characteristics and synaptic connectivity of tyrosine hydroxylase-expressing neurons in adult mouse striatum. *J Neurosci* 30:6999-7016.
- Ibanez-Sandoval O, Tecuapetla F, Unal B, Shah F, Koos T, Tepper JM (2011) A novel functionally distinct subtype of striatal neuropeptide y interneuron. *J Neurosci* 31:16757-16769.
- Jin X, Costa RM (2010) Start/stop signals emerge in nigrostriatal circuits during sequence learning. *Nature* 466:457-462.
- Jin X, Tecuapetla F, Costa RM (2014) Basal ganglia subcircuits distinctively encode the parsing and concatenation of action sequences. *Nat Neurosci* 17:423-430.

- Joel D, Weiner I (1994) The organization of the basal ganglia-thalamocortical circuits: open interconnected rather than closed segregated. *Neuroscience* 63:363-379.
- John CE, Jones SR (2007) Fast Scan Cyclic Voltammetry of Dopamine and Serotonin in Mouse Brain Slices.
- Johnson A, van der Meer MA, Redish AD (2007) Integrating hippocampus and striatum in decision-making. *Curr Opin Neurobiol* 17:692-697.
- Jollivet C, Montero-Menei CN, Venier-Julienne MC, Sapin A, Benoit JP, Menei P (2004) Striatal tyrosine hydroxylase immunoreactive neurons are induced by L-dihydroxyphenylalanine and nerve growth factor treatment in 6-hydroxydopamine lesioned rats. *Neurosci Lett* 362:79-82.
- Kageyama T, Nakamura M, Matsuo A, Yamasaki Y, Takakura Y, Hashida M, Kanai Y, Naito M, Tsuruo T, Minato N, Shimohama S (2000) The 4F2hc/LAT1 complex transports L-DOPA across the blood-brain barrier. *Brain Res* 879:115-121.
- Kaneda N, Sasaoka T, Kobayashi K, Kiuchi K, Nagatsu I, Kurosawa Y, Fujita K, Yokoyama M, Nomura T, Katsuki M, et al. (1991) Tissue-specific and high-level expression of the human tyrosine hydroxylase gene in transgenic mice. *Neuron* 6:583-594.
- Kawaguchi Y (1992) Large aspiny cells in the matrix of the rat neostriatum in vitro: physiological identification, relation to the compartments and excitatory postsynaptic currents. *J Neurophysiol* 67:1669-1682.
- Kawaguchi Y (1993) Physiological, morphological, and histochemical characterization of three classes of interneurons in rat neostriatum. *J Neurosci* 13:4908-4923.
- Kawaguchi Y, Aosaki T, Kubota Y (1997) Cholinergic and GABAergic interneurons in the striatum. *Nihon Shinkei Seishin Yakurigaku Zasshi* 17:87-90.
- Kawaguchi Y, Wilson CJ, Augood SJ, Emson PC (1995) Striatal interneurons: chemical, physiological and morphological characterization. *Trends Neurosci* 18:527-535.
- Kim KS, Kim CH, Hwang DY, Seo H, Chung S, Hong SJ, Lim JK, Anderson T, Isacson O (2003) Orphan nuclear receptor Nurr1 directly transactivates the promoter activity of the tyrosine hydroxylase gene in a cell-specific manner. *J Neurochem* 85:622-634.
- Kimura M, Yamada H, Matsumoto N (2003) Tonically active neurons in the striatum encode motivational contexts of action. *Brain Dev* 25 Suppl 1:S20-23.
- Kita H (1993) GABAergic circuits of the striatum. *Prog Brain Res* 99:51-72.
- Kita H (1996) Glutamatergic and GABAergic postsynaptic responses of striatal spiny neurons to intrastriatal and cortical stimulation recorded in slice preparations. *Neuroscience* 70:925-940.
- Kita H, Kosaka T, Heizmann CW (1990) Parvalbumin-immunoreactive neurons in the rat neostriatum: a light and electron microscopic study. *Brain Res* 536:1-15.
- Knopfel T, Lin MZ, Levskaya A, Tian L, Lin JY, Boyden ES (2010) Toward the second generation of optogenetic tools. *J Neurosci* 30:14998-15004.
- Koller WC, Rueda MG (1998) Mechanism of action of dopaminergic agents in Parkinson's disease. *Neurology* 50:S11-14; discussion S44-18.

- Kölliker A (1896) *Handbuch der Gewebelehre des Menschen*, Vol 2, Nervensystem. Leipzig: Engelmann.
- Komiskey HL, Bossart JF, Miller DD, Patil PN (1978) Conformation of dopamine at the dopamine receptor. *Proc Natl Acad Sci U S A* 75:2641-2643.
- Komori K, Fujii T, Nagatsu I (1991) Do some tyrosine hydroxylase-immunoreactive neurons in the human ventrolateral arcuate nucleus and globus pallidus produce only L-dopa? *Neurosci Lett* 133:203-206.
- Koos T, Tepper JM (1999) Inhibitory control of neostriatal projection neurons by GABAergic interneurons. *Nat Neurosci* 2:467-472.
- Koos T, Tepper JM (2002) Dual cholinergic control of fast-spiking interneurons in the neostriatum. *J Neurosci* 22:529-535.
- Koos T, Tepper JM, Wilson CJ (2004) Comparison of IPSCs evoked by spiny and fast-spiking neurons in the neostriatum. *J Neurosci* 24:7916-7922.
- Kravitz AV, Kreitzer AC (2011) Optogenetic manipulation of neural circuitry in vivo. *Curr Opin Neurobiol* 21:433-439.
- Kravitz AV, Freeze BS, Parker PR, Kay K, Thwin MT, Deisseroth K, Kreitzer AC (2010) Regulation of parkinsonian motor behaviours by optogenetic control of basal ganglia circuitry. *Nature* 466:622-626.
- Kress GJ, Yamawaki N, Wokosin DL, Wickersham IR, Shepherd GM, Surmeier DJ (2013) Convergent cortical innervation of striatal projection neurons. *Nat Neurosci* 16:665-667.
- Kubota Y, Kawaguchi Y (1993) Spatial distributions of chemically identified intrinsic neurons in relation to patch and matrix compartments of rat neostriatum. *J Comp Neurol* 332:499-513.
- Kubota Y, Kawaguchi Y (2000) Dependence of GABAergic synaptic areas on the interneuron type and target size. *J Neurosci* 20:375-386.
- Lanciego JL, Luquin N, Obeso JA (2012) Functional neuroanatomy of the basal ganglia. *Cold Spring Harb Perspect Med* 2:a009621.
- Lee CR, Tepper JM (2007) A calcium-activated nonselective cation conductance underlies the plateau potential in rat substantia nigra GABAergic neurons. *J Neurosci* 27:6531-6541.
- Lee CR, Machold RP, Witkovsky P, Rice ME (2013) TRPM2 channels are required for NMDA-induced burst firing and contribute to H₂O₂-dependent modulation in substantia nigra pars reticulata GABAergic neurons. *J Neurosci* 33:1157-1168.
- Lenartowski R, Goc A (2011) Epigenetic, transcriptional and posttranscriptional regulation of the tyrosine hydroxylase gene. *Int J Dev Neurosci* 29:873-883.
- Leventhal DK, Gage GJ, Schmidt R, Pettibone JR, Case AC, Berke JD (2012) Basal ganglia beta oscillations accompany cue utilization. *Neuron* 73:523-536.
- Li JY, Popovic N, Brundin P (2005) The use of the R6 transgenic mouse models of Huntington's disease in attempts to develop novel therapeutic strategies. *NeuroRx* 2:447-464.
- Lima SL, Valone TJ, Caraco T (1985) Foraging-efficiency-predation-risk trade-off in the grey squirrel. *Anim Behav* 33:155-165.
- Liu X, Tonegawa S (2010) Optogenetics 3.0. *Cell* 141:22-24.
- Lomb NR (1976) Least-squares frequency analysis of unequally spaced data. *Astrophys Space Sci* 39:447-462.
- Lopez-Real A, Rodriguez-Pallares J, Guerra MJ, Labandeira-Garcia JL (2003) Localization and functional significance of striatal neurons

- immunoreactive to aromatic L-amino acid decarboxylase or tyrosine hydroxylase in rat Parkinsonian models. *Brain Res* 969:135-146.
- Lovinger DM (2010) Neurotransmitter roles in synaptic modulation, plasticity and learning in the dorsal striatum. *Neuropharmacology* 58:951-961.
- Luo R, Janssen MJ, Partridge JG, Vicini S (2013) Direct and GABA-mediated indirect effects of nicotinic ACh receptor agonists on striatal neurones. *J Physiol* 591:203-217.
- Mao L, Lau YS, Petroske E, Wang JQ (2001) Profound astrogenesis in the striatum of adult mice following nigrostriatal dopaminergic lesion by repeated MPTP administration. *Brain Res Dev Brain Res* 131:57-65.
- Marshall DL, Redfern PH, Wonnacott S (1997) Presynaptic nicotinic modulation of dopamine release in the three ascending pathways studied by in vivo microdialysis: comparison of naive and chronic nicotine-treated rats. *J Neurochem* 68:1511-1519.
- Martin LJ (2007) Transgenic mice with human mutant genes causing Parkinson's disease and amyotrophic lateral sclerosis provide common insight into mechanisms of motor neuron selective vulnerability to degeneration. *Rev Neurosci* 18:115-136.
- Martone ME, Young SJ, Armstrong DM, Groves PM (1994) The distribution of cholinergic perikarya with respect to enkephalin-rich patches in the caudate nucleus of the adult cat. *J Chem Neuroanat* 8:47-59.
- Matsuda W, Furuta T, Nakamura KC, Hioki H, Fujiyama F, Arai R, Kaneko T (2009) Single nigrostriatal dopaminergic neurons form widely spread and highly dense axonal arborizations in the neostriatum. *J Neurosci* 29:444-453.
- Matsumoto M, Hikosaka O (2009) Two types of dopamine neuron distinctly convey positive and negative motivational signals. *Nature* 459:837-841.
- Mazloom M, Smith Y (2006) Synaptic microcircuitry of tyrosine hydroxylase-containing neurons and terminals in the striatum of 1-methyl-4-phenyl-1,2,3,6-tetrahydropyridine-treated monkeys. *J Comp Neurol* 495:453-469.
- McCool MF, Patel S, Talati R, Ragozzino ME (2008) Differential involvement of M1-type and M4-type muscarinic cholinergic receptors in the dorsomedial striatum in task switching. *Neurobiol Learn Mem* 89:114-124.
- McHaffie JG, Stanford TR, Stein BE, Coizet V, Redgrave P (2005) Subcortical loops through the basal ganglia. *Trends Neurosci* 28:401-407.
- McRae-Degueurce A, Geffard M (1986) One perfusion mixture for immunocytochemical detection of noradrenaline, dopamine, serotonin and acetylcholine in the same rat brain. *Brain Res* 376:217-219.
- Medina L, Reiner A (1995) Neurotransmitter organization and connectivity of the basal ganglia in vertebrates: implications for the evolution of basal ganglia. *Brain Behav Evol* 46:235-258.
- Meredith GE, Farrell T, Kellaghan P, Tan Y, Zahm DS, Totterdell S (1999) Immunocytochemical characterization of catecholaminergic neurons in the rat striatum following dopamine-depleting lesions. *Eur J Neurosci* 11:3585-3596.
- Mikula S, Parrish SK, Trimmer JS, Jones EG (2009) Complete 3D visualization of primate striosomes by KChIP1 immunostaining. *J Comp Neurol* 514:507-517.

- Millar J, Pelling CW (2001) Improved methods for construction of carbon fibre electrodes for extracellular spike recording. *J Neurosci Methods* 110:1-8.
- Miller DW, Abercrombie ED (1999) Role of high-affinity dopamine uptake and impulse activity in the appearance of extracellular dopamine in striatum after administration of exogenous L-DOPA: studies in intact and 6-hydroxydopamine-treated rats. *J Neurochem* 72:1516-1522.
- Mura A, Linder JC, Young SJ, Groves PM (2000) Striatal cells containing aromatic L-amino acid decarboxylase: an immunohistochemical comparison with other classes of striatal neurons. *Neuroscience* 98:501-511.
- Mura A, Jackson D, Manley MS, Young SJ, Groves PM (1995) Aromatic L-amino acid decarboxylase immunoreactive cells in the rat striatum: a possible site for the conversion of exogenous L-DOPA to dopamine. *Brain Res* 704:51-60.
- Nagatsu I, Sakai M, Takeuchi T, Arai R, Karasawa N, Yamada K, Nagatsu T (1997) Tyrosine hydroxylase (TH)-only-immunoreactive non-catecholaminergic neurons in the brain of wild mice or the human TH transgenic mice do not contain GTP cyclohydrolase I. *Neurosci Lett* 228:55-57.
- Nair-Roberts RG, Chatelain-Badie SD, Benson E, White-Cooper H, Bolam JP, Ungless MA (2008) Stereological estimates of dopaminergic, GABAergic and glutamatergic neurons in the ventral tegmental area, substantia nigra and retrorubral field in the rat. *Neuroscience* 152:1024-1031.
- Nairne JS, Pandeirada JNS (2008) Adaptive memory: Is survival processing special? *J Mem Lang* 59:377-388.
- Nairne JS, Pandeirada JN, Thompson SR (2008) Adaptive memory: the comparative value of survival processing. *Psychol Sci* 19:176-180.
- Ng GY, Mouillac B, George SR, Caron M, Dennis M, Bouvier M, O'Dowd BF (1994) Desensitization, phosphorylation and palmitoylation of the human dopamine D1 receptor. *Eur J Pharmacol* 267:7-19.
- Ogren SO, Hall H, Kohler C, Magnusson O, Sjostrand SE (1986) The selective dopamine D2 receptor antagonist raclopride discriminates between dopamine-mediated motor functions. *Psychopharmacology (Berl)* 90:287-294.
- Oldenburg IA, Ding JB (2011) Cholinergic modulation of synaptic integration and dendritic excitability in the striatum. *Curr Opin Neurobiol* 21:425-432.
- Orduz D, Bishop DP, Schwaller B, Schiffmann SN, Gall D (2013) Parvalbumin tunes spike-timing and efferent short-term plasticity in striatal fast spiking interneurons. *J Physiol* 591:3215-3232.
- Pakhotin P, Bracci E (2007) Cholinergic interneurons control the excitatory input to the striatum. *J Neurosci* 27:391-400.
- Palfi S, Leventhal L, Chu Y, Ma SY, Emborg M, Bakay R, Deglon N, Hantraye P, Aebischer P, Kordower JH (2002) Lentivirally delivered glial cell line-derived neurotrophic factor increases the number of striatal dopaminergic neurons in primate models of nigrostriatal degeneration. *J Neurosci* 22:4942-4954.
- Panayotacopoulou MT, Raadsheer FC, Swaab DF (1994) Colocalization of tyrosine hydroxylase with oxytocin or vasopressin in neurons of the human paraventricular and supraoptic nucleus. *Brain Res Dev Brain Res* 83:59-66.

- Parent A (1986) *Comparative Neurobiology of the Basal Ganglia*. New York: John Wiley & Sons.
- Park CH, Minn YK, Lee JY, Choi DH, Chang MY, Shim JW, Ko JY, Koh HC, Kang MJ, Kang JS, Rhie DJ, Lee YS, Son H, Moon SY, Kim KS, Lee SH (2005) In vitro and in vivo analyses of human embryonic stem cell-derived dopamine neurons. *J Neurochem* 92:1265-1276.
- Parush N, Tishby N, Bergman H (2011) Dopaminergic Balance between Reward Maximization and Policy Complexity. *Front Syst Neurosci* 5:22.
- Patel J, Rice ME (2006) Dopamine Release in Brain Slices. In: *Encyclopedia of Sensors*, Vol 6 (Grimes CA, Dickey EC, Pishko MV, eds), pp 313-334. Stevenson Ranch, California: American Scientific.
- Pawlak V, Kerr JN (2008) Dopamine receptor activation is required for corticostriatal spike-timing-dependent plasticity. *J Neurosci* 28:2435-2446.
- Pei Y, Rogan SC, Yan F, Roth BL (2008) Engineered GPCRs as tools to modulate signal transduction. *Physiology (Bethesda)* 23:313-321.
- Peled A (2011) Optogenetic neuronal control in schizophrenia. *Med Hypotheses* 76:914-921.
- Pennartz CM, Ito R, Verschure PF, Battaglia FP, Robbins TW (2011) The hippocampal-striatal axis in learning, prediction and goal-directed behavior. *Trends Neurosci* 34:548-559.
- Pennartz CM, Berke JD, Graybiel AM, Ito R, Lansink CS, van der Meer M, Redish AD, Smith KS, Voorn P (2009) Corticostriatal Interactions during Learning, Memory Processing, and Decision Making. *J Neurosci* 29:12831-12838.
- Perez-Rosello T, Figueroa A, Salgado H, Vilchis C, Tecuapetla F, Guzman JN, Galarraga E, Bargas J (2005) Cholinergic control of firing pattern and neurotransmission in rat neostriatal projection neurons: role of CaV2.1 and CaV2.2 Ca²⁺ channels. *J Neurophysiol* 93:2507-2519.
- Petroske E, Meredith GE, Callen S, Totterdell S, Lau YS (2001) Mouse model of Parkinsonism: a comparison between subacute MPTP and chronic MPTP/probenecid treatment. *Neuroscience* 106:589-601.
- Pikaart MJ, Recillas-Targa F, Felsenfeld G (1998) Loss of transcriptional activity of a transgene is accompanied by DNA methylation and histone deacetylation and is prevented by insulators. *Genes Dev* 12:2852-2862.
- Piochon C, Kruskal P, Maclean J, Hansel C (2012) Non-Hebbian spike-timing-dependent plasticity in cerebellar circuits. *Front Neural Circuits* 6:124.
- Pivonello R, Ferone D, Lombardi G, Colao A, Lamberts SW, Hofland LJ (2007) Novel insights in dopamine receptor physiology. *Eur J Endocrinol* 156 Suppl 1:S13-21.
- Plenz D (2003) When inhibition goes incognito: feedback interaction between spiny projection neurons in striatal function. *Trends Neurosci* 26:436-443.
- Plenz D, Kitai ST (1998) Up and down states in striatal medium spiny neurons simultaneously recorded with spontaneous activity in fast-spiking interneurons studied in cortex-striatum-substantia nigra organotypic cultures. *J Neurosci* 18:266-283.
- Popescu AT, Popa D, Pare D (2009) Coherent gamma oscillations couple the amygdala and striatum during learning. *Nat Neurosci* 12:801-807.

- Porritt MJ, Kingsbury AE, Hughes AJ, Howells DW (2006) Striatal dopaminergic neurons are lost with Parkinson's disease progression. *Mov Disord* 21:2208-2211.
- Porritt MJ, Batchelor PE, Hughes AJ, Kalnins R, Donnan GA, Howells DW (2000) New dopaminergic neurons in Parkinson's disease striatum. *Lancet* 356:44-45.
- Power JM, Sah P (2008) Competition between calcium-activated K⁺ channels determines cholinergic action on firing properties of basolateral amygdala projection neurons. *J Neurosci* 28:3209-3220.
- Quinones H, Collazo R, Moe OW (2004) The dopamine precursor L-dihydroxyphenylalanine is transported by the amino acid transporters rBAT and LAT2 in renal cortex. *Am J Physiol Renal Physiol* 287:F74-80.
- Ramon y Cajal S (1911) *Histologie du Systeme Nerveux de l'Homme et des Vertébrés*. Paris: Maloine.
- Redgrave P, Prescott TJ, Gurney K (1999) The basal ganglia: a vertebrate solution to the selection problem? *Neuroscience* 89:1009-1023.
- Redgrave P, Rodriguez M, Smith Y, Rodriguez-Oroz MC, Lehericy S, Bergman H, Agid Y, DeLong MR, Obeso JA (2010) Goal-directed and habitual control in the basal ganglia: implications for Parkinson's disease. *Nat Rev Neurosci* 11:760-772.
- Reiner A (2002) Functional circuitry of the avian basal ganglia: implications for basal ganglia organization in stem amniotes. *Brain Res Bull* 57:513-528.
- Reiner A, Medina L, Veenman CL (1998) Structural and functional evolution of the basal ganglia in vertebrates. *Brain Res Brain Res Rev* 28:235-285.
- Rivera A, Alberti I, Martin AB, Narvaez JA, de la Calle A, Moratalla R (2002) Molecular phenotype of rat striatal neurons expressing the dopamine D5 receptor subtype. *Eur J Neurosci* 16:2049-2058.
- Robinson DL, Wightman RM (2004) Nomifensine amplifies subsecond dopamine signals in the ventral striatum of freely-moving rats. *J Neurochem* 90:894-903.
- Robinson DL, Heien ML, Wightman RM (2002) Frequency of dopamine concentration transients increases in dorsal and ventral striatum of male rats during introduction of conspecifics. *J Neurosci* 22:10477-10486.
- Roitman MF, Stuber GD, Phillips PE, Wightman RM, Carelli RM (2004) Dopamine operates as a subsecond modulator of food seeking. *J Neurosci* 24:1265-1271.
- Ruf T (1999) The Lomb-Scargle Periodogram in Biological Rhythm Research: Analysis of Incomplete and Unequally Spaced Time-Series. *Biol Rhythm Res* 30:178-201.
- Rymar VV, Sasseville R, Luk KC, Sadikot AF (2004) Neurogenesis and stereological morphometry of calretinin-immunoreactive GABAergic interneurons of the neostriatum. *J Comp Neurol* 469:325-339.
- Saka E, Iadarola M, Fitzgerald DJ, Graybiel AM (2002) Local circuit neurons in the striatum regulate neural and behavioral responses to dopaminergic stimulation. *Proc Natl Acad Sci U S A* 99:9004-9009.
- Sakai M, Fujii T, Karasawa N, Arai R, Nagatsu I (1995) Enhanced expression of tyrosine hydroxylase and aromatic L-amino acid decarboxylase in cerebellar Purkinje cells of mouse after hyperosmotic stimuli. *Neurosci Lett* 194:142-144.

- Sakurada K, Ohshima-Sakurada M, Palmer TD, Gage FH (1999) Nurr1, an orphan nuclear receptor, is a transcriptional activator of endogenous tyrosine hydroxylase in neural progenitor cells derived from the adult brain. *Development* 126:4017-4026.
- Salin P, Lopez IP, Kachidian P, Barroso-Chinea P, Rico AJ, Gomez-Bautista V, Coulon P, Kerkerian-Le Goff L, Lanciego JL (2009) Changes to interneuron-driven striatal microcircuits in a rat model of Parkinson's disease. *Neurobiol Dis* 34:545-552.
- Sardo P, Ferraro G, Di Giovanni G, Galati S, La Grutta V (2002) Inhibition of nitric oxide synthase influences the activity of striatal neurons in the rat. *Neurosci Lett* 325:179-182.
- Scargle JD (1982) Studies in astronomical time series analysis. II - Statistical aspects of spectral analysis of unevenly spaced data. *ApJ* 263:835-853.
- Schlosser B, Klaus G, Prime G, Ten Bruggencate G (1999) Postnatal development of calretinin- and parvalbumin-positive interneurons in the rat neostriatum: an immunohistochemical study. *J Comp Neurol* 405:185-198.
- Schultz W (1998) Predictive reward signal of dopamine neurons. *J Neurophysiol* 80:1-27.
- Schultz W (1999) The Reward Signal of Midbrain Dopamine Neurons. *News Physiol Sci* 14:249-255.
- Schultz W (2002) Getting formal with dopamine and reward. *Neuron* 36:241-263.
- Schultz W (2006) Behavioral theories and the neurophysiology of reward. *Annu Rev Psychol* 57:87-115.
- Schultz W (2007) Behavioral dopamine signals. *Trends Neurosci* 30:203-210.
- Schultz W (2010a) Multiple functions of dopamine neurons. *F1000 Biol Rep* 2.
- Schultz W (2010b) Dopamine signals for reward value and risk: basic and recent data. *Behav Brain Funct* 6:24.
- Sciamanna G, Wilson CJ (2011) The ionic mechanism of gamma resonance in rat striatal fast-spiking neurons. *J Neurophysiol* 106:2936-2949.
- Seeman P (1987) Dopamine receptors and the dopamine hypothesis of schizophrenia. *Synapse* 1:133-152.
- Sen D, Balakrishnan B, Gabriel N, Agrawal P, Roshini V, Samuel R, Srivastava A, Jayandharan GR (2013) Improved adeno-associated virus (AAV) serotype 1 and 5 vectors for gene therapy. *Sci Rep* 3:1832.
- Sharott A, Moll CK, Engler G, Denker M, Grun S, Engel AK (2009) Different subtypes of striatal neurons are selectively modulated by cortical oscillations. *J Neurosci* 29:4571-4585.
- Shen H, Kannari K, Yamato H, Arai A, Matsunaga M (2003) Effects of benserazide on L-DOPA-derived extracellular dopamine levels and aromatic L-amino acid decarboxylase activity in the striatum of 6-hydroxydopamine-lesioned rats. *Tohoku J Exp Med* 199:149-159.
- Shen W, Hamilton SE, Nathanson NM, Surmeier DJ (2005) Cholinergic suppression of KCNQ channel currents enhances excitability of striatal medium spiny neurons. *J Neurosci* 25:7449-7458.
- Shen W, Flajolet M, Greengard P, Surmeier DJ (2008) Dichotomous dopaminergic control of striatal synaptic plasticity. *Science* 321:848-851.

- Shen W, Tian X, Day M, Ulrich S, Tkatch T, Nathanson NM, Surmeier DJ (2007) Cholinergic modulation of Kir2 channels selectively elevates dendritic excitability in striatopallidal neurons. *Nat Neurosci* 10:1458-1466.
- Sjostrom PJ, Nelson SB (2002) Spike timing, calcium signals and synaptic plasticity. *Curr Opin Neurobiol* 12:305-314.
- Skaper SD, Giusti P (2010) Transgenic mouse models of Parkinson's disease and Huntington's disease. *CNS Neurol Disord Drug Targets* 9:455-470.
- Smeets WJ, Marin O, Gonzalez A (2000) Evolution of the basal ganglia: new perspectives through a comparative approach. *J Anat* 196 (Pt 4):501-517.
- Soares-da-Silva P, Serrao MP (2004) High- and low-affinity transport of L-leucine and L-DOPA by the hetero amino acid exchangers LAT1 and LAT2 in LLC-PK1 renal cells. *Am J Physiol Renal Physiol* 287:F252-261.
- Spacek J (1992) Dynamics of Golgi impregnation in neurons. *Microsc Res Tech* 23:264-274.
- Spencer JP, Murphy KP (2000) Bi-directional changes in synaptic plasticity induced at corticostriatal synapses in vitro. *Exp Brain Res* 135:497-503.
- Stephenson-Jones M, Ericsson J, Robertson B, Grillner S (2012) Evolution of the basal ganglia: dual-output pathways conserved throughout vertebrate phylogeny. *J Comp Neurol* 520:2957-2973.
- Stott SR, Barker RA (2013) Time course of dopamine neuron loss and glial response in the 6-OHDA striatal mouse model of Parkinson's disease. *Eur J Neurosci*.
- Stuber GD, Sparta DR, Stamatakis AM, van Leeuwen WA, Hardjoprajitno JE, Cho S, Tye KM, Kempadoo KA, Zhang F, Deisseroth K, Bonci A (2011) Excitatory transmission from the amygdala to nucleus accumbens facilitates reward seeking. *Nature* 475:377-380.
- Sullivan MA, Chen H, Morikawa H (2008) Recurrent inhibitory network among striatal cholinergic interneurons. *J Neurosci* 28:8682-8690.
- Surmeier DJ, Kitai ST (1993) D1 and D2 dopamine receptor modulation of sodium and potassium currents in rat neostriatal neurons. *Prog Brain Res* 99:309-324.
- Surmeier DJ, Kitai ST (1994) Dopaminergic regulation of striatal efferent pathways. *Curr Opin Neurobiol* 4:915-919.
- Surmeier DJ, Carrillo-Reid L,argas J (2011) Dopaminergic modulation of striatal neurons, circuits, and assemblies. *Neuroscience* 198:3-18.
- Surmeier DJ,argas J, Hemmings HC, Jr., Nairn AC, Greengard P (1995) Modulation of calcium currents by a D1 dopaminergic protein kinase/phosphatase cascade in rat neostriatal neurons. *Neuron* 14:385-397.
- Surmeier DJ, Ding J, Day M, Wang Z, Shen W (2007) D1 and D2 dopamine-receptor modulation of striatal glutamatergic signaling in striatal medium spiny neurons. *Trends Neurosci* 30:228-235.
- Surmeier DJ, Shen W, Day M, Gertler T, Chan S, Tian X, Plotkin JL (2010) The role of dopamine in modulating the structure and function of striatal circuits. *Prog Brain Res* 183:149-167.
- Tande D, Hoglinger G, Debeir T, Freundlieb N, Hirsch EC, Francois C (2006) New striatal dopamine neurons in MPTP-treated macaques result from a phenotypic shift and not neurogenesis. *Brain* 129:1194-1200.

- Tank AW, Xu L, Chen X, Radcliffe P, Sterling CR (2008) Post-transcriptional regulation of tyrosine hydroxylase expression in adrenal medulla and brain. *Ann N Y Acad Sci* 1148:238-248.
- Tashiro Y, Kaneko T, Sugimoto T, Nagatsu I, Kikuchi H, Mizuno N (1989a) Striatal neurons with aromatic L-amino acid decarboxylase-like immunoreactivity in the rat. *Neurosci Lett* 100:29-34.
- Tashiro Y, Sugimoto T, Hattori T, Uemura Y, Nagatsu I, Kikuchi H, Mizuno N (1989b) Tyrosine hydroxylase-like immunoreactive neurons in the striatum of the rat. *Neurosci Lett* 97:6-10.
- Tecuapetla F, Carrillo-Reid L, Vargas J, Galarraga E (2007) Dopaminergic modulation of short-term synaptic plasticity at striatal inhibitory synapses. *Proc Natl Acad Sci U S A* 104:10258-10263.
- Tecuapetla F, Patel JC, Xenias H, English D, Tadros I, Shah F, Berlin J, Deisseroth K, Rice ME, Tepper JM, Koos T (2010) Glutamatergic signaling by mesolimbic dopamine neurons in the nucleus accumbens. *J Neurosci* 30:7105-7110.
- Tepper JM (2006) Microcircuits in the Striatum: Striatal Cell Types and Their Interaction. In: *Microcircuits: The Interface between Neurons and Global Brain Function*. Dahlem Workshop Report 93 (Grillner S, Graybiel AM, eds), pp 127-148. Cambridge, MA: : The MIT Press.
- Tepper JM, Bolam JP (2004) Functional diversity and specificity of neostriatal interneurons. *Curr Opin Neurobiol* 14:685-692.
- Tepper JM, Koos T, Wilson CJ (2004) GABAergic microcircuits in the neostriatum. *Trends Neurosci* 27:662-669.
- Tepper JM, Wilson CJ, Koos T (2008) Feedforward and feedback inhibition in neostriatal GABAergic spiny neurons. *Brain Res Rev* 58:272-281.
- Tepper JM, Sharpe NA, Koos TZ, Trent F (1998) Postnatal development of the rat neostriatum: electrophysiological, light- and electron-microscopic studies. *Dev Neurosci* 20:125-145.
- Tepper JM, Tecuapetla F, Koos T, Ibanez-Sandoval O (2010) Heterogeneity and diversity of striatal GABAergic interneurons. *Front Neuroanat* 4:150.
- Threlfell S, Cragg SJ (2011) Dopamine signaling in dorsal versus ventral striatum: the dynamic role of cholinergic interneurons. *Front Syst Neurosci* 5:11.
- Threlfell S, Lalic T, Platt NJ, Jennings KA, Deisseroth K, Cragg SJ (2012) Striatal dopamine release is triggered by synchronized activity in cholinergic interneurons. *Neuron* 75:58-64.
- Tritsch NX, Ding JB, Sabatini BL (2012) Dopaminergic neurons inhibit striatal output through non-canonical release of GABA. *Nature* 490:262-266.
- Ugrumov M, Melnikova V, Ershov P, Balan I, Calas A (2002) Tyrosine hydroxylase- and/or aromatic L-amino acid decarboxylase-expressing neurons in the rat arcuate nucleus: ontogenesis and functional significance. *Psychoneuroendocrinology* 27:533-548.
- Ugrumov MV (2009) Non-dopaminergic neurons partly expressing dopaminergic phenotype: distribution in the brain, development and functional significance. *J Chem Neuroanat* 38:241-256.
- Ugrumov MV, Melnikova VI, Lavrentyeva AV, Kudrin VS, Rayevsky KS (2004) Dopamine synthesis by non-dopaminergic neurons expressing individual complementary enzymes of the dopamine synthetic pathway in the arcuate nucleus of fetal rats. *Neuroscience* 124:629-635.

- Unal B, Shah F, Kothari J, Tepper JM (2013) Anatomical and electrophysiological changes in striatal TH interneurons after loss of the nigrostriatal dopaminergic pathway. *Brain Struct Funct*.
- Unal B, Ibanez-Sandoval O, Shah F, Abercrombie ED, Tepper JM (2011) Distribution of tyrosine hydroxylase-expressing interneurons with respect to anatomical organization of the neostriatum. *Front Syst Neurosci* 5:41.
- Ungless MA, Grace AA (2012) Are you or aren't you? Challenges associated with physiologically identifying dopamine neurons. *Trends Neurosci* 35:422-430.
- Veenman CL (1997) Pigeon basal ganglia: insights into the neuroanatomy underlying telencephalic sensorimotor processes in birds. *Eur J Morphol* 35:220-233.
- Vogt C, Vogt O (1920) Zur Lehre der Erkrankungen des striären Systems. *J Psychol Neurol (Leipzig)* 25:627-846.
- Wanat MJ, Willuhn I, Clark JJ, Phillips PE (2009) Phasic dopamine release in appetitive behaviors and drug addiction. *Curr Drug Abuse Rev* 2:195-213.
- Weihe E, Depboylu C, Schutz B, Schafer MK, Eiden LE (2006) Three types of tyrosine hydroxylase-positive CNS neurons distinguished by dopa decarboxylase and VMAT2 co-expression. *Cell Mol Neurobiol* 26:659-678.
- West AR, Grace AA (2004) The nitric oxide-guanylyl cyclase signaling pathway modulates membrane activity States and electrophysiological properties of striatal medium spiny neurons recorded in vivo. *J Neurosci* 24:1924-1935.
- Westin JE, Andersson M, Lundblad M, Cenci MA (2001) Persistent changes in striatal gene expression induced by long-term L-DOPA treatment in a rat model of Parkinson's disease. *Eur J Neurosci* 14:1171-1176.
- Wiedemann DJ, Kawagoe KT, Kennedy RT, Ciolkowski EL, Wightman RM (1991) Strategies for low detection limit measurements with cyclic voltammetry. *Anal Chem* 63:2965-2970.
- Williams SC, Deisseroth K (2013) Optogenetics. *Proc Natl Acad Sci U S A* 110:16287.
- Wilson CJ (2004) Basal Ganglia. In: *The Synaptic Organization of the Brain*, 5 Edition, pp 361-414. Oxford: Oxford Uni. Press.
- Wilson CJ (2005) The mechanism of intrinsic amplification of hyperpolarizations and spontaneous bursting in striatal cholinergic interneurons. *Neuron* 45:575-585.
- Wilson CJ (2007) GABAergic inhibition in the neostriatum. *Prog Brain Res* 160:91-110.
- Wilson CJ, Kawaguchi Y (1996) The origins of two-state spontaneous membrane potential fluctuations of neostriatal spiny neurons. *J Neurosci* 16:2397-2410.
- Witten IB, Lin SC, Brodsky M, Prakash R, Diester I, Anikeeva P, Gradinaru V, Ramakrishnan C, Deisseroth K (2010) Cholinergic interneurons control local circuit activity and cocaine conditioning. *Science* 330:1677-1681.
- Yamada H, Matsumoto N, Kimura M (2004) Tonically active neurons in the primate caudate nucleus and putamen differentially encode instructed motivational outcomes of action. *J Neurosci* 24:3500-3510.
- Yamaguchi T, Sheen W, Morales M (2007) Glutamatergic neurons are present in the rat ventral tegmental area. *Eur J Neurosci* 25:106-118.

- Yang J, Ye M, Tian C, Yang M, Wang Y, Shu Y (2013) Dopaminergic modulation of axonal potassium channels and action potential waveform in pyramidal neurons of prefrontal cortex. *J Physiol* 591:3233-3251.
- Yizhar O, Fenno LE, Davidson TJ, Mogri M, Deisseroth K (2011) Optogenetics in neural systems. *Neuron* 71:9-34.
- Zeiss CJ (2005) Neuroanatomical phenotyping in the mouse: the dopaminergic system. *Vet Pathol* 42:753-773.
- Zhang F, Wang LP, Boyden ES, Deisseroth K (2006) Channelrhodopsin-2 and optical control of excitable cells. *Nat Methods* 3:785-792.
- Zhang F, Gradinaru V, Adamantidis AR, Durand R, Airan RD, de Lecea L, Deisseroth K (2010) Optogenetic interrogation of neural circuits: technology for probing mammalian brain structures. *Nat Protoc* 5:439-456.
- Zhang RL, Zhang L, Zhang ZG, Morris D, Jiang Q, Wang L, Zhang LJ, Chopp M (2003) Migration and differentiation of adult rat subventricular zone progenitor cells transplanted into the adult rat striatum. *Neuroscience* 116:373-382.
- Zhou FM, Wilson CJ, Dani JA (2002) Cholinergic interneuron characteristics and nicotinic properties in the striatum. *J Neurobiol* 53:590-605.
- Zhou FM, Wilson C, Dani JA (2003) Muscarinic and nicotinic cholinergic mechanisms in the mesostriatal dopamine systems. *Neuroscientist* 9:23-36.
- Zigmond MJ, Hastings TG, Abercrombie ED (1992) Neurochemical responses to 6-hydroxydopamine and L-dopa therapy: implications for Parkinson's disease. *Ann N Y Acad Sci* 648:71-86.
- Zoli M, Agnati LF, Tinner B, Steinbusch HW, Fuxe K (1993) Distribution of dopamine-immunoreactive neurons and their relationships to transmitter and hypothalamic hormone-immunoreactive neuronal systems in the rat mediobasal hypothalamus. A morphometric and microdensitometric analysis. *J Chem Neuroanat* 6:293-310.

VITA

Harry S. Xenias

EDUCATION

2006 - 2014	Rutgers University, New Jersey, Ph. D.
2003	Columbia University, New York, B. S., Physics,
2003	Columbia University, New York, B. A., Mathematics

ACADEMIC RESEARCH

Rutgers University

2009 – 2014	Dr. James M. Tepper Lab Striatal Interneuron Network Research
-------------	--

2006-2009	Dr. Kenneth Harris Lab, 2006-2009 Auditory Multi-unit Recordings Activity-dependent Neurodevelopment
-----------	--

TECHNICAL SKILLS

Whole-cell patch electrophysiology
Optogenetics
Voltammetry
Immunocytochemistry
Intracellular electrophysiology
Dynamic clamp electrophysiology
Cell culture

HONORS AND REWARDS

2013	·	CMBN Travel Grant for SfN 2013
2013	·	Annual Communication Excellence in Scholarship
2007 -	·	HHMI Interface Scholar
2000 - 2003	·	Columbia University Dean's List
2000 - 2003	·	GS Scholarship for three consecutive years
2002	·	Hettena Scholarship for Physics and Chemistry

PROFESSIONAL ORGANIZATIONS AND SOCIETIES

Society for Neuroscience (SfN)
International Basal Ganglia Society (IBAGs)
American Association for the Advancement of Science
Golden Key National Honor Society